

Latent Noise Injection for Private and Statistically Aligned Synthetic Data Generation

Rex Shen *
Stanford University

Lu Tian †
Stanford University

June 19, 2025

Abstract

Synthetic Data Generation has become essential for scalable, privacy-preserving statistical analysis. While standard approaches based on generative models, such as Normalizing Flows, have been widely used, they often suffer from slow convergence in high-dimensional settings, frequently converging more slowly than the canonical $1/\sqrt{n}$ rate when approximating the true data distribution.

To overcome these limitations, we propose a Latent Noise Injection method using Masked Autoregressive Flows (MAF). Instead of directly sampling from the trained model, our method perturbs each data point in the latent space and maps it back to the data domain. This construction preserves a one to one correspondence between observed and synthetic data, enabling synthetic outputs that closely reflect the underlying distribution, particularly in challenging high-dimensional regimes where traditional sampling struggles.

Our procedure satisfies local (ϵ, δ) -differential privacy and introduces a single perturbation parameter to control the privacy-utility trade-off. Although estimators based on individual synthetic datasets may converge slowly, we show both theoretically and empirically that aggregating across K studies in a meta analysis framework restores classical efficiency and yields consistent, reliable inference. We demonstrate that with a well-calibrated perturbation parameter, Latent Noise Injection achieves strong statistical alignment with the original data and robustness against membership inference attacks. These results position our method as a compelling alternative to conventional flow-based sampling for synthetic data sharing in decentralized and privacy-sensitive domains, such as biomedical research.

1 Introduction

Recently, the exponential growth of data has underscored the increasing need for synthetic data generation to replicate observed datasets. While extensive research has been conducted in this area, a fundamental challenge remains: generating high-quality synthetic samples that accurately preserve the statistical distributions and key properties of the original data. Ensuring the quality and fidelity of these synthetic samples helps address various challenges, such as protecting data confidentiality while enabling statistically valid analyses. In addition, synthetic data generation can reduce the need for extensive real-world experiments, thereby lowering costs and improving scalability.

In this work, we focus on Normalizing Flows as a powerful generative modeling approach for producing synthetic data. Among the variety of generative methods available, Normalizing Flows possess unique advantages. Unlike models such as Variational Autoencoders (VAEs) or Generative Adversarial Networks (GANs) (Goodfellow et al., 2020; Kingma, Diederik P and Welling, Max and Others, 2019), which rely on approximate reconstruction losses, Normalizing Flows leverage explicit likelihood-based training, enabling both density estimation and efficient sampling. More importantly, Normalizing Flows permit fast inversion and can transform complex data distributions into simple base distributions, typically standard Gaussian distributions, where adding random noise is often more natural. These properties make Normalizing Flows

*rshen0@alumni.stanford.edu

†lutian@stanford.edu

particularly well-suited for synthetic data generation, especially in multi-dimensional settings where capturing intricate dependencies is essential.

Among the family of Normalizing Flows, Masked Autoregressive Flows (MAFs) stand out for their balance of flexibility and tractability. MAF extends autoregressive models by stacking multiple transformations, each representing a learned, invertible map from latent variables to the data space. This increases model expressiveness while maintaining computational efficiency (Papamakarios et al., 2017). The architecture of MAF builds upon the Masked Autoencoder for Distribution Estimation (MADE) (Germain et al., 2015), which enforces the autoregressive property by applying binary masks to a feedforward neural network. This property makes MAF—and Normalizing Flows more broadly—particularly well-suited for applications that require exact and tractable density evaluation, in contrast to VAEs and GANs, which lack closed-form likelihoods. Beyond generative modeling, density estimators like MAF have been successfully integrated into Bayesian workflows. They have been used as surrogates for posterior distributions (Papamakarios and Murray, 2016), as proposal distributions in importance sampling (Paige and Wood, 2016), and as key components in amortized inference frameworks for simulation-based models (Greenberg et al., 2019). While MAF provides strong performance across a wide range of tasks, the broader family of Normalizing Flows includes several notable variants, each offering different trade-offs in expressiveness, computational efficiency, and applicability. For example, Continuous Normalizing Flows (CNFs) (Chen et al., 2018; Gao et al., 2024; Du et al., 2022) model data transformations as solutions to ordinary differential equations (ODEs), enabling highly flexible and adaptive mappings. However, their expressiveness comes at the cost of greater computational complexity due to the need to solve ODEs during training and sampling.

On the other hand, discrete-time flows such as RealNVP (Dinh et al., 2016) and GLOW (Kingma and Dhariwal, 2018) utilize coupling layers and invertible transformations to scale effectively to high-dimensional data, especially in image domains. The foundational NICE model (Dinh et al., 2014) introduced volume-preserving flows with additive coupling layers, paving the way for these architectures. In contrast to MAF, which is optimized for fast likelihood computation, Inverse Autoregressive Flows (IAF) (Kingma et al., 2016) are designed for fast sampling, making them particularly suitable for variational inference tasks. More expressive models such as Neural Spline Flows (Durkan et al., 2019) enhance flexibility by replacing affine transformations with monotonic rational-quadratic splines, allowing construction of richer yet still tractable mappings. Finally, Conditional Normalizing Flows (Ardizzone et al., 2019; Winkler et al., 2019) extend standard flows by incorporating conditioning variables, supporting tasks such as class-conditional generation, structured prediction, and simulation-based inference. While we choose MAF as the basis for synthetic data generation in this paper due to the aforementioned considerations, we don’t claim it is the best choice. As the field continues to advance, hybrid architectures that combine the strengths of discrete-time flows (i.e., MAF) with continuous-time models (i.e., CNFs) represent a promising direction for developing new techniques for synthetic data generation.

To formalize a common setting in the literature, consider an observed dataset consisting of features and relevant outcomes from n observations, denoted by $\mathbf{X} = \{X_1, \dots, X_n\}$, where each $X_i \in \mathbb{R}^d$. The goal is to generate a synthetic dataset $\tilde{\mathbf{X}} = \{\tilde{X}_1, \dots, \tilde{X}_m\}$, where $\tilde{X}_i \in \mathbb{R}^d$, such that

$$\tilde{\mathbf{X}} \stackrel{d}{\sim} \mathbf{X}$$

i.e., the synthetic data are drawn from a distribution similar to the underlying distribution of observed data. Importantly, the sample sizes n and m need not be equal.

The resulting synthetic dataset $\{\tilde{X}_1, \dots, \tilde{X}_m\}$ can be used as a substitute for the original data in downstream statistical analyses without requiring access to original observations. This objective is closely aligned with the goals of Federated Learning (FL), where models are trained across distributed data sources without centralized data sharing on the individual level (McMahan et al., 2017). However, FL typically involves iterative communication between local clients and a central server—transmitting gradients, parameter updates, or summary statistics across multiple rounds—which can impose substantial communication overhead, especially in large or bandwidth-constrained networks.

Moreover, FL workflows must be tailored to specific analyses. The summary statistics and updates required to fit a linear regression model, for example, differ from those of logistic regression. Consequently, FL generally requires the analytical objectives to be pre-specified, limiting its flexibility. In scenarios involving exploratory or sequential analyses—where subsequent steps depend on earlier results—FL becomes cumbersome and, in some cases, infeasible.

By contrast, our synthetic data strategy enables a one-shot solution: once the synthetic data is generated and shared, users can directly conduct statistical analyses without requiring repeated interactions or communication rounds. This approach offers significant flexibility and efficiency. However, it is important to acknowledge a key limitation: synthetic data, even when generated using state-of-the-art generative models, often fails to fully replicate results obtained from the original raw data. This shortfall arises from the intrinsic difficulty of nonparametrically estimating the joint distribution of a high-dimensional random vector with the typical sample sizes available in practice. A more subtle practical difficulty is that even if we can generate the synthetic data from a distribution that closely approximates that of X , one may expect to reproduce a parameter estimate but certainly not the associated uncertainty measure such as the standard error due to the simple fact that the sample size of the synthetic data potentially can be arbitrarily big, which may yield artificially small standard errors of any sensible parameter estimates. This inflated confidence on parameter estimates from the synthetic data is due to the fact that users of the synthetic data neither account nor know how to account for the intrinsic randomness in estimating the generative model from observed data of finite sample size.

To mitigate this issue, it is desirable for synthetic data to resemble the observed data not only in distribution, but also in their actual values, i.e.,

$$\tilde{X} \approx X.$$

At the same time, \tilde{X} must not be too close to X , as this would compromise privacy. Ideally, we aim to generate synthetic data that preserves analytical utility while satisfying formal privacy guarantees, such as local differential privacy (Local DP) (Ji et al., 2014; Dwork et al., 2006; Yang et al., 2024), which provides a quantifiable bound on privacy loss and supports controlled data sharing.

Accordingly, the main contribution of our work is a method for generating synthetic data that:

1. is sampled from a distribution closely matching that of the original data X ;
2. remains sufficiently close to the observed data to reproduce results of statistical analysis based on original data;
3. introduces sufficient perturbation to satisfy the differential privacy guarantees.

Specifically, we propose a procedure that diverges from traditional resampling methods by instead generating synthetic data through a latent-space transformation. Specifically, we map the observed data into a latent space, inject random perturbations, and then map the perturbed representations back to the data space. This approach induces a one to one correspondence between the original and synthetic datasets when $m = n$, ensuring that each synthetic observation reflects a controlled deviation from a specific real data point.

Another appealing feature of our method is its applicability to meta analysis for synthesizing evidence across multiple studies. In particular, traditional meta analysis does not require individual level data; instead, study-specific estimators are extracted and aggregated to form a combined estimate of the parameter of interest. However, similar to Federated Learning, meta analysis is only feasible when the relevant summary statistics in the form of parameter estimates, CIs, and related inferential quantities are available from all participating studies. These summary statistics are typically obtained either from published results or by request from data custodians. As a result, meta analysis cannot be conducted in an exploratory or flexible manner for arbitrary parameters without access to individual level data.

In practice, especially in fields such as healthcare and the social sciences, individual level data often cannot be shared due to privacy concerns (Riley et al., 2010; Shen et al., 2022). To address this challenge, our method facilitates the generation and sharing of privacy-preserving synthetic datasets from multiple studies, thereby enabling meta analysis for any parameter of interest. Crucially, our data generation strategy is designed to preserve the statistical integrity of each study, ensuring that downstream aggregation yields valid inference. Specifically, although standard Normalizing Flow models may converge slowly to the true distribution, our Latent Noise Injection method enhances fidelity at the study level. When synthetic datasets from multiple studies are combined, the resulting aggregate estimates exhibit greater stability than those derived from individual synthetic datasets. For example, one may expect that its result (1) is robust to sharing synthetic data of poor quality from a few studies and (2) may average out the difference between synthetic data and original data across all studies of interest. This makes our approach particularly advantageous for multi-site meta analyses.

Taken together, our method offers a practical middle ground—reducing the communication burden relative to Federated Learning while enabling access to statistically valid, privacy-preserving samples. This makes it especially suitable for decentralized scientific collaboration in sensitive domains, such as healthcare and finance. Moreover, future work may explore hybrid frameworks that integrate synthetic data generation with formal differential privacy guarantees or adaptive strategies that balance fidelity and privacy depending on the intended downstream analysis.

The structure of this paper is as follows. We begin by introducing Normalizing Flows, outlining their mathematical foundations and their role in generative modeling. We then describe our proposal for generating high-quality synthetic samples based on Normalizing Flows. We also present theoretical guarantees showing that our method can produce inference results equivalent to those based on the original data, while simultaneously providing privacy protection under the framework of Local DP (Ji et al., 2014). Next, we examine the operating characteristics of our method through extensive simulation studies and applications to real-world datasets. Finally, we conclude by discussing the broader implications of our findings and outline future research directions, including integrating transfer learning to further improve synthetic data quality, and extending our framework to more general meta analytic settings.

2 Method

In the following, we first provide a detailed overview of the Normalizing Flow framework and highlight the Masked Autoregressive Flow (MAF) architecture, which underpins our proposed methodology (Section 2.1). Then, we introduce meta analysis (Section 2.2). Lastly, we present our main contribution in proposing a new synthetic data generation method with its applications in meta analysis (Section 2.3).

2.1 Normalizing Flows

Normalizing Flows have emerged as a compelling framework for generative modeling due to their ability to combine expressive power with exact likelihood computation. Normalizing Flows construct complex data distributions from a simple base distribution by composing a series of invertible transformations. The architecture of Normalizing Flows enables efficient training via maximum likelihood and tractable sampling, while preserving the distributional structure of the data.

In the context of privacy-preserving synthetic data generation, these properties are particularly advantageous. The invertibility ensures a one to one correspondence between a real observation and its “projection” into a latent space that follows a simple base distribution allowing controlled perturbations. Moreover, the explicit likelihood evaluation permits rigorous evaluation of distributional fidelity. Thus, Normalizing Flows provide an ideal foundation for generating high-fidelity synthetic data that balance statistical utility and privacy guarantees.

The general framework of the Normalizing Flow revolves around learning models in multi-dimensional continuous spaces. The objective of Normalizing Flows is to learn a bijective function $f : \mathbb{R}^d \rightarrow \mathbb{R}^d$ based on our observed data $\mathbf{X} = \{X_1, \dots, X_n\}$ consisting of n independently identically distributed (i.i.d.) copies of a random vector $X \in \mathbb{R}^d$, such that $X = f(Z)$, where Z follows a simple base distribution of the same dimension of X (e.g., a standard multivariate Gaussian). The rationale of training f is as follows: given a simple base distribution p_Z on a latent variable space and a bijection $f(\cdot)$, the change of variables formula defines a distribution on $X = f(Z)$ by

$$p_X(X) = p_Z \{f^{-1}(X)\} |\det(\nabla f^{-1}(X))|,$$

or equivalently

$$\log\{p_X(X)\} = \log[p_Z \{f^{-1}(X)\}] + \log\{|\det \{\nabla f^{-1}(X)\}|\}, \quad (1)$$

where $p_Z(\cdot)$ is the density function of Z . One may want to train f to maximize the observed log-likelihood function

$$l(f) = \sum_{i=1}^n \log\{p_X(X_i)\}.$$

However, directly computing the Jacobian in (1) for large d is expensive and even intractable. On the other hand, if we carefully design a parametrization of f to make the computation of likelihood function simple

and efficient, then the bijective function f can be learned accordingly. Specifically, Normalizing Flows can be formed by composing k invertible “simple” transformations $\{f_j\}_{j=1}^k$ allowing a fast computation of the Jacobian and

$$X = f_k \circ f_{k-1} \circ \dots \circ f_1(Z) = f(Z).$$

Using the change-of-variables formula, the log-likelihood at observation X can be computed as:

$$\log\{p_X(X)\} = \log[p_Z\{f^{-1}(X)\}] + \sum_{j=1}^k \log|\det[\nabla f_j^{-1}\{f_j^{-1} \circ \dots \circ f_{k-1}^{-1} \circ f_k^{-1}(X)\}]|. \quad (2)$$

In the next subsection, we provide a detailed overview of Normalizing Flows with a particular focus on the Masked Autoregressive Flow (MAF) architecture, which is a special type of Normalizing Flow and permits fast computation of the log-likelihood function in (2). The MAF forms the backbone of our approach.

2.1.1 Masked Autoregressive Flow (MAF) Methodology

MAF (Papamakarios et al., 2017) is a generative model designed to learn complex data distributions through a sequence of invertible transformations. It trains the Normalizing Flow by leveraging the autoregressive structure to parameterize a flexible transformation of a base probability distribution, typically a standard Gaussian distribution, to match a complex target distribution p_X .

The MAF Model is constructed using multiple autoregressive transformations, implemented via the Masked Autoencoder for Distribution Estimation (MADE). The key components of the MAF model include:

- **Base Distribution:** The latent variable typically follows an isotropic Gaussian, $Z \sim N(0, \mathbf{I}_d)$, and transformations are applied to map it to a more complex target distribution, P_X , where \mathbf{I}_d is a d by d identity matrix. In a typical application, the target distribution P_X is unknown, but one observes n i.i.d. samples X_1, X_2, \dots, X_n from P_X .
- **MADE Layers:** The backbone of MAF is the MADE network, which is a masked feedforward map enforcing autoregressive dependencies. Specifically, suppose that $X = (x_1, \dots, x_d)'$ and $Z = (z_1, \dots, z_d)'$. The MADE network determines a one to one correspondence between X and Z as

$$z_i = \frac{x_i - \mu_i(x_1, \dots, x_{i-1})}{\sigma_i(x_1, \dots, x_{i-1})}, i = 1, 2, \dots, d,$$

where $\mu_i(\cdot)$ and $\sigma_i(\cdot)$ are individual neural networks with (x_1, \dots, x_{i-1}) as input.

- **Permutation Layers:** Since MAF relies on autoregressive factorization, the ordering of variables influences the model’s expressiveness. The Permutation Layer reorders inputs and re-trains a fresh MADE network. This step ensures training multiple invertible transformations to capture dependencies among individual components of X in different orders. The final transport map is the composition of all resulting MADE networks.

The key motivation in designing MAF is that the joint distribution of $X = (x_1, \dots, x_d)'$ is determined by a set of conditional distributions: $x_i | x_1, \dots, x_{i-1}, i = 1, \dots, d$, as

$$p_X(X) = \prod_{i=1}^d p(x_i | x_1, \dots, x_{i-1}).$$

In MAF, these conditional distributions are modeled with Gaussian autoregressive working models:

$$x_i | x_1, \dots, x_{i-1} \sim N\{\mu_i(x_1, \dots, x_{i-1}), \sigma_i^2(x_1, \dots, x_{i-1})\},$$

where $\mu_i(\cdot)$ and $\sigma_i(\cdot)$ are flexible neural networks. This transformation ensures that each output variable can be generated sequentially. Figure 1 illustrates the case with three variables x_1, x_2 , and x_3 , where x_2 depends only on x_1 , and x_3 depends on both x_2 and x_1 . The orange arrows represent the dependency paths relevant to modeling $p(x_2 | x_1)$, and black arrows represent the dependency paths relevant to modeling $p(x_3 | x_2, x_1)$.

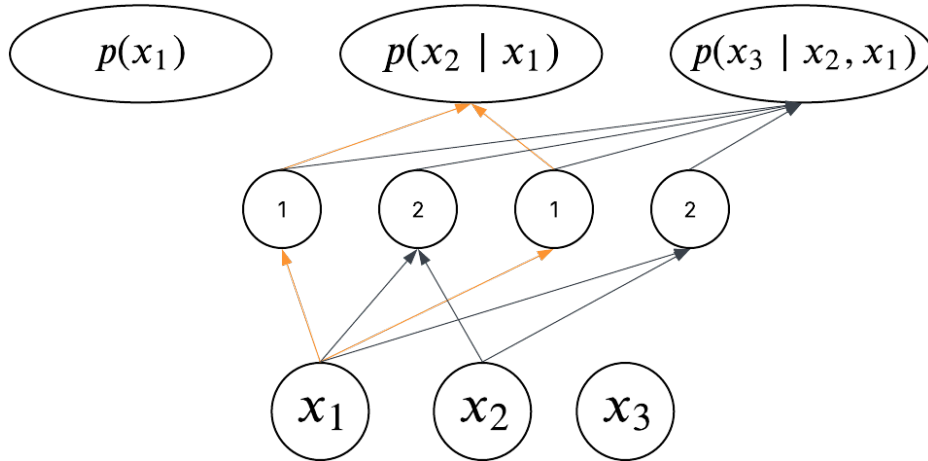


Figure 1: An autoregressive structure of a MADE layer corresponding to the factorization $p(x_1, x_2, x_3) = p(x_1)p(x_2|x_1)p(x_3|x_1, x_2)$.

Note, each unit is assigned a number indicating which inputs it can depend on. This network ensures that the output for each variable x_i depends only on x_1, \dots, x_{i-1} , preserving the autoregressive structure. Moreover, unlike typical autoregressive models that require sequential updates, MAF benefits from MADE's structure to compute the density at any data point in a single forward pass, making it highly suitable for GPU acceleration in training.

To see how MADE integrates into the Masked Autoregressive Flow (MAF), recall that Normalizing Flows transform a simple base distribution into a complex one using invertible mappings. In a simple MAF with a single MADE layer, the forward and inverse mappings are given by:

$$x_i = \mu_i(x_1, \dots, x_{i-1}) + z_i \cdot \sigma_i(x_1, \dots, x_{i-1}), \quad (3)$$

and

$$z_i = \frac{x_i - \mu_i(x_1, \dots, x_{i-1})}{\sigma_i(x_1, \dots, x_{i-1})} \quad (4)$$

for $i = 1, \dots, d$, respectively. Thus, the log-determinant of the Jacobian simplifies to

$$\log |\det \nabla f^{-1}(X)| = - \sum_{i=1}^d \log \{\sigma_i(x_1, \dots, x_{i-1})\}.$$

This formulation allows for efficient likelihood computation. Specifically, the log-likelihood function at X can be evaluated as

$$\log \{p_X(X)\} = \log \{p_Z(Z)\} - \sum_{i=1}^d \log \{\sigma_i(x_1, \dots, x_{i-1})\},$$

where $Z = f^{-1}(X)$ can be calculated via (4). Therefore, we can train $\{\mu_i(\cdot), \sigma_i(\cdot), i = 1, \dots, d\}$ to maximize the empirical log-likelihood:

$$l(f) = \sum_{i=1}^n \log \{p_X(X_i)\},$$

via the stochastic gradient descent algorithm. If there is more than one MADE layer, the log-likelihood function can still be efficiently calculated as

$$\log \{p_X(X)\} = \log \{p_Z(Z)\} + \sum_{i=1}^k \log |\det (\nabla f_i^{-1})|,$$

where $f = f_k \circ f_{k-1} \circ \dots \circ f_1$. In the following, we give an example of MAF with three MADE layers. With a given observation $X = (x_1, x_2, x_3)'$, we proceed with the following steps to calculate $Z = f^{-1}(X)$ and the log-determinant of the Jacobian.

1. First MAF Layer:

(a) We use an autoregressive transformation:

$$(z_{11}, z_{12}, z_{13}) = \left(\frac{x_1 - \mu_{31}}{\sigma_{31}}, \frac{x_2 - \mu_{32}(x_1)}{\sigma_{32}(x_1)}, \frac{x_3 - \mu_{33}(x_1, x_2)}{\sigma_{33}(x_1, x_2)} \right).$$

(b) Output: $Z_1 = f_3^{-1}(x)$, where $Z_1 = (z_{11}, z_{12}, z_{13})'$.

2. Second MAF Layer:

(a) Permutation: the variable order is shuffled. For instance,

$$(1, 2, 3) \rightarrow (3, 1, 2).$$

(b) We use a new auto-regressive transformation on the permuted variables:

$$(z_{23}, z_{21}, z_{22}) = \left(\frac{z_{13} - \mu_{23}}{\sigma_{23}}, \frac{z_{11} - \mu_{21}(z_{13})}{\sigma_{21}(z_{13})}, \frac{z_{12} - \mu_{22}(z_{13}, z_{11})}{\sigma_{22}(z_{13}, z_{11})} \right);$$

(c) Output: $Z_2 = f_2^{-1}(Z_1)$, where $Z_2 = (z_{21}, z_{22}, z_{23})'$.

3. Third MAF Layer:

(a) Permutation: the variable order is shuffled again. For instance,

$$(1, 2, 3) \rightarrow (2, 3, 1).$$

(b) We use a new auto-regressive transformation on the permuted variables:

$$(z_{32}, z_{33}, z_{31}) = \left(\frac{z_{22} - \mu_{12}}{\sigma_{12}}, \frac{z_{23} - \mu_{13}(z_{22})}{\sigma_{13}(z_{22})}, \frac{z_{21} - \mu_{11}(z_{22}, z_{23})}{\sigma_{11}(z_{22}, z_{23})} \right);$$

(c) Output: $Z_3 = f_1^{-1}(Z_2)$, where $Z_3 = (z_{31}, z_{32}, z_{33})'$.

4. The Final Output:

$$Z = f_1^{-1} \circ f_2^{-1} \circ f_3^{-1}(X) = f^{-1}(X) = Z_3,$$

where the transport map, $f = f_3 \circ f_2 \circ f_1$, is characterized by $\mu_{ij}(\cdot)$ and $\sigma_{ij}(\cdot)$ with $i = 1, 2, 3$ being the index for the MAF layer and $j = 1, 2, 3$ being the index for the individual components of X or $Z \in \mathbb{R}^d$, and the log-determinant of the Jacobian is

$$\begin{aligned} \log |\det(\nabla f^{-1}(X))| &= -[\log(\sigma_{31}) + \log\{\sigma_{32}(x_1)\} + \log\{\sigma_{33}(x_1, x_2)\}] \\ &\quad - [\log(\sigma_{23}) + \log\{\sigma_{21}(z_{13})\} + \log\{\sigma_{22}(z_{13}, z_{11})\}] \\ &\quad - [\log(\sigma_{12}) + \log\{\sigma_{13}(z_{22})\} + \log\{\sigma_{11}(z_{22}, z_{23})\}]. \end{aligned}$$

Therefore, the log-likelihood function value at observation X is

$$\begin{aligned} &\log[p_Z\{f^{-1}(X)\}] + \log |\det\{\nabla f^{-1}(X)\}| \\ &= -3 \log(\sqrt{2\pi}) - \frac{z_{31}^2 + z_{32}^2 + z_{33}^2}{2} \\ &\quad - [\log(\sigma_{31}) + \log\{\sigma_{32}(x_1)\} + \log\{\sigma_{33}(x_1, x_2)\}] \\ &\quad - [\log(\sigma_{23}) + \log\{\sigma_{21}(z_{13})\} + \log\{\sigma_{22}(z_{13}, z_{11})\}] \\ &\quad - [\log(\sigma_{12}) + \log\{\sigma_{13}(z_{22})\} + \log\{\sigma_{11}(z_{22}, z_{23})\}], \end{aligned}$$

which is very easy to compute.

So far, we have introduced MAF that applies a finite sequence of invertible maps to a random variable. However, there are other versions of Normalizing Flows as discussed in the Introduction. Specifically, there is a class of Continuous Normalizing Flows that realize the continuous limit as $k \rightarrow \infty$ in (2).

Remark 1. *Instead of a finite sequence of k invertible maps from (2), a Continuous Normalizing Flow (CNF) models an infinitesimal transformation governed by an initial-value problem*

$$\frac{dX_t}{dt} = v_\theta(t, X_t), \quad X_0 = Z, \quad t \in [0, 1], \quad (5)$$

where the velocity field $v_\theta(t, x) : [0, 1] \times \mathbb{R}^d \rightarrow \mathbb{R}^d$ is a neural network with parameters θ that can be estimated from the data (e.g. Chen et al., 2018; Grathwohl et al., 2018). The basic idea is to find an appropriate velocity field such that the terminal-time random variable approximates the target distribution p_X , when the base distribution

$$X_0 = Z \sim N(0, \mathbf{I}_d).$$

The solution of this initial value problem generates a smoothing path between the base and target distribution. Combining the Ordinary Differential Equation with the instantaneous change-of-variables formula gives

$$\partial_t \begin{bmatrix} X_t \\ \log p(X_t) \end{bmatrix} = \begin{bmatrix} v_\theta(t, X_t) \\ -\text{Tr}\{\nabla_x v_\theta(t, X_t)\} \end{bmatrix}, \quad (6)$$

where $\text{Tr}(\cdot)$ denotes the trace and $\nabla_x v_\theta(t, X_t)$ is the Jacobian Matrix of the velocity field with respect to X_t . Integrating (5) and (6) over time yields the exact log-density:

$$\log p_X(X) = \log\{p_Z(Z)\} + \int_0^1 \text{Tr}\{\nabla_x v_\theta(t, X_t)\} dt. \quad (7)$$

Crucially, the sum of log-determinants in (2) collapses to a single time-integral of a Jacobian Trace. There are several benefits of this approach. First, it drops the raw complexity of calculating the determinant from $O(d^3)$ in (2) to $O(d^2)$, or even $O(d)$ when a particular trace estimator (i.e., the Hutchinson Stochastic Trace Estimator) is employed (Grathwohl et al., 2018). Second, it provides architectural freedom in that because (6) involves only the trace of the Jacobian, any neural architecture can parameterize v_θ without sacrificing exact likelihoods, while every discrete layer must admit a tractable determinant. The corresponding analogous likelihood to be trained on is the one that maximizes the observed log-likelihood function

$$\sum_{i=1}^n \left[\log\{p_Z(X_{i0})\} + \int_0^1 \text{Tr}\{\nabla_x v_\theta(t, X_{it})\} dt \right],$$

whose gradients are efficiently obtained via the adjoint sensitivity method (Cao et al., 2002). One advantage of considering CNF is the presence of theoretical guarantees on the convergence rate of the estimated transport map (Gao et al., 2024).

2.2 Meta Analysis

Having already introduced the methodology of Normalizing Flows in Section 2.1, we now turn to meta analysis, which is a statistical methodology used to combine results from multiple independent studies or datasets. In particular, suppose that we have K datasets, denoted by $\mathbf{X}_1, \dots, \mathbf{X}_K$, each providing a point estimator $\hat{\theta}_k$ for an underlying parameter θ_0 of interest. The goal of meta analysis is to synthesize these estimates into a more robust and generalizable consensus estimator $\hat{\theta}_0$.

In many real-world scenarios, especially those involving privacy-sensitive data (e.g., medical records or proprietary datasets), direct access to individual level data \mathbf{X}_k may not be feasible due to regulatory or ethical constraints. Fortunately, meta analysis can often still be conducted in such settings by leveraging summary statistics only. Specifically, if each site or study can share the pair $(\hat{\theta}_k, \sigma_k^2)$ —that is, the point estimate and its associated variance—then classical statistical techniques such as fixed-effects or random-effects models (e.g., the DerSimonian-Laird Method by (DerSimonian and Laird, 1986)) can be employed to compute $\hat{\theta}_0$ in meta analysis.

There are two general classes of methods used for meta analysis: the fixed effects model and the random effects model. A fixed effects model assumes that all $\hat{\theta}_k$ estimates a common parameter θ_0 in the sense that

$$\hat{\theta}_k \sim N(\theta_0, \sigma_k^2), k = 1, \dots, K, \quad (8)$$

and we are interested in estimating θ_0 based on $\{(\hat{\theta}_k, \sigma_k^2), k = 1, \dots, K\}$. The corresponding estimator is the well-known inverse variance estimator

$$\hat{\theta}_F = \frac{\sum_{k=1}^K \sigma_k^{-2} \hat{\theta}_k}{\sum_{k=1}^K \sigma_k^{-2}}. \quad (9)$$

The variance of $\hat{\theta}_F$ is simply

$$\sigma_F^2 = \left(\sum_{k=1}^K \sigma_k^{-2} \right)^{-1}.$$

This estimator would be the optimal estimator with the smallest variance under (8). Oftentimes, the fixed effects model may be too restrictive and a natural extension allowing more between study heterogeneity is the random effects model, which assumes a hierarchical model

$$\hat{\theta}_k \sim N(\theta_k, \sigma_k^2),$$

$$\text{where } \theta_k \sim N(\theta_0, \tau_0^2), k = 1, \dots, K. \quad (10)$$

In other words, each estimator $\hat{\theta}_k$ estimates a study-specific population parameter θ_k , which can be different across studies. To facilitate the evidence synthesis, the random effects model assumes that all θ_k 's are drawn from a common population $N(\theta_0, \tau_0^2)$ and the center of the population, θ_0 , is the parameter of interest, which can be used to summarize information from all studies. τ_0^2 characterizes the between study heterogeneity and is also a parameter of interest. The fixed effects model (8) is a special case of the random effects model (10), as the random effects model degenerates into a fixed effects model when $\tau_0^2 = 0$. To estimate θ_0 in the random effects model (10), one needs to notice that

$$\hat{\theta}_k \sim N(\theta_0, \sigma_k^2 + \tau_0^2), k = 1, \dots, K,$$

and an inverse variance estimator for θ_0 would still be optimal. However, the marginal variance of $\hat{\theta}_k$ is unknown, as it contains τ_0^2 . Therefore, an estimator for θ_0 can be constructed by first estimating τ_0^2 via the following steps:

1. obtain an initial estimator of θ_0 as $\hat{\theta}_F$ given in (9).
2. estimate τ_0^2 as

$$\hat{\tau}^2 = \max \left\{ 0, \frac{\sum_{k=1}^K (\hat{\theta}_k - \hat{\theta}_F)^2 / \sigma_k^2 - (K - 1)}{\sum_{k=1}^K \sigma_k^{-2} - (\sum_{k=1}^K \sigma_k^{-4}) / (\sum_{k=1}^K \sigma_k^{-2})} \right\}.$$

3. update the initial estimator of θ_0 as

$$\hat{\theta}_R = \frac{\sum_{k=1}^K (\sigma_k^2 + \hat{\tau}^2)^{-1} \hat{\theta}_k}{\sum_{k=1}^K (\sigma_k^2 + \hat{\tau}^2)^{-1}}. \quad (11)$$

4. approximate the variance of $\hat{\theta}_R$ by

$$\hat{\sigma}_R^2 = \left\{ \sum_{k=1}^K (\sigma_k^2 + \hat{\tau}^2)^{-1} \right\}^{-1},$$

based on which the Wald-Type confidence interval (CI) for θ_0 can be constructed as

$$[\hat{\theta}_R - 1.96\hat{\sigma}_R, \hat{\theta}_R + 1.96\hat{\sigma}_R].$$

This estimator was originally proposed in DerSimonian and Laird (1986). Since then, various estimators for θ_0 have been proposed under the same random effects model framework, such as MLE, RMLE, Sidik-Jonkman Estimator, and Hunter-Schmidt Estimator, with different finite-sample performance (Harville, 1977; IntHout et al., 2014; Hunter, 2004; Michael et al., 2019). However, the DL Estimator (DerSimonian and Laird, 1986) remains to be one of the most popular choice in practice, and it is optimal when $K \rightarrow \infty$. In summary, meta analysis can be conducted without access to individual level data, once relevant summary statistics from individual studies are available.

However, challenges arise when the analyst has not yet decided on a specific parameter of interest and instead wishes to explore multiple candidate estimands. In such exploratory analyses—common in early-stage research or hypothesis generation—summary statistics are not always available. This brings the need for access to individual level data, which is typically required to flexibly define and estimate new parameters post hoc.

To reconcile this need for analytic flexibility with privacy protection, one potential solution is to share perturbed or synthetic data that mimics the statistical properties of the original datasets while preserving individual privacy. These synthetic datasets enable flexible exploratory analyses without compromising the confidentiality of the original individual records. We propose a novel method to create such perturbed datasets in Section 2.3 using the Normalizing Flows described in Section 2.1.

2.3 Our Contribution

2.3.1 Synthetic Data Generation

In this subsection, we describe how to generate a synthetic dataset preserving the distribution of the observed data, while providing appropriate privacy protection via MAF. Specifically, given one observed dataset

$$\mathbf{X} = \{X_1, X_2, \dots, X_n\},$$

where X_1, X_2, \dots, X_n are i.i.d. copies of $X \sim P_X$, which is an unknown distribution, the perturbation procedure is as follows. Let $f = f_k \circ f_{k-1} \circ \dots \circ f_1$ be a composition of K bijective and invertible functions $\{f_1, f_2, \dots, f_k\}$ in a MAF, such that $X = f(Z)$, where Z follows a standard Gaussian distribution, $N(0, \mathbf{I}_d)$, and $X \sim P_X$. Then, perturbing an observed observation X without changing its marginal distribution can be achieved via

$$f[\mathcal{M}\{f^{-1}(X)\}],$$

where $f^{-1}(\cdot)$ is the inverse function of $f(\cdot)$ and $\mathcal{M}(Z)$ is an appropriate random perturbation of a random variable $Z \sim N(0, \mathbf{I}_d)$.

In practice, $f(\cdot)$ is unknown and needs to be estimated. This can be done with any type of Normalizing Flow. For this paper, we propose to use the MAF for efficient, higher quality training. There are several advantages of using MAF for synthetic data generation. First, the observations in generated synthetic data are expected to follow a distribution similar to P_X . Second, unlike other synthetic data generation methods, observations in the perturbed dataset $\tilde{\mathbf{X}}$ have a one to one correspondence with data points in the original data, i.e.,

$$X_i \leftrightarrow \tilde{X}_i,$$

where \tilde{X}_i is the generated synthetic observation by perturbing X_i , with a tuning parameter controlling the “distance” between X_i and \tilde{X}_i . Lastly, by transforming the original data into a latent space, where transformed observations approximately follow a standard Gaussian distribution, injecting independent Gaussian noise becomes a very natural way to introduce random perturbation. This perturbation approach accounts for the varying marginal distributions of different components of X and their potential complex correlations. Therefore, we propose Algorithm 1 (Latent Noise Injection) for synthetic data generation.

Algorithm 1 Synthetic Data Generation (Latent Noise Injection)

train our flow on observed data \mathbf{X} , for which we denote trained functions as $\{\hat{f}_i\}_{i=1}^K$.
for $i \in \{1, \dots, n\}$ **do** perturb sample $X_i \in \mathbf{X}$ as

$$X_i \xrightarrow{\hat{f}^{-1}} f^{-1}(X_i) \rightarrow \sqrt{w}\hat{f}^{-1}(X_i) + \sqrt{1-w}Z_i \xrightarrow{\hat{f}} \tilde{X}_i, \quad (12)$$

where $\hat{f} = \hat{f}_k \circ \hat{f}_{k-1} \dots \hat{f}_1$, $\hat{f}^{-1}(\cdot)$ is the inverse function of $\hat{f}(\cdot)$ and $w \in (0, 1)$ is a tuning parameter controlling the privacy protection, and $Z_i \sim N(0, \mathbf{I}_d)$ is a Gaussian random variable independent of observed data \mathbf{X} .
end for

return the perturbed synthetic dataset

$$\tilde{\mathbf{X}} = \{\tilde{X}_1, \dots, \tilde{X}_n\}.$$

The proposed Latent Noise Injection method bridges different privacy-utility regimes via the perturbation parameter $w \in [0, 1]$. When $w = 1$, the generative distribution matches the empirical distribution of observed data. As $w \rightarrow 0$, however, the algorithm behaves like independent sampling from a distribution estimated by Normalizing Flows to approximate P_X , as there is no direct one to one correspondence between original data and perturbed data. This resembles the classical generative sampling approach, where differences between analysis results based on synthetic and original data may remain substantial, as nonparametrically matching a target distribution can be challenging.

2.3.2 Theoretical Properties of Perturbed Estimator $\tilde{\theta}_w$ based on Synthetic Data

Now, we analyze the asymptotic properties of estimators derived from generated synthetic data. To this end, we first investigate the convergence behavior of a general estimator $\tilde{\theta}_w = \theta(\hat{P}_w)$ obtained from our perturbed synthetic data, compared to its counterpart $\hat{\theta}$ from observed data. Let

$$\mathbf{X} = \{X_1, X_2, \dots, X_n\} \quad \text{and} \quad \tilde{\mathbf{X}} = \{\tilde{X}_{1w}, \tilde{X}_{2w}, \dots, \tilde{X}_{nw}\},$$

be observed and perturbed data, respectively, where $X_i, i = 1, \dots, n$ are n i.i.d. copies of a d -dimensional random vector $X \sim P_X$, \tilde{X}_{iw} is perturbed X_i with a transport map \hat{f} and $w \in [0, 1]$. Let the empirical distribution of \mathbf{X} and $\tilde{\mathbf{X}}$ be denoted by \hat{P} and \hat{P}_w respectively. Here, we assume that the transport map \hat{f} is trained based on an independent dataset consisting of $O(n)$ i.i.d. observations following the distribution P_X such that $\hat{f}^{-1}(X)$ approximately follows a standard Gaussian distribution $N(0, \mathbf{I}_d)$. In practice, $\hat{f}(\cdot)$ is oftentimes trained on \mathbf{X} as well and induces a correlation between $\hat{f}(\cdot)$ and summary statistics of \mathbf{X} , which we ignore in our subsequent discussion.

In classical settings, an empirical parameter estimator converges to a population parameter θ with the root n convergence rate, i.e.,

$$\hat{\theta} - \theta = \theta(\hat{P}) - \theta(P_X) = O_p\left(\frac{1}{\sqrt{n}}\right).$$

One may hope that the estimator based on synthetic data, $\tilde{\theta}_w = \theta(\hat{P}_w)$, is close to $\hat{\theta}$, so that

$$\tilde{\theta}_w - \theta \approx \hat{\theta} - \theta,$$

i.e., as an estimator of θ , $\tilde{\theta}_w$ is almost as good as $\hat{\theta}$. Unfortunately, this is not true in general, as \hat{P}_w may not be sufficiently close to either P_X or its empirical counterpart \hat{P} . Although we do not provide a formal theorem, existing theoretical results suggest that convergence rates for estimators under generative sampling without a linkage to original observations are typically slower than the classical $O_p(n^{-1/2})$ rate when the data dimension $d > 2$ (Tian and Shen, 2024; Fournier and Guillin, 2015). In particular, under suitable regularity conditions, Tian and Shen (2024) show that the 1-Wasserstein Distance between P_X and the distribution induced by the trained Normalizing Flow $P_{\hat{f}} = \hat{f}\{N(0, \mathbf{I}_d)\}$ is:

$$E\left\{\mathcal{W}_1(P_X, P_{\hat{f}})\right\} = O\left(n^{-\frac{r}{2r+d}} \log^{5/2} n\right), \quad (13)$$

where the density function of P_X has a continuous r th derivative. Noting that $r/(2r+d) < 1/2$ regardless of “smoothness” of P_X , this convergence rate in Wasserstein Distance is slower than the regular root n rate with an approximation error that may be propagated into the estimation of θ , causing $\theta(P_X) - \theta(P_{\hat{f}})$ to converge at a rate slower than root n as well.

Remark 2. Note, an intrinsic estimation error term ϵ^z arises as an additional term in (13), but was omitted. It captures the excess risk in estimating the synthetic data distribution when the latent input $Z \sim N(0, \mathbf{I}_d)$ is passed through the learned transport map \hat{f} . We assume that ϵ^z is negligible compared to the overall generation error of the flow-based model because Lemma 39 of Tian and Shen (2024) suggests that $\epsilon^z = O_p(n^{-r_z/(2r_z+d)} \log^{5/2} n)$, where the base density function of Z has continuous r_z th derivative. Since our base distribution is $N(0, \mathbf{I}_d)$, which is infinitely smooth, ϵ^z is negligible.

Noting that $\theta(\hat{P}_0)$ with $w = 0$ is a finite sample approximation to $\theta(P_{\hat{f}})$ with a precision of $O(n^{-1/2})$,

$$\tilde{\theta}_w - \theta = \left\{ \theta(\hat{P}_w) - \theta(P_{\hat{f}}) \right\} + \left\{ \theta(P_{\hat{f}}) - \theta(P_X) \right\}$$

also cannot converge at the regular root n rate for $w = 0$. Indeed, our simulation results suggest that for many w away from 1,

$$\tilde{\theta}_w - \theta \neq O_p\left(\frac{1}{\sqrt{n}}\right),$$

and instead, the convergence is slower. Therefore, in general, one may not be able to replace $\hat{\theta}$ from the original observed data by $\tilde{\theta}_w$ from the synthetic data without losing efficiency. We also note that when $w \rightarrow 1$, $\tilde{\theta}_w$ also approaches θ . However, if w is too close to 1, then the privacy protection would be lost as the injected noise level would be too small. We hope that when w is sufficiently but not too close to 1, a good transport map trained via Normalizing Flows can still guarantee that the difference between $\tilde{\theta}_w$ and $\hat{\theta}$ is small, such that we may replace the original data with the synthetic data without losing asymptotic efficiency for the purpose of estimating θ . The following Theorem 1 ensures that this is possible.

Theorem 1. Let $\hat{\theta} = \theta(\hat{P})$ be the estimator computed from the empirical distribution \hat{P} for a study, where \hat{P} is the probability measure induced by n i.i.d. observations in observed data $\mathbf{X} = \{X_1, \dots, X_n\}$. Similarly, $\tilde{\theta}_w = \theta(\hat{P}_w)$ is the estimator computed from the synthetic distribution \hat{P}_w generated by our mechanism with perturbation weight w . Here, $\theta(\cdot)$ is a functional with the first order expansion

$$\theta(\hat{P}) = \theta(\mathcal{P}) + \frac{1}{n} \sum_{i=1}^n l(\mathcal{X}_i) + o_p(n^{-1}),$$

where \hat{P} is the probability measure induced by the empirical distribution of n i.i.d. observations $\mathcal{X}_1, \dots, \mathcal{X}_n \sim \mathcal{P}$. We assume the following:

1. P_X has a continuously differentiable density function over a compact support on \mathbb{R}^d .
2. invertible transport map trained from the MAF, $\hat{f}(\cdot)$, converges to a deterministic invertible transport map $f(\cdot)$ in probability, where $Z = f^{-1}(X) \sim N(0, \mathbf{I}_d)$. Specifically, $\|\hat{f} - f\|_2 = O_p(\delta_{1n})$ for $\delta_{1n} = o(1)$.
3. $\hat{f}(\cdot)$ and $f(\cdot)$ are uniformly bi-Lipchitz Continuous on the support of X .
4. Both f and \hat{f} are members of a class of functions $\mathcal{F} = \{f_\theta\}$, and the class of functions

$$\mathcal{L} = \left\{ l \left[\tilde{f} \left(\sqrt{w} \tilde{f}^{-1}(x) + \sqrt{1-w} z \right) \right] \mid w \in [0, 1], \|\tilde{f} - f\|_2 \leq \epsilon_n, \tilde{f}(\cdot) \in \mathcal{F} : \mathbb{R}^d \rightarrow \mathbb{R}^d \right\}$$

is a Donsker Class.

5. $l(\cdot)$ is continuously differentiable on \mathbb{R}^d .
6. $1 - w = o(\delta_{2n})$ for $\delta_{2n} = o(1)$.

Then, we have

$$\theta(\hat{P}_w) - \theta(\hat{P}) = O_p\left(\delta_{1n}^2 + \delta_{1n} \sqrt{\delta_{2n}}\right) + o_p(n^{-1/2}).$$

Theorem 1 provides a rate for the distance between perturbed estimator $\tilde{\theta}_w$ and the non-private estimator $\hat{\theta}$ as $n \rightarrow \infty$ and $w \rightarrow 1$. More importantly, this convergence rate can be faster than the regular rate $O_p(n^{-1/2})$ under appropriate conditions. In such a case, both $\tilde{\theta}_w$ and $\hat{\theta}$ estimate θ with the same asymptotic precision. Specifically, if we let $w = 1 - O(n^{-2/d})$ and $\|\hat{f} - f\|_2 = O_p(n^{-1/2+\delta_0})$, where $\delta_0 < \min(1/4, 1/d)$, then

$$\sqrt{n}(\tilde{\theta}_w - \hat{\theta}) = o_p(1) \implies \sqrt{n}(\tilde{\theta}_w - \theta) \sim N\{0, \sigma^2(P_X)\}$$

in distribution, as $n \rightarrow \infty$. On the other hand, this convergence rate can be substantially slower than the regular rate, if either $|w - 1|$ or $\|\hat{f} - f\|_2$ goes to zero too slowly. In Section 3.1.2, we have performed a numerical study to empirically confirm our observations on this convergence rate.

Note that although in theory w is a user-specified tuning parameter that can be arbitrarily close to 1, in practice, we don't want to use a w too close to 1. Otherwise, the privacy protection will be lost due to the simple fact that the synthetic dataset $\tilde{\mathbf{X}}$ becomes the observed dataset \mathbf{X} as $w \rightarrow 1$. In Section 2.3.3, we argue that $w = 1 - O(n^{-2/d})$ is both small enough to provide sufficient privacy protection and big enough to ensure the asymptotic equivalence between $\tilde{\theta}_w$ and $\hat{\theta}$.

Now, we discuss the possibility of constructing a transport map \hat{f} such that $\|\hat{f} - f\|_2 = O_p(n^{-1/2+\delta_0})$ for a sufficiently small constant $\delta_0 > 0$. Theorem 5.12 of Gao et al. (2024) proves that under regularity conditions for Continuous Normalizing Flows with time component $t \in [0, 1]$ as in (5), the estimated velocity field $v_{\hat{\theta}}(t, X_t)$ converges to the true velocity field $v_{\theta}(t, x) \in W^{1,\infty}$ in (6), where $W^{1,\infty}$ is the Sobolev Space of Lipschitz Functions whose first weak derivatives are bounded in L^∞ , satisfying

$$\|v_{\hat{\theta}}(t, x) - v_{\theta}(t, x)\|_2 = O(n^{-1/(d+3)}). \quad (14)$$

The estimated transport map is determined by the velocity field and can be approximated as

$$\begin{aligned} \hat{f}(z) &= \hat{x}_{J_n-1} + \delta_n v_{\hat{\theta}}(t_{J_n-1}, \hat{x}_{J_n-1}) \\ \hat{x}_{J_n-1} &= \hat{x}_{J_n-2} + \delta_n v_{\hat{\theta}}(t_{J_n-2}, \hat{x}_{J_n-2}) \\ &\dots \\ \hat{x}_2 &= x_1 + \delta_n v_{\hat{\theta}}(t_1, \hat{x}_1) \\ \hat{x}_1 &= z + \delta_n v_{\hat{\theta}}(t_0, z) \\ \hat{x}_0 &= z, \end{aligned}$$

where $0 = t_0, t_1, \dots, t_{J_n-1}, t_{J_n} = 1$ are $J_n + 1$ equal-spaced points in the unit interval $[0, 1]$ and $\delta_n = J_n^{-1}$ is the step size dependent on sample size n . The limit transport map f can be defined similarly based on v_{θ} with $J_n \rightarrow \infty$. If $v_{\hat{\theta}}(t, x)$ and $v_{\theta}(t, x)$ are Lipschitz Continuous with a uniform bound, (29) also suggests that

$$\|\hat{f} - f\|_2 = O(n^{-1/(d+3)}).$$

We provide a more generic result by adopting Theorem 5.12's proof in Gao et al. (2024) to generalize the result of (29) for $v_{\theta} \in W^{s,\infty}$ with arbitrary smoothness s . Specifically, by assuming more smoothness on v_{θ} , we can establish a new convergence rate

$$\|\hat{f} - f\|_2 = o(n^{-s/(2s+d+1)+\delta_0}),$$

for any $\delta_0 > 0$. See Appendix 7.1 for the proof sketch. This provides a theoretical justification for achieving a sufficiently fast convergence rate of the estimated transport map $\hat{f}(\cdot)$ to a underlying true optimal transporter f , if f is sufficiently smooth. Note that this convergence rate of the transport map estimation is consistent with the convergence rate in Wasserstein Distance between the induced distribution given in (13).

The proof of Theorem 1 is provided in Appendix 7. The rational for the convergence can be explained by a simple example, where $\theta(P_X) = E(X)$. In such a case,

$$\begin{aligned} \sqrt{n}\{\theta(\hat{P}) - \theta(P_X)\} &= \frac{1}{\sqrt{n}} \sum_{i=1}^n X_i, \\ \sqrt{n}\{\theta(\hat{P}_w) - \theta(P_w)\} &= \frac{1}{\sqrt{n}} \sum_{i=1}^n \hat{f}(\sqrt{w}\hat{f}^{-1}(X_i) + \sqrt{1-w}Z_i). \end{aligned}$$

It follows from the stochastic equi-continuity guaranteed by the assumption on Donsker Class that

$$\sqrt{n} \{ \theta(\hat{P}) - \theta(\hat{P}_w) \} = \sqrt{n} \{ \theta(P_X) - \theta(P_w) \} + o_p(1),$$

for $1 - w = o(1)$. Note that if $w = 1$, then

$$\theta(P_w) = E \{ \hat{f}(\hat{f}^{-1}(X)) \} = E(X) = \theta(P_X).$$

Also, if $\hat{f} = f$,

$$\theta(P_w) = E \{ f(\sqrt{w}f^{-1}(X) + \sqrt{1-w}Z) \} = E \{ f(Z) \} = E(X) = \theta(P_X).$$

Thus, one may expect that $|\theta(P_X) - \theta(P_w)|$ is small, when either $|w - 1|$ or $\|\hat{f} - f\|_2$ is close to zero. Indeed, we may bound this difference by

$$C (\|\hat{f} - f\|_2^2 + \sqrt{1-w}\|\hat{f} - f\|_2),$$

where C is a constant multiplier. The main conclusion of Theorem 1 follows.

We now turn to a formal privacy analysis of the perturbation mechanism applied within a single dataset. This begins with a proof of its compliance with Local Differential Privacy guarantees.

2.3.3 Privacy Protection of Our Perturbation for a Single Dataset

Local Differential Privacy (Local DP) has become a foundational framework for formalizing privacy guarantees in data analysis. At its core, Local DP ensures that the presence or absence of a single individual in the dataset has a limited effect on the output of a randomized mechanism. While the standard Local (ϵ, δ) -DP Formulation is widely used (Dwork et al., 2014), it can be challenging to analyze under composition or continuous settings. To address these limitations, Local Rényi Differential Privacy (Local RDP) was introduced as a generalization of Local DP using Rényi Divergence, offering a more structured and flexible privacy accounting mechanism (Mironov, 2017). In the following, we present formal definitions of both Local (ϵ, δ) -DP and RDP, followed by a key result (Theorem 2) showing how privacy guarantees are preserved under the perturbation mechanism (12). First, we introduce the concept of Local DP.

Definition 1. *Local Differential Privacy (Local DP).* A randomized mechanism \mathcal{M} satisfies (ϵ, δ) -Local DP if for each individual z and any possible values z' and for any output y in the output space of \mathcal{M} :

$$\mathbb{P}[\mathcal{M}(z) = y] \leq e^\epsilon \mathbb{P}[\mathcal{M}(z') = y] + \delta,$$

where the probability is taken over the randomness of the mechanism \mathcal{M} and ϵ and δ are two positive constants that can be arbitrarily close to zero.

Definition 2. *Rényi Divergence.* The Rényi Divergence of Order $\alpha > 1$ between two probability distributions P and Q over a domain \mathcal{X} is defined as:

$$D_\alpha(P\|Q) = \frac{1}{\alpha - 1} \log E_{x \sim Q} \left[\left(\frac{P(x)}{Q(x)} \right)^\alpha \right]. \quad (15)$$

For $\alpha \rightarrow 1$, the Rényi Divergence is equivalent to the Kullback-Leibler (KL) Divergence:

$$D_{\alpha \rightarrow 1}(P\|Q) = E_{x \sim P} \left[\log \frac{P(x)}{Q(x)} \right]. \quad (16)$$

This can be seen by L'Hopital.

Definition 3. *Local Rényi Differential Privacy.* A randomized mechanism $\mathcal{M} : \mathcal{X} \rightarrow \mathbb{R}^d$ satisfies (α, ϵ) -Local Rényi Differential Privacy (Local RDP) if for all inputs $y, z \in \mathcal{X}$ satisfying $\|y - z\|_2 \leq b$ for some constant b ,

$$D_\alpha(\mathcal{M}(y)\|\mathcal{M}(z)) \leq \epsilon, \quad (17)$$

where $D_\alpha(\cdot\|\cdot)$ denotes the Rényi Divergence of Order $\alpha > 1$.

Remark 3. *Local Rényi Differential Privacy (Local RDP) provides a structured and flexible framework for analyzing privacy guarantees at the level of individual data entries, in comparison to standard (ϵ, δ) -Local Differential Privacy (Local DP) because of the following advantages:*

- **Tighter Composition Bounds:** *Local RDP provides a control over cumulative privacy loss when composing multiple locally private mechanisms. Unlike (ϵ, δ) -Local DP, where composition of multiple random mechanisms requires complex summation or amplification arguments, Local RDP obeys a simple additive property:*

$$\mathcal{M}_j(\cdot) \text{ is } (\alpha, \epsilon_j)\text{-Local RDP, } j = 1, 2 \Rightarrow \mathcal{M}_1\{\mathcal{M}_2(\cdot)\} \text{ is } (\alpha, \epsilon_1 + \epsilon_2)\text{-Local RDP.}$$

- **Conversion to (ϵ, δ) -Local DP:** *Proposition 3 of (Mironov, 2017) shows that any (α, ϵ) Local RDP guarantee can be converted into an (ϵ', δ) -Local DP guarantee, where*

$$\epsilon' = \epsilon + \frac{\log(1/\delta)}{\alpha - 1}. \quad (18)$$

This allows for finer-grained tracking of privacy loss while still being able to express results in the standard (ϵ, δ) -LDP form.

- **Stronger Privacy Guarantees:** *Local RDP offers stronger tail bounds on privacy loss compared to (ϵ, δ) -Local DP. While (ϵ, δ) -Local DP allows for a small probability δ of an unbounded privacy breach, Local RDP ensures that extreme deviations are tightly controlled, thereby preventing catastrophic privacy failure, however small the probability is.*
- **Compatibility with Continuous Domains:** *Local RDP is naturally defined over probability distributions rather than discrete databases. This makes it particularly well-suited for continuous data settings, where inputs may differ smoothly or infinitesimally, which is common in high-dimensional generative modeling.*
- **Intuitive Interpretation:** *The core intuition behind Local RDP is that it measures how distinguishable the outputs of a mechanism are on neighboring individual inputs, using the Rényi Divergence rather than the standard likelihood ratio. This provides a more nuanced and robust quantification of privacy leakage.*

Now, with Definitions 1, 2, and 3, we move on to Lemma 1 and Theorem 2 below, which ultimately provide a nice result of how $\hat{f} \{ \sqrt{w} \hat{f}^{-1}(x) + \sqrt{1-w}Z \}$ satisfies (ϵ^*, δ) -Differential Privacy with high probability as sample size $n \rightarrow \infty$, where $Z \sim N(0, \mathbf{I}_d)$ and \hat{f} is the estimated invertible transport map from MAF.

Lemma 1. *Set $\mathcal{M}(\cdot)$ to be the perturbation generated by applying Gaussian noise*

$$\mathcal{M}(g(x)) = g(x) + N(0, \sigma^2 \mathbf{I}_d), \quad (19)$$

where $g(x) \in \mathbb{R}^d$ is a function such that its sensitivity

$$\Delta_2(g) = \sup_{\|x-y\|_2 \leq 1} \|g(x) - g(y)\|_2 \quad (20)$$

is bounded, i.e., $\Delta_2(g) \leq B$, for a constant $B > 0$. Then, the mechanism $\mathcal{M}(\cdot)$ satisfies (α, ϵ_R) Local RDP of order α with

$$\epsilon_R = \frac{\alpha \times \Delta_2(g)^2}{2\sigma^2}.$$

Note that the noise injection on the latent space in our method for the true transport map f is

$$X \rightarrow \mathcal{M} \{ f^{-1}(X) \} = \sqrt{w} f^{-1}(X) + N(0, (1-w)\mathbf{I}_d).$$

It can be viewed as a special case of the Gaussian Mechanism (31) in Lemma 1 for both f and when replacing f with estimated \hat{f} . Coupled with the boundedness of $\Delta_2(f^{-1})$, Lemma 1 provides a theoretical backbone for Theorem 2 below.

Theorem 2. *First, consider a trained MAF transport map, $\hat{f} = \hat{f}_k \circ \dots \circ \hat{f}_1$, where each $\hat{f}_j, j \in \{1, \dots, k\}$ has mapping defined in (3). We assume the following:*

1. *each function $\mu_i(\cdot)$ and $\sigma_i(\cdot)$ in (3) are trained neural networks whose layers are spectrally normalized with the same number of layers L for each $\hat{f}_j, j \in \{1, \dots, k\}$. That is, each weight matrix has spectral norm at most 1.*
2. *the data domain $\mathcal{X} \subset \mathbb{R}^d$ is compact.*
3. *\hat{f} converges to a deterministic transport map f uniformly in probability as the sample size increases and the sensitivity of f^{-1} is bounded, i.e., $\Delta_2(f^{-1}) < C$ for a constant C .*

Now, let

$$\tilde{\mathcal{M}}(x) = \sqrt{w}\hat{f}^{-1}(x) + \sqrt{1-w}Z, \quad (21)$$

where $w \in (0, 1)$ is a parameter controlling the perturbation size and $Z \sim N(0, \mathbf{I}_d)$. Then, the mechanism $\hat{f}\{\tilde{\mathcal{M}}(\cdot)\}$ satisfies (ϵ^*, δ) -Local DP for any $0 < \delta < 1$ and a prescribed $\epsilon^* > 0$ and some constant $C' > 0$, with

$$\epsilon^* = \frac{wC^2}{2(1-w)} + \frac{C\sqrt{2w\log(1/\delta)}}{\sqrt{1-w}}$$

in probability, i.e.,

$$\mathbb{P}\left(\mathbb{P}[\hat{f}\{\tilde{\mathcal{M}}(x)\} = y] \leq e^{\epsilon^*} \mathbb{P}[\hat{f}\{\tilde{\mathcal{M}}(x')\} = y] + \delta\right) \rightarrow 1$$

as $n \rightarrow \infty$ for any x, x' and y .

The proof of Lemma 1 and Theorem 2 are provided in Appendix 7.2. Note that Lemmas 2 and 3 imply that f^{-1} is Lipschitz and $\Delta_2(f^{-1})$ is bounded, which justifies bounding $\Delta_2(f^{-1})$ by a positive constant C . The interpretation is that as $w \rightarrow 0$, the mechanism becomes more private, i.e., $\epsilon \rightarrow 0$, and as $w \rightarrow 1$, the mechanism becomes more accurate at the cost of weaker privacy.

Theorem 2 suggests that when the perturbation parameter w is sufficiently close to zero, privacy can be well protected. However, to preserve the utility of the synthetic data, namely its ability to reproduce statistical analysis results from the original data, we prefer to use a value of w that is not too small. This raises the question: what is the largest value of w that still provides a meaningful level of privacy protection? To explore this, let $X \in \mathbf{X} = \{X_1, \dots, X_n\}$, and let \tilde{X} be its perturbed version using a given w . To ensure adequate privacy protection, the distance between X and \tilde{X} should exceed the minimum distance between X and any other data point in the database \mathbf{X} :

$$d_{\min}(X) = \min_{X_i \in \mathbf{X} - \{X\}} \|X_i - X\|_2.$$

Otherwise, \tilde{X} would be closet to its original counterpart X , making it identifiable and compromising privacy. Under mild regularity conditions, i.e., assuming X_1, \dots, X_n are i.i.d. observations from a smooth distribution on a compact set, it is well known that $d_{\min}(X)$ is in the order of $O(n^{-1/d})$, where d is the data dimension. On the other hand, the distance between X and \tilde{X} is approximately proportional to $\sqrt{1-w}$ for w close 1. Equating this with $d_{\min}(X)$, we find that to match the perturbation magnitude with the minimal pairwise distance, w should be in the order of

$$1 - O(n^{-2/d}).$$

This suggests that choosing w on the order of $1 - O(n^{-2/d})$ may provide a basic level of privacy protection, ensuring that synthetic points are not trivially matched to their original counterparts.

Despite this theoretical rate, the perturbation parameter w must still be selected empirically in practice. Following the same rational, w can be chosen such that

$$\mathbb{P}\left(\|X_j - X_i\|_2 < \|\tilde{X}_i - X_i\|_2\right) \approx \frac{1}{n(n-1)} \sum_{1 \leq i < j \leq n} I(\|X_j - X_i\|_2 < \|\tilde{X}_i - X_i\|_2) \quad (22)$$

exceeds a pre-specified threshold. This criterion ensures that, for a randomly selected observation X_i from the original dataset \mathbf{X} , there is a reasonable chance that another real observation X_j is closer to X_i than

its synthetic counterpart \tilde{X}_i . Selecting w in this way helps reduce the risk that synthetic samples closely replicate their original inputs, thereby mitigating potential memorization and enhancing privacy protection.

w selected based on this criterion ensures that there is a reasonable probability that for a random selected observation in \mathbf{X} , there is another real observation closer to it than its perturbed value in the synthetic dataset, reducing the risk that synthetic samples memorize their original inputs.

Alternatively, we can split observed data into two sets: a training set D_1 and a test set D_0 . We then train a MAF model using D_1 and then generate a synthetic dataset \tilde{D}_1 by perturbing observations in D_1 using the trained MAF model and a given perturbation size w . For each $X \in D_1 \cup D_0$, we compute a membership score

$$d_{\tilde{D}_1}(X) = \min_{\tilde{X} \in \tilde{D}_1} \|X - \tilde{X}\|_2,$$

where a smaller value suggests that X may have been memorized by the generative model as an observation from the original training set D_1 . We assign binary membership labels: $Y = 1$ if $X \in D_1$ (training set) and $Y = 0$ if $X \in D_0$ (test set), and then compute the AUC under the ROC curve (Hayes et al., 2017; Chen et al., 2020) using pairs $\{d_{\tilde{D}_1}(X), Y\}$, $X \in D_1 \cup D_0$. An AUC value close to 0.5 indicates that the synthetic data does not reveal whether a given data point was part of the training set, thus suggesting low risk of privacy leakage. In practice, we may choose the largest perturbation parameter w such that the resulting AUC remains below a pre-specified threshold (e.g., 0.55). This criterion is closely related to Membership Inference Attacks (MIAs), which assesses whether a particular observation was used to train the generative model. More discussion on MIA can be found in Section 3.1.1

2.3.4 Meta Analysis based on Synthetic Data

Suppose that there are K datasets $\mathbf{X}_1, \dots, \mathbf{X}_K$ with their observations being drawn from distributions P_1, \dots, P_K , respectively. We generate perturbed versions of the original data in each of the K studies using Algorithm 1. This produces K synthetic sets $\tilde{\mathbf{X}}_1, \dots, \tilde{\mathbf{X}}_K$, which can be used to enable exploratory and inferential analyses without compromising the confidentiality of the original individual level records. Specifically, let

$$\mathbf{X}_k = \{X_{k1}, \dots, X_{kn_k}\} \quad \text{and} \quad \tilde{\mathbf{X}}_k = \{\tilde{X}_{k1w}, \dots, \tilde{X}_{kn_kw}\},$$

where X_{ki} , $i = 1, \dots, n_k$ are n_k i.i.d. copies of a d -dimensional random vector $X_k \sim P_k$, \tilde{X}_{kiw} is perturbed X_{ki} with an estimated transport map \hat{f} and a tuning parameter $w \in [0, 1]$. Also, let the empirical distribution of \mathbf{X}_k and $\tilde{\mathbf{X}}_k$ be denoted by \hat{P}_k and $\hat{P}_{w,k}$ respectively. The justification of privacy protection is already established in Section 2.3.3 under appropriate regularity conditions. We are focusing on validity of meta analysis based on synthetic data in this section. After generating these synthetic datasets, we may estimate the parameter of interest based on them, i.e., obtaining

$$\{\theta(\hat{P}_{w,k}), \sigma^2(\hat{P}_{w,k}) \mid k = 1, \dots, K\}$$

and proceed with a meta analytic model to combine the results. Here, we used the notations $\theta(\hat{P}_{w,k})$ and $\sigma^2(\hat{P}_{w,k})$ to emphasize their dependence on synthetic data $\tilde{\mathbf{X}}_k$, where $\hat{P}_{w,k}$ is the probability measure induced by the empirical distribution of n_k observations in $\tilde{\mathbf{X}}_k$. When there is no ambiguity, we also use $\tilde{\theta}_{w,k}$ and $\tilde{\sigma}_{w,k}^2$ to replace $\theta(\hat{P}_{w,k})$ and $\sigma^2(\hat{P}_{w,k})$, respectively.

In the random effects model for meta analysis,

$$\theta(\hat{P}_{w,k}) \sim N(\theta_0, \sigma^2(\hat{P}_{w,k}) + \tau_0^2), \quad k = 1, \dots, K.$$

Moreover, θ_0 can be estimated as in Section 2.2, i.e., by

$$\tilde{\theta}_R = \frac{\sum_{k=1}^K (\sigma^2(\hat{P}_{w,k}) + \tilde{\tau}^2)^{-1} \theta(\hat{P}_{w,k})}{\sum_{k=1}^K (\sigma^2(\hat{P}_{w,k}) + \tilde{\tau}^2)^{-1}}, \quad (23)$$

where

$$\tilde{\tau}^2 = \max \left\{ 0, \frac{\sum_{k=1}^K (\theta(\hat{P}_{w,k}) - \tilde{\theta}_R)^2 / \sigma^2(\hat{P}_{w,k}) - (K-1)}{\sum_{k=1}^K 1 / \sigma^2(\hat{P}_{w,k}) - (\sum_{k=1}^K 1 / \sigma^4(\hat{P}_{w,k})) / (\sum_{k=1}^K 1 / \sigma^2(\hat{P}_{w,k}))} \right\}$$

and

$$\tilde{\theta}_F = \frac{\sum_{k=1}^K \theta(\hat{P}_{w,k}) / \sigma^2(\hat{P}_{w,k})}{\sum_{k=1}^K 1 / \sigma^2(\hat{P}_{w,k})}.$$

As $K \rightarrow \infty$, we have

$$\sqrt{K}(\tilde{\theta}_R - \theta_0) \rightarrow N(0, \sigma_R^2)$$

in distribution, where

$$\sigma_R^2 = \left(\sum_{k=1}^K (\sigma_k^2(P_k) + \tau_0^2)^{-1} \right)^{-1},$$

which can be estimated as

$$\tilde{\sigma}_R^2 = \left(\sum_{k=1}^K (\sigma_k^2(\hat{P}_{w,k}) + \tilde{\tau}_0^2)^{-1} \right)^{-1}.$$

Consequently, the 95% CI for θ_0 can be constructed as

$$(\tilde{\theta}_R - z_{\alpha/2} \times \tilde{\sigma}_R, \tilde{\theta}_R + z_{\alpha/2} \times \tilde{\sigma}_R)$$

where $z_{\alpha/2}$ is the critical value from the standard Gaussian distribution. On the other hand, a parallel meta analysis based on observed data $\mathbf{X}_1, \dots, \mathbf{X}_K$ can also be conducted to obtain

$$(\hat{\theta}_R, \hat{\sigma}_R^2).$$

A natural question is if there is any efficiency loss due to the fact that the synthetic rather than observed data is used to obtain an estimator for θ_k in individual studies and θ_0 in the subsequent meta analysis.

Now, we analyze the asymptotic properties of the meta analysis estimator $\tilde{\theta}_R$ derived from generated synthetic data based on the results in Section 2.3.2. The basic idea is that while each study may incur perturbation bias, aggregation across K studies mitigates this effect. Indeed, under appropriate regularity conditions, the perturbed estimator remains asymptotically equivalent to the non-private estimator, as shown below.

Theorem 3. *Now, let $n = (n_1 + \dots + n_K)/K$ be the average sample size of K studies and $n_k/n, k = 1, \dots, K$ is uniformly bounded below away from zero and above. Suppose that data from different studies are independent and the regularity conditions in Theorem 1 hold for all studies. In addition, we assume the following:*

1. $K^{1/2}(\delta_{1n}^2 + \delta_{1n}\sqrt{\delta_{2n}}) = o(1)$.
2. $K/n = o(1)$.
3. $\tau_0 > 0$.

Then,

$$\sqrt{K}(\tilde{\theta}_R - \hat{\theta}_R) = o_p(1)$$

and

$$\sqrt{K}(\tilde{\theta}_R - \theta_0) \xrightarrow{d} N\left(0, \frac{1}{K^{-1} \sum_{k=1}^K (\sigma_k^2 + \tau_0^2)^{-1}}\right).$$

The justification is straightforward. Based on Theorem 1,

$$\theta(\hat{P}_{w,k}) - \theta(\hat{P}_k) = O_p(\delta_{1n}^2 + \delta_{1n}\sqrt{\delta_{2n}}) + o_p(n^{-1/2}).$$

Since $\hat{\theta}_R$ and $\tilde{\theta}_R$ are a weighted average of $\{\theta(\hat{P}_k), k = 1, \dots, K\}$ and $\{\theta(\hat{P}_{w,k}), k = 1, \dots, K\}$ respectively, with equivalent weighting schemes, i.e., the weight for the k th study $\propto (\sigma^2(P_k) + \tau_0^2)^{-1}$,

$$\sqrt{K}(\tilde{\theta}_R - \hat{\theta}_R) = O_p(1)$$

under the assumption $\sqrt{K}(\delta_{1n}^2 + \delta_{1n}\sqrt{\delta_{2n}}) = o(1)$. The weights for constructing $\hat{\theta}_R$ and $\tilde{\theta}_R$ are equivalent, which is due to the equivalence of $\hat{\theta}_F$ and $\tilde{\theta}_F$. Since K is typically substantially smaller than n_k , the

approximation of $\tilde{\theta}_R$ to $\hat{\theta}_R$ is oftentimes better than the approximation of $\theta(\hat{P}_{w,k})$ to $\theta(\hat{P}_k)$ at the individual study level. Therefore, the reproducibility of meta analysis based on synthetic data is expected to be high.

In summary, Theorem 3 implies that, asymptotically, the perturbed meta analysis estimator $\tilde{\theta}_R$ shares the same limiting distribution as the non-private estimator $\hat{\theta}_R$. Thus, privacy-preserving estimators retain consistency and asymptotic normality in meta analysis under appropriate regularity conditions. Although the perturbation error may decay slowly within each study, it can be effectively mitigated through aggregation. When the number of studies satisfies $K = O(n^{1/2+\epsilon})$, the aggregate error vanishes asymptotically, rendering $\tilde{\theta}_R$ an efficient estimator. These results illustrate a favorable privacy-utility trade-off: valid inference based on synthetic and private data is attainable when combining information across studies. In this way, meta analysis based on generated synthetic data provides a powerful framework for conducting statistically valid inference under privacy constraints.

3 Numerical Study

In this section, we have performed several simulation studies to examine the finite-sample performance of proposal. The simulation studies have two objectives: (1) to examine the effect of using generated synthetic data to replace the originally observed data in subsequent statistical inference; (2) to examine the privacy protection provided by sharing the synthetic data.

3.1 Simulation Experiments

3.1.1 Convergence Rate of $\tilde{\theta}$ in a fixed Study based on the Synthetic Data

In this section, a simulation study is conducted to evaluate the performance of several methods of generating synthetic data for downstream statistical analysis. Specifically, the study compares three techniques:

1. **Flow Sampling:** Synthetic Data are sampled directly from a trained MAF based on observed data. The sample size of the synthetic data can be determined by the user.
2. **Latent Noise Injection:** Observed Data are mapped to a latent space, perturbed by noise injection, and then reconstructed. The mapping to the latent space and subsequent reconstruction are based on trained MAF described in Section 2.3.
3. **Direct Noise Injection:** Observed Data are perturbed by directly injecting an independent Gaussian noise.

The goal is to analyze how well a simple correlation coefficient estimator based on synthetic data estimates the true correlation coefficient. Specifically, we are interested in the relationship between estimation precision and sample size of observed data for each aforementioned method generating synthetic data.

In one iteration of the simulation study, the ‘‘observed’’ data of size n are generated from a multivariate Gaussian distribution with a compound symmetric variance-covariance matrix of

$$\Sigma = (1 - \rho)\mathbf{I}_5 + \rho\mathbf{1}\mathbf{1}^T,$$

which gives a correlation coefficient of $\rho = 0.9$ between any two different components of $X \in \mathbb{R}^5$. A MAF is then trained on the generated dataset such that $X = \hat{f}(Z)$ is approximately $N(0, \Sigma)$, the distribution used to generate the observed data, where $Z \sim N(0, \mathbf{I}_5)$. The model consists of one hidden layer of size 50 with 5 autoregressive flow transformations. We train > 100 iteration steps using the Adam Optimizer to maximize the corresponding log-likelihood function. We simply set the batch size to be n , the total sample size of generated data, in maximizing the objective function. We also normalize the weight matrix by its maximum singular value to improve training stability and for enforcing Lipschitz Continuity (Miyato et al., 2018). See Lemma 2 in Appendix. With trained MAF, $\hat{f}(\cdot)$, we then generate

- a synthetic dataset based on the MAF model (Method 1: Flow Sampling),

$$\mathcal{D}_1 = \{\hat{f}(Z_i) \mid Z_i \sim N(0, \mathbf{I}_5), i = 1, \dots, 50,000\},$$

where the sample size of \mathcal{D}_1 can be arbitrarily large, and we select 50,000.

- a synthetic dataset of size n by perturbing “observed data” on the latent space (Method 2: Latent Noise Injection),

$$\mathcal{D}_2 = \{\hat{f}(\sqrt{w}\hat{f}^{-1}(x_i) + \sqrt{1-w}Z_i) \mid Z_i \sim N(0, \mathbf{I}_5), i = 1, \dots, n\},$$

where w is a tuning parameter between 0 and 1.

- a synthetic dataset of size n by injecting a random noise to “observed data” (Method 3: Direct Noise Injection),

$$\mathcal{D}_3 = \{\sqrt{w}x_i + \sqrt{1-w}\text{diag}\{\hat{\sigma}_1, \dots, \hat{\sigma}_d\}Z_i \mid Z_i \sim N(0, \mathbf{I}_5), i = 1, \dots, n\},$$

where $\hat{\sigma}_k$ is the empirical standard deviation of the k th component of X , $Z_i \sim N(0, \mathbf{I}_d)$ and $w \in (0, 1)$ is a tuning parameter.

To assess the performance of correlation coefficient estimator based on synthetic data, we compute the MLE of ρ for each synthetic dataset under the compound symmetry assumption for the variance-covariance matrix:

$$\frac{2}{p(p-1)} \sum_{1 \leq i < j \leq p} \hat{\rho}_{ij},$$

where $\hat{\rho}_{ij}$ is the sample Pearson’s correlation coefficient between the i th and j th components of X . Now, let the estimator based on synthetic data \mathcal{D}_j be $\hat{\rho}_j$, $j = 1, 2, 3$. In addition, for Latent Noise Injection and Direct Noise Injection methods, different w ’s are used to control the perturbation size. Specifically, we use $w = 0, 0.25, 0.5, 0.75$ and 1. When $w = 0$, synthetic dataset generated via Latent Noise Injection degenerates into a data generated via Flow Sampling (Method 1) except with a sample size of n instead of 50000. When $w = 1$, synthetic datasets generated via Latent Noise Injection and Direct Noise Injection are identical to the original “observed” data, since the injected noises become zero.

After repeating this process $B = 100$ times, the mean absolute difference (MAD) and empirical bias (EB) are computed as

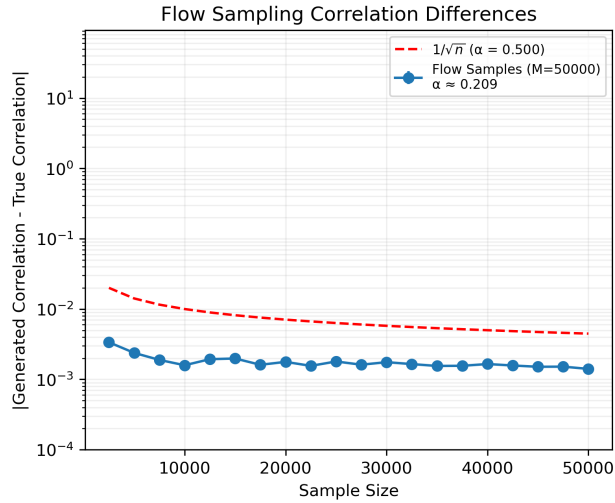
$$MAD_j = \frac{1}{B} \sum_{b=1}^B |\hat{\rho}_j^{(b)} - \rho| \quad \text{and} \quad Bias_j = \frac{1}{B} \sum_{b=1}^B \hat{\rho}_j^{(b)} - \rho,$$

respectively, where $\hat{\rho}_j^{(b)}$ is the MLE for ρ in the b th iteration of the simulation based on synthetic dataset \mathcal{D}_j , $j = 1, 2, 3$, and $\rho = 0.9$ is the true correlation coefficient. This simulation is repeated for different sample sizes $n \in \{2500k \mid k = 1, 2, \dots, 20\}$. We then examine if a power law of the form $MAD_j \propto n^{-\alpha}$ can characterize the impact of sample size of observed data on the estimation precision for estimators from synthetic data measured by MAD and EB. If $\alpha \approx 0.5$, then the estimator based on synthetic data has the same convergence rate as the MLE based on “observed” data, i.e., converges to the true parameter at the regular root n rate (Casella, 2001). $\alpha < 0.5$ indicates that there is nontrivial information loss due to the use of synthetic data rather than “observed” data for estimating parameters of interest.

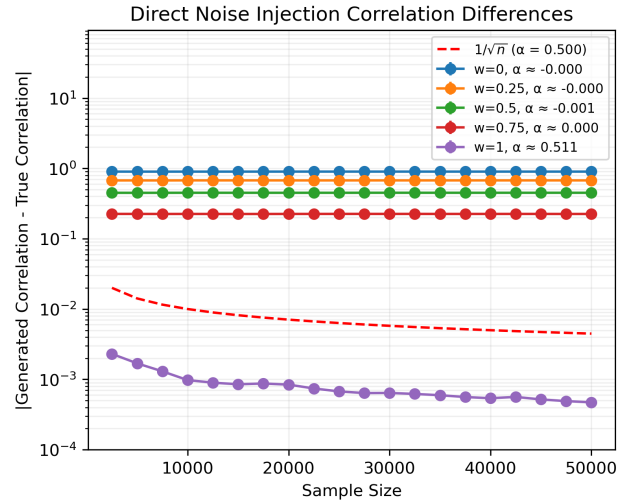
The simulation results are summarized in Figures 2, 3, and Tables 1, 2. Figure 2 presents the MAD between estimated and true correlation coefficient for each method as a function of sample size of observed data. The theoretical convergence rate, $O_p(n^{-1/2})$, is plotted as a reference. Panel (a) of Figure 1 indicates that the estimator based on synthetic data generated via Flow Sampling exhibits a slower than the regular root n rate in estimating the true correlation coefficient. It may be due to the fact that the transport map trained via MAF fails to generate synthetic data from a distribution that is sufficiently close to the underlying distribution for the “observed” data even if the sample size n is large. Indeed, we know that in general, the Wasserstein Distance between the true distribution and the distribution induced by a Normalizing Flow trained based on a training dataset of size n is slower than the regular root n rate, suggesting that the estimator based on synthetic data also converges at a slower than root n rate. Panel (b) of Figure 2 demonstrates that the estimator based on synthetic data generated via Latent Noise Injection converges to the true correlation coefficient at approximately a root n rate when w is close to 1. The convergence rate is slower than the root n rate when w is close to 0, as in Panel (a). This observation suggests that perturbing the observed data by injecting a random noise at a controlled level in the latent space can replace the original “observed” data for downstream analysis without sacrificing the estimation precision. Finally, directly injecting independent noise to observed data distorts the distribution of observed data and may

severely bias the related parameter estimation, especially when w is away from 1. In the current case, injecting a Gaussian noise component wise would dilute the correlation coefficient, leading to a downward bias in estimating ρ . This bias doesn't diminish with increased sample size as shown in Panel (c) of Figure 2, since it is caused by the perturbation mechanism itself. The detailed results on MAD from the simulation study are also reported in Tables 1 and 2. Note, we only plot for $n \in \{10000, 20000, 30000, 40000, 50000\}$ to avoid verbosity.

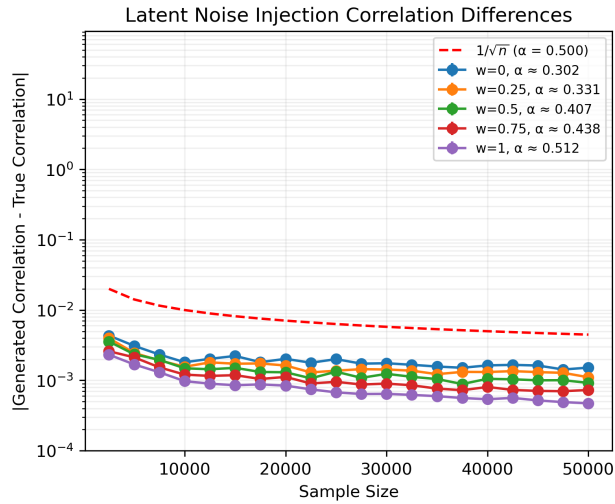
Figure 3 presents the EB for correlation coefficient estimator as a function of sample size of observed data. Panel (a) of Figure 3 indicates that the estimator based on synthetic data generated via Flow Sampling exhibits a near zero bias even when the sample size is as small as 2500. It is expected that the transport map trained via MAF can induce a distribution consistently approximating the true distribution of X . Panel (b) of Figure 3 demonstrates that the estimator based on synthetic data generated via Latent Noise Injection is approximately unbiased for all w and all sample sizes investigated. This observation further supports using synthetic data generated via the proposed Latent Noise Injection to replace the original data for statistic analysis. Finally, the Direct Noise Injection method introduces a downward bias in estimating the correlation coefficient, and this bias persists with increasing sample size in Panel (c) of Figure 3. The detailed results on EB from the simulation study are also reported in Table 2.



(a) Flow Sampling Absolute Correlation Differences

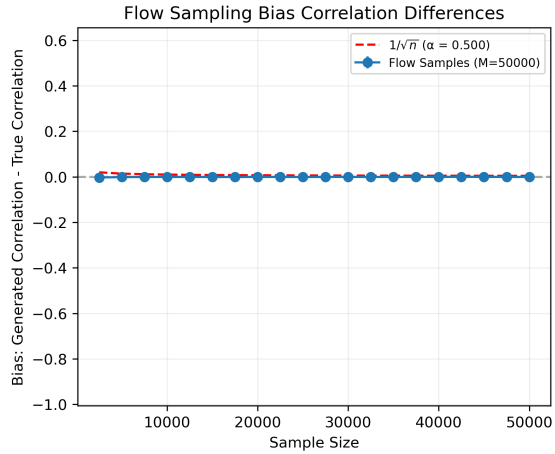


(b) Direct Noise Injection Absolute Correlation Differences

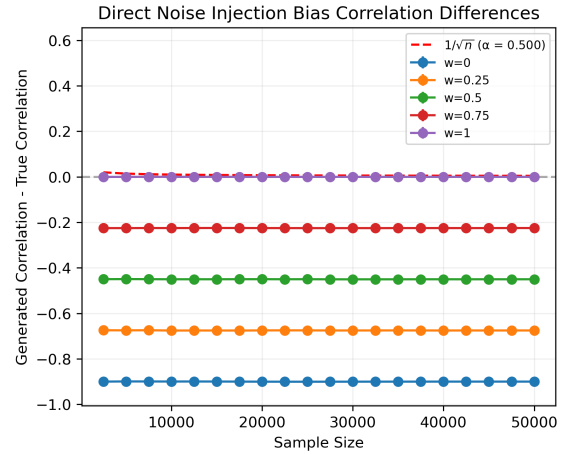


(c) Latent Noise Injection Absolute Correlation Differences

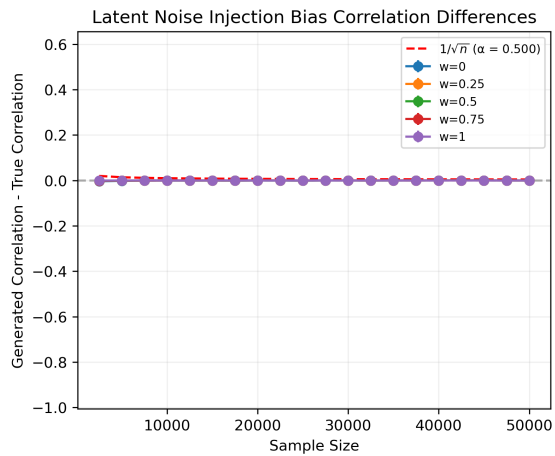
Figure 2: A comparison of mean absolute differences in estimating the correlation coefficient based on 3 synthetic data generation schemes (100 simulations); the red curve represents the benchmark $n^{-1/2}$ rate.



(a) Flow Sampling Bias Correlation Differences



(b) Direct Noise Injection Bias Correlation Differences



(c) Latent Noise Injection Bias Correlation Differences

Figure 3: A comparison of biases in estimating the correlation coefficient based on 3 synthetic data generation schemes (100 simulations).

Table 1: The mean absolute distances, $\text{average}|\hat{\rho}_{MLE}-\rho|$, estimates over 100 simulations for different methods and sample sizes ($\rho = 0.9$) with $w \in \{0, 0.25, 0.5, 0.75, 1\}$.

n	Method	w = 0	w = 0.25	w = 0.5	w = 0.75	w = 1
10000	Flow Sampling	0.0016	-	-	-	-
	Latent Noise Injection	0.0018	0.0016	0.0015	0.0012	0.0010
	Direct Noise Injection	0.8996	0.6755	0.4502	0.2251	0.0010
20000	Flow Sampling	0.0018	-	-	-	-
	Latent Noise Injection	0.0020	0.0016	0.0013	0.0011	0.0008
	Direct Noise Injection	0.9003	0.6750	0.4498	0.2251	0.0008
30000	Flow Sampling	0.0018	-	-	-	-
	Latent Noise Injection	0.0018	0.0014	0.0012	0.0009	0.0006
	Direct Noise Injection	0.9003	0.6753	0.4505	0.2252	0.0006
40000	Flow Sampling	0.0017	-	-	-	-
	Latent Noise Injection	0.0016	0.0013	0.0011	0.0008	0.0005
	Direct Noise Injection	0.9000	0.6754	0.4502	0.2251	0.0005
50000	Flow Sampling	0.0014	-	-	-	-
	Latent Noise Injection	0.0015	0.0011	0.0009	0.0007	0.0005
	Direct Noise Injection	0.9000	0.6752	0.4501	0.2250	0.0005

Table 2: The empirical bias, $\text{average}(\hat{\rho}_{MLE}) - \rho$, over 100 simulations for different methods and sample sizes ($\rho = 0.9$) with $w \in \{0, 0.25, 0.5, 0.75, 1\}$.

n	Method	w = 0	w = 0.25	w = 0.5	w = 0.75	w = 1
10000	Flow Sampling	-0.0004	-	-	-	-
	Latent Noise Injection	-0.0007	-0.0004	-0.0002	-0.0001	0.0000
	Direct Noise Injection	-0.8996	-0.6755	-0.4502	-0.2251	0.0001
20000	Flow Sampling	-0.0002	-	-	-	-
	Latent Noise Injection	-0.0005	-0.0002	-0.0001	0.0000	0.0000
	Direct Noise Injection	-0.9003	-0.6750	-0.4498	-0.2251	0.0001
30000	Flow Sampling	-0.0003	-	-	-	-
	Latent Noise Injection	-0.0004	-0.0002	-0.0001	-0.0001	-0.0000
	Direct Noise Injection	-0.9003	-0.6753	-0.4505	-0.2252	-0.0000
40000	Flow Sampling	-0.0001	-	-	-	-
	Latent Noise Injection	-0.0003	-0.0000	-0.0002	-0.0000	-0.0000
	Direct Noise Injection	-0.9000	-0.6754	-0.4502	-0.2251	-0.0000
50000	Flow Sampling	-0.0004	-	-	-	-
	Latent Noise Injection	-0.0006	-0.0003	-0.0002	-0.0001	0.0000
	Direct Noise Injection	-0.9000	-0.6752	-0.4501	-0.2250	0.0000

Next, we assess empirical privacy leakage through membership inference attacks (MIA) and monitor how attack success varies with the perturbation parameter w . A particularly informative variant of MIA is the distance-to-synthetic attack, applicable to models such as GANs, VAEs, and Diffusion (Chen et al., 2020). Unlike binary classification approaches that attempt to distinguish synthetic from real data, this method instead focuses on identifying which real data points were likely seen during training and perturbed to generate synthetic observations. Specifically, we generate synthetic data with different w 's in our proposed Latent Noise Injection method. To quantify the privacy protection via MIA, we attempt to differentiate originally observed data, whose privacy needs to be protected, from freshly generated new observations based

on the synthetic dataset $\tilde{\mathbf{X}}$. If there is no or very little difference between them, i.e., based on synthetic data one can't tell if a given observation X is from observed data or a fresh independent observation, then there is a strong privacy protection.

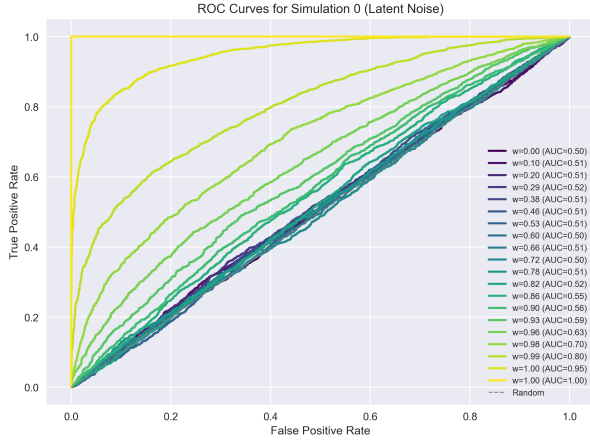
In this simulation study, we examine the performance of a specific classifier based on the distance between observation of interest X_0 and synthetic data $\tilde{\mathbf{X}}$ released for public use:

$$d_{\tilde{\mathbf{X}}}(X_0) = \min_{\tilde{X} \in \tilde{\mathbf{X}}} \|X_0 - \tilde{X}\|_2. \quad (24)$$

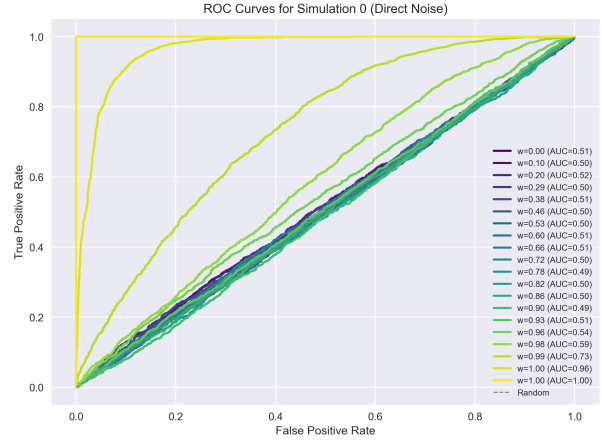
The performance of this classifier can be measured by the AUC under the ROC curve. If the AUC is close to 0.5, then this classifier can't effectively separate fresh observations from old observations in the original dataset, i.e., a good privacy protection. Based on this observation, for each pair of observed and synthetic datasets in our simulation, we also generate a fresh dataset from the same distribution of observed data with the same sample size and then calculate the AUC under the ROC curve for $d_{\tilde{\mathbf{X}}}(X)$. In particular, the AUC can be calculated as

$$\frac{1}{n^2} \sum_{i=1}^n \sum_{j=1}^n \left[I \{d_{\tilde{\mathbf{X}}}(X_i) < d_{\tilde{\mathbf{X}}}(X_j^*)\} + \frac{1}{2} I \{d_{\tilde{\mathbf{X}}}(X_i) = d_{\tilde{\mathbf{X}}}(X_j^*)\} \right], \quad (25)$$

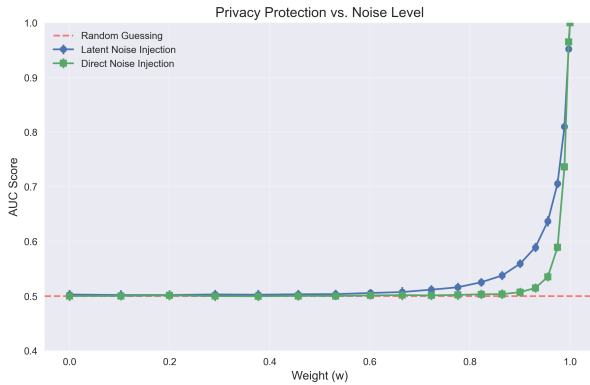
where the observed data consists of $\{X_1, \dots, X_n\}$ and freshly generated independent data consists of $\{X_1^*, \dots, X_n^*\}$. We use a sample size of $n = 2500$ across $B = 100$ simulation runs. We summarize the AUC for different methods and different w for Latent Noise Injection and Direct Noise Injection methods in Figure 4. Panels (a) and (b) display the AUC-ROC curves for one simulation for illustration, and Panel (c) displays the mean AUC across all $B = 100$ runs as a function of $w \in [0, 1]$ for both Latent and Direct Noise Injection methods. In particular, when $w = 0.75$, the mean AUC for Latent Noise Injection is 0.52, implying a fairly good privacy protection. On the other hand, when $w = 0.975$, the mean AUC for Latent Noise Injection method is 0.71, suggesting loss in privacy protection.



(a) ROC curves of membership scores in MIA based on one set of synthetic data generated via the Latent Noise Injection method.



(b) ROC curves of membership scores in MIA based on one set of synthetic data generated via Direct Noise Injection method.



(c) AUC under the ROC curve of membership scores from MIA for synthetic data generated via Latent and Direct Noise Injection Methods with different w .

Figure 4: A privacy protection assessment for synthetic data generated using Noise Injection Techniques.

A justification for why Direct Noise Injection allows for a larger noise weight without immediately compromising privacy protection, as seen in Panel (c) of Figure 4, is that it perturbs the output data more “chaotically” and directly in the observation space. This unstructured distortion makes it more difficult to identify specific individuals, thereby impeding the model’s ability to extract structured, sensitive patterns. However, while this approach may better obfuscate identifiable information, it comes at the cost of degrading the underlying data structure essential for statistical inference.

In contrast, our Latent Noise Injection method strikes a more favorable balance. Specifically, at a noise weight of $w = 0.75$, it achieves two key advantages. First, the resulting synthetic data retains a high degree of utility: estimates of key statistical quantities (e.g., precision or model parameters) are comparable to those obtained using the original data, as seen in Figures 2 and 3. Second, privacy protection remains strong, with AUC scores close to random guessing. By comparison, although Direct Noise Injection offers similar privacy at higher noise levels, it fails to preserve inferential fidelity, significantly compromising precision, as seen in Figures 2 and 3. Thus, our approach outperforms existing methods by achieving both privacy and utility simultaneously.

Overall, this study provides insights into the efficacy of Normalizing Flows and perturbation-based reconstruction methods in preserving correlation structures in generated data. The key findings suggest Flow Sampling maintains correlation fidelity but does not fully reach the theoretical decay rate. Second, the La-

tent Noise Injection method improves with increasing reconstruction weight w , making it a viable method for structure-preserving data generation. Finally, the Direct Noise Injection method fails to maintain correlation, especially for higher values of w .

We note that future work may explore adaptive perturbation strategies or alternative generative models to further enhance correlation preservation.

3.1.2 Validity of Meta Analysis Results

The goal of this simulation study is to evaluate the ability of MAF to generate synthetic datasets that preserve key statistical properties of real data across multiple studies to permit meta analysis based on synthetic data. Specifically, we assess how well synthetic data can reproduce regression coefficient estimates obtained from “originally observed” data using synthetic data generated via the Latent Noise Injection method in light of the findings in Chapter 4. This is particularly relevant for generating and sharing synthetic data for subsequent meta analysis with a good privacy protection.

Specifically, for each simulation iteration, we simulate data from $K = 10$ independent studies. In particular, data for study k consists of n_k i.i.d. copies of (X_1, X_2, X_3, X_4, Y) following a simple linear model:

$$Y = \beta_{0k} + \beta_{1k}X_1 + \beta_{2k}X_2 + \beta_{3k}X_3 + \beta_{4k}X_4 + \varepsilon, \quad \varepsilon \sim N(0, \sigma_\varepsilon^2)$$

where $(X_1, X_2, X_3, X_4)' \sim N(0, \mathbf{I}_4)$, and $\sigma_\varepsilon^2 = 0.5$. Moreover, the regression coefficients $(\beta_{0k}, \beta_{1k}, \beta_{2k}, \beta_{3k}, \beta_{4k})'$ for each study are drawn from a multivariate Gaussian distribution:

$$\begin{bmatrix} \beta_{0k} \\ \beta_{1k} \\ \beta_{2k} \\ \beta_{3k} \\ \beta_{4k} \end{bmatrix} \sim N \left\{ \begin{bmatrix} \beta_0 \\ \beta_1 \\ \beta_2 \\ \beta_3 \\ \beta_4 \end{bmatrix}, \Sigma_\beta \right\} = N \left\{ \begin{bmatrix} 0 \\ 1 \\ 1 \\ 1 \\ 1 \end{bmatrix}, \begin{bmatrix} 10^{-4} & 5 \cdot 10^{-5} & 5 \cdot 10^{-5} & 5 \cdot 10^{-5} & 5 \cdot 10^{-5} \\ 5 \cdot 10^{-5} & 5 \cdot 10^{-3} & 5 \cdot 10^{-5} & 5 \cdot 10^{-5} & 5 \cdot 10^{-5} \\ 5 \cdot 10^{-5} & 5 \cdot 10^{-5} & 10^{-4} & 5 \cdot 10^{-5} & 5 \cdot 10^{-5} \\ 5 \cdot 10^{-5} & 5 \cdot 10^{-5} & 5 \cdot 10^{-5} & 10^{-4} & 5 \cdot 10^{-5} \\ 5 \cdot 10^{-5} & 5 \cdot 10^{-5} & 10^{-4} \cdot 10^{-5} & 5 \cdot 10^{-5} & 10^{-4} \end{bmatrix} \right\}.$$

The sample size n_k for each study is drawn uniformly from the range $[750, 1000]$. For each study, MAF is trained on observed data. After training, synthetic data is generated by the proposed Latent Noise Injection method using the resulting MAF. 13 synthetic datasets are generated corresponding with $w = \{0, 0.1, \dots, 1.0\}$, as seen in the legends of Figure 5, controlling the perturbation size. In generating these 13 synthetic datasets, the same set of $Z_i \in N(0, \mathbf{I}_5)$ in (12) is used to ensure consistency in the evaluating the effect of the perturbation size on statistical analysis based on synthetic data. The parameter of interest is the common regression slope of X_2 , i.e., $\beta_2 = 1$, which can be estimated via meta analysis. Note that we specify the variance of β_{1k} to be $5 \cdot 10^{-3}$, compared to 10^{-4} for other components $\beta_{jk}, j \neq 1$. In each iteration, we

1. generate K observed datasets for K studies;
2. compute $\hat{\beta}_{2k}$ and its variance $\hat{\sigma}_{2k}^2$ using ordinary least square method for each study based on observed data;
3. use the DerSimonian-Laird Method from Section 2.2 to compute an aggregated estimator of β_2 , $\hat{\beta}_2$, and its standard error based on $(\hat{\beta}_{2k}, \hat{\sigma}_{2k}^2), k = 1, \dots, K$;
4. generate K synthetic datasets for K studies using the Latent Noise Injection method for each $w \in \{0, 0.1, \dots, 1.0\}$ as seen in the legends of Figure 5;
5. compute $\tilde{\beta}_{2k}(w)$ and its variance $\tilde{\sigma}_{2k}^2(w)$ using the ordinary least square method for each study based on synthetic data generated with a given w ;
6. use the DerSimonian-Laird method to compute a aggregated estimator of β_2 , $\tilde{\beta}_2(w)$, and its standard error based on $(\tilde{\beta}_{2k}, \tilde{\sigma}_{2k}^2), k = 1, \dots, K$.

We train the MAF based on observed data with a hidden size of 32 and only one hidden layer. The model is composed of 2 flow steps and is trained with a 70% – 30% train-validation split to select the number of iterations (up to 1000). Specifically, we continue to train MAF for an additional 100 steps with a learning

rate of 10^{-4} after the loss in the validation set stops to improve. The process is repeated $B = 500$ times. Then, we compare the meta analysis estimator based on observed data with its counterpart based on synthetic data using different w .

The choice of the tuning parameter w controlling the perturbation size plays a critical role in balancing the trade-off between privacy protection and data fidelity. A lower value of w typically provides stronger privacy protection, but can come at the cost of reduced inferential performance based on synthetic data. Therefore, selecting an appropriate w is essential to ensure the synthetic data remains a useful replacement of original data, while limiting potential information leakage. In our simulation study, we assessed the AUC of MIA in a range of w values for each study with (24) and (25). Using a single simulation realization as an illustrative example, we have reported ROC curves for the generated 10 studies with different w in Figure 5. We also report the average AUC across 500 simulation runs for each study and as a function of $w \in [0, 1]$ in Figure 6. The ROC curves show that as w increases, the ability to distinguish between real and synthetic data also increases. In general, $w = 0.8$, which is highlighted in bold red in Figure 5, was found to offer a practical balance, as the average AUC is approximately 55% across the 10 studies.

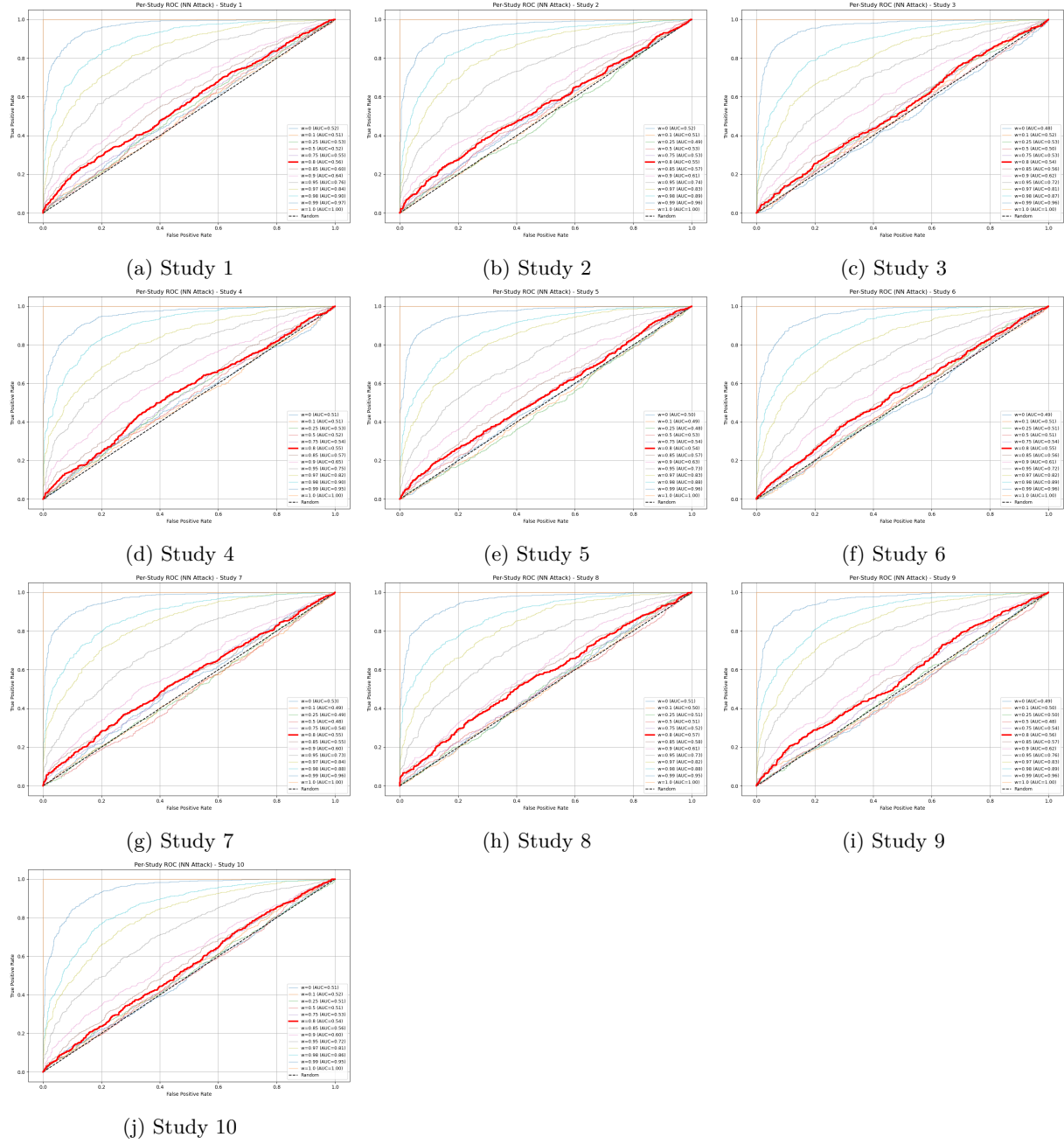


Figure 5: ROC Curves of membership scores in MIA for each study for one simulation iteration. ROC curves are color-coded according to perturbation weight w .

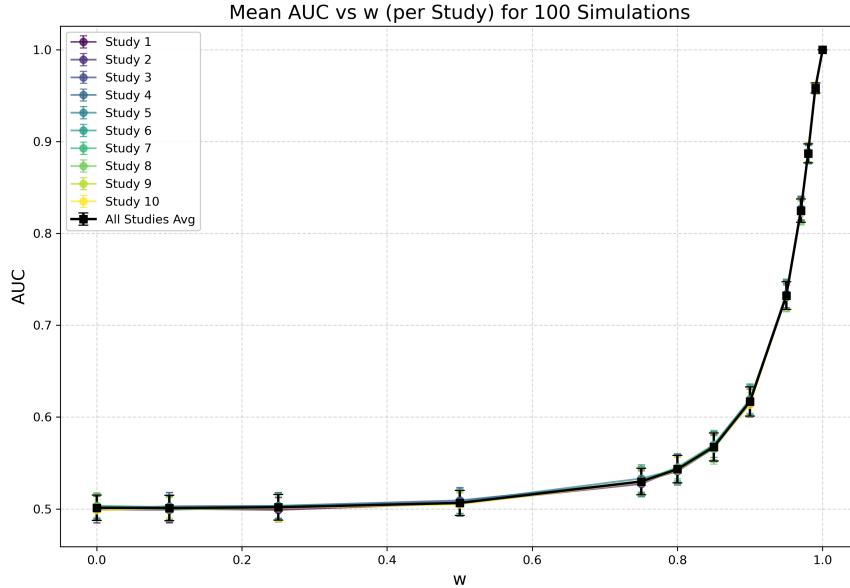


Figure 6: Mean AUC under ROC curve of membership scores in MIA for synthetic data generated with different w across 100 simulations. For each of the ten studies (colored lines), the curve represents the relationship between average AUC and w , and the vertical short bars show the mean AUC \pm one standard error.

With $w = 0.8$ fixed as our chosen tuning parameter, we next investigate how well synthetic data generated under this choice supports downstream meta analytic inference. The results are summarized in Figures 7, 8, 9. Figure 7 shows study level estimates of β_{2k} and their corresponding 95% CIs as well as the meta analysis estimator of β_2 and its 95% CI based on the random effects model from a single simulation run for illustrative purposes. The synthetic data is generated with $w = 0, 0.8$ and 1.0 . Note, synthetic data generated with $w = 0$ does not retain any one to one correspondence at the individual level and offers full privacy protection. On the other hand, synthetic data generated with $w = 1$ is identical to the real data, and the results from meta analysis should be identical to that based on real data. This case is presented for a sanity check. While there are noticeable differences in point estimators and 95% CIs between observed and synthetic data for some individual studies, e.g., Study 1, the aggregated results from meta analysis based on synthetic data are very similar to those based on original data. Figure 8 presents a scatterplot comparing aggregated β_2 estimates from observed data with those from synthetic data across 500 simulations. Note that the strong linear relationship, evident from the tight clustering around the diagonal line, indicates high fidelity between estimates from real and synthetic data in general. When the perturbation size w is close to 1 ($w = 0.8$), the concordance between estimates from original and synthetic data becomes high (i.e., light blue dots in Figure 8). The concordance is substantially diluted when the synthetic data is generated with $w = 0$. The MAD between $\hat{\beta}_2$ and $\tilde{\beta}_2(w)$ is 0.0042 for $w = 0.8$ and almost doubled to 0.0089 for $w = 0$. Obviously, when $w = 1$, $\hat{\beta}_2 = \tilde{\beta}_2(w)$ as indicated in Figure 8, since there is essentially no perturbation. In addition, the MAD between the true parameter $\beta_2 = 1$ and $\tilde{\beta}_2(w)$ based on synthetic data, or $\hat{\beta}_2$ based on original data, is 0.0067 for $w = 1$ (i.e., no perturbation), 0.0080 for $w = 0.8$, and 0.0111 for $w = 0$, suggesting that the estimation precision for $w = 0$ is the poorest and substantially improved after anchoring synthetic data with original data by setting $w = 0.8$. We further plot the densities of $\hat{\beta}_2$ from original data and $\tilde{\beta}_2(w)$ from synthetic data in Figure 9, demonstrating that the variance of the estimator based on synthetic data with a perturbation size of $w = 0.8$ is indeed similar to that based on observed data and substantially smaller than the variance of the estimator based on synthetic data with a perturbation size of $w = 0$.

In general, these results collectively validate the synthetic data generation pipeline, demonstrating that it reliably reproduces both point estimates and CIs in the meta analysis setting beyond a single study, when w is appropriately selected to balance the privacy-reproducibility trade-off.

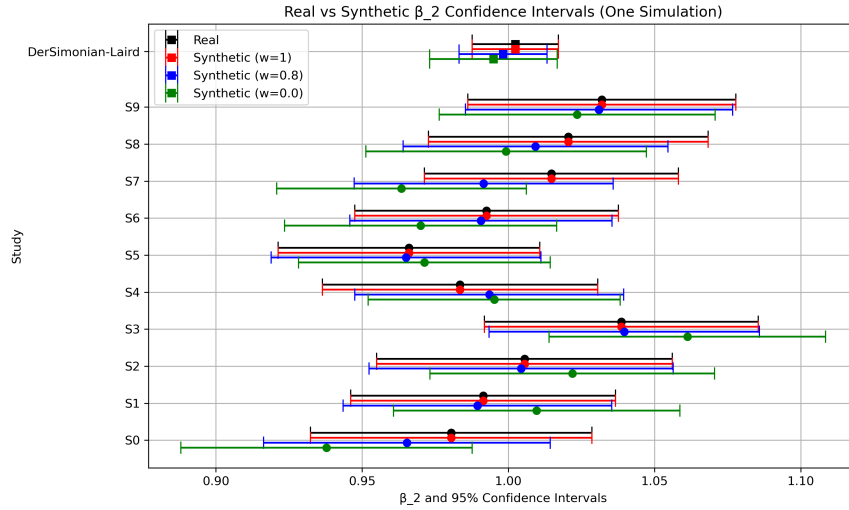


Figure 7: A forest plot for one simulation run. The point estimator and associated 95% CIs from individual studies as well as the meta analysis are reported; estimates based on synthetic data with different w are colored differently: green ($w = 0$), blue ($w = 0.8$), and red ($w = 1.0$).

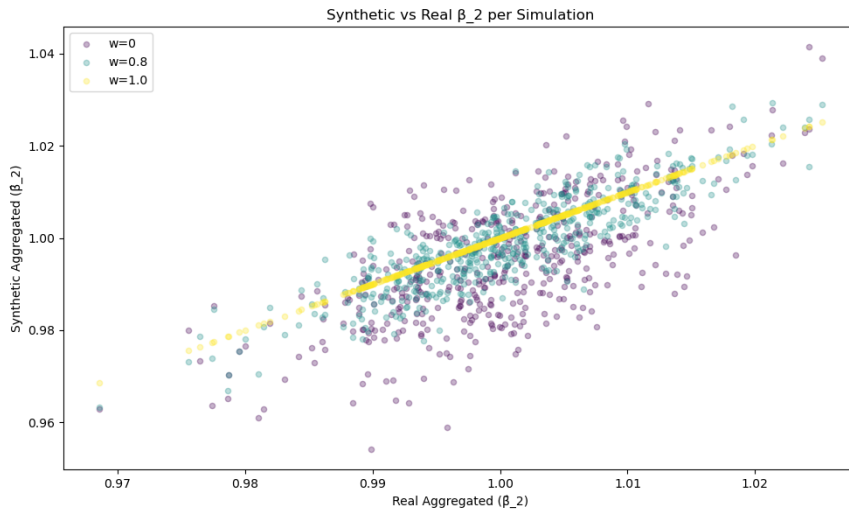


Figure 8: The scatter plot of point estimates of β_2 from meta analysis based on real vs synthetic data (500 simulations); estimates based on synthetic data generated with different w are color-coded differently: purple ($w = 0$), teal ($w = 0.8$), and yellow ($w = 1.0$).

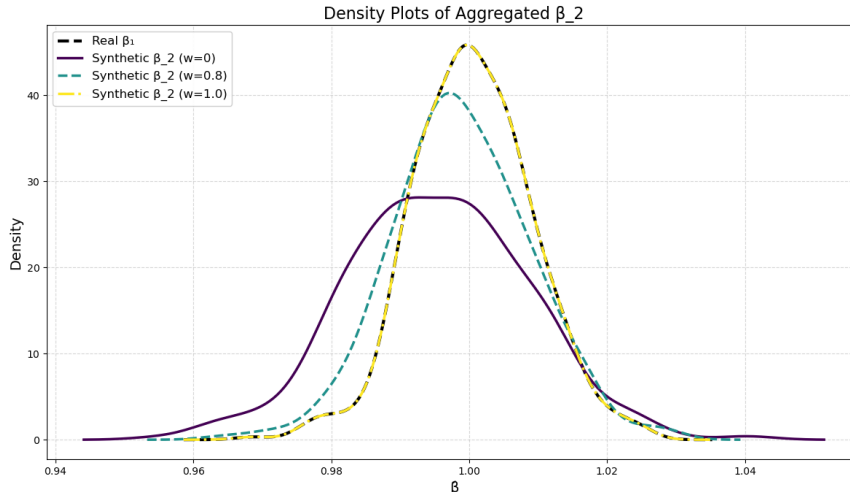


Figure 9: The density estimates of the estimator of β_2 from meta analysis (500 simulations); estimates based on synthetic data generated with different w are color-coded differently: purple ($w = 0$), teal ($w = 0.8$), and yellow ($w = 1.0$). The estimates based on original data are colored as black.

4 Real Data Example

We conduct experiments to evaluate the effectiveness of the proposed Latent Noise Injection method in generating synthetic data while preserving statistical and predictive properties of real data. The dataset used consists of common clinical variables including time from baseline to the first cardiovascular disease (CVD) event subjective to right censoring, sex, baseline age, baseline total cholesterol level, baseline high-density lipoprotein cholesterol level (HDL), and baseline systolic blood pressure (SBP) from six cohort studies established for studying risk factors associated with cardiovascular health: Atherosclerosis Risk in Communities study (ARIC) (Liao et al., 1999; Schmidt et al., 2005), Coronary Artery Risk Development in Young Adults (CARDIA) study (Carnethon et al., 2004; Friedman et al., 1988), Cardiovascular Health (CHS) study (Fried et al., 1991), Multi-Ethnic Study of Atherosclerosis (MESA) study (Bild et al., 2002), Framingham Offspring study (Feinleib et al., 1975), and Jackson Heart study (Sempos et al., 1999). ARIC, MESA, and the Jackson Heart studies probe novel risk factors for sub-clinical atherosclerosis and their downstream impact on heart failure across diverse U.S. populations. CARDIA and CHS follow participants longitudinally to chart how cardiovascular and stroke risks evolve with age. The Framingham Offspring study focuses on the heritable nature of cardiovascular disease across generations.

4.1 Original Data Analysis

After excluding participants with missing data, there are a total of 8101 female and 6762 male participants in ARIC, 2743 female and 2297 male participants in CARDIA, 3254 female and 2413 male participants in CHS, 3552 female and 3176 male participants in MESA, 1766 female and 1608 male participants for Framingham Offspring study, and 1913 female and 1196 male participants for Jackson Heart study. We divide each cohort study into male and female subgroups, yielding a total of 12 “sub-studies”. We select age, total cholesterol level, HDL, and SBP as potential CVD risk factors with a special interest in SBP. We have summarized their distribution in 12 sub-studies in Table 3. The continuous measurements are summarized by mean and standard deviation and the binary variable is summarized by proportion.

Table 3: The baseline summary statistics for the 12 sub-studies: mean (standard deviation) for continuous measures (time to CVD, Age, total cholesterol level, HDL and SBP) and percentage of participants who experienced a CVD Event.

Study	n	CVD Event (%)	TIME TO CVD (year)	AGE (year)	CHL (mg/dL)	HDL (mg/dL)	SBP (mmHg)
ARIC (F)	8101	16	20 (6)	54 (6)	218 (43)	57 (17)	120 (19)
ARIC (M)	6762	26	18 (7)	55 (6)	211 (40)	44 (14)	122 (18)
CARDIA (F)	2743	4	33 (4)	25 (4)	177 (33)	56 (13)	107 (10)
CARDIA (M)	2297	7	32 (6)	25 (4)	176 (34)	50 (13)	115 (10)
CHS (F)	3254	42	13 (7)	72 (5)	221 (39)	59 (16)	137 (22)
CHS (M)	2413	50	10 (7)	73 (6)	198 (36)	48 (13)	136 (21)
MESA (F)	3552	9	14 (4)	62 (10)	200 (36)	56 (15)	127 (23)
MESA (M)	3176	13	14 (4)	62 (10)	188 (35)	45 (12)	126 (19)
Framingham (F)	1766	13	27 (7)	44 (10)	201 (40)	54 (13)	118 (17)
Framingham (M)	1608	22	25 (9)	44 (10)	204 (37)	43 (11)	126 (16)
Jackson Heart (F)	1913	4	10 (2)	50 (12)	197 (38)	54 (14)	124 (17)
Jackson Heart (M)	1196	5	9 (2)	49 (12)	197 (40)	45 (12)	126 (16)

The objective of the statistical analysis is to examine the associations between SBP level at the baseline and the hazard of subsequent CVD events. To this end, we fit two Cox regression models on data from each sub-study and obtain the estimated regression coefficient of SBP and the corresponding CI: one without any adjustment and one with adjustment of age, total cholesterol level, and HDL. Then, we aggregate results from all 12 sub-studies into one point estimator with a CI for the hazard ratio (HR) associated with a change of 10 mmHg in SBP using a random effects model-based meta analysis (10). In particular, the Dersimonian-Laird Method to aggregate information from all 12 sub-studies is used. The results are reported in Figure 15. Without any adjustment of potential confounders, the estimated HR of 10 mmHg increase in SBP is 1.277 (95% CI: 1.221 to 1.333). After adjusting for age, total cholesterol level, and HDL, the estimated hazard ratio is 1.171 (95% CI: 1.134 to 1.207), suggesting that a higher SBP is statistically significantly associated with increased CVD risk. Specifically, every 10 mmHg higher in SBP corresponds to a 17.1% increase in CVD hazard after adjusting for other common CVD risk factors.

4.2 MAF Training

Suppose that individual level data from the aforementioned studies cannot be shared due to privacy concerns. We plan to generate synthetic data using the proposed Latent Noise Injection method and conduct meta analysis based on generated data. To this end, we need to first train MAF as a generative model for each sub-study. Before MAF training, we transform the event time using a scaled min-max logit transformation since event time always falls into a range determined by the maximum study follow-up time. For binary censoring indicator, we continualize it by adding an independent noise from $U(0,1)$ to their original binary values. Moreover, all other variables were standardized by applying Z -score normalization to improve training stability. After training MAF, all the variables were transformed back to their original scales by inverting the standardization steps when generating the final synthetic data. Specifically, for censoring indicator, this means values less than 0 are set to 0, and values greater than or equal to 0 are set to 1. All training is conducted with PyTorch as the deep learning framework. We apply an initial learning rate of 10^{-4} with a minimum threshold of 10^{-7} . In addition, we tune our MAF to select the "best" model configuration by optimizing the validation loss using 80% vs 20% cross-validation across multiple candidate configurations specified apriori for each sub-study. Specifically, we perform a grid search over the following hyperparameters: hidden layer size, number of hidden layers, and number of Normalizing Flow layers. The parameter grids varied by study according to respective sample size, and the final selected configuration is reported in Table 4.

4.3 Selection of Perturbation Size

Once the MAF is trained for each sub-study, we need to determine the optimal perturbation size w in our Latent Noise Injection method. To select a w to ensure sufficient privacy protection, we assess empirical privacy leakage through MIA described in Section 3.1.1 with different w values for each sub-study. Unfortunately, we don't have access to a fresh new dataset. Thus, we randomly split observed data into two sets: D_1 , a training set consisting of 80% of the original data, and D_0 , a test set consisting of 20% of the original data. We then train a MAF based on the training set D_1 and use the Latent Noise Injection method with trained MAF and given perturbation size w to generate a synthetic dataset \tilde{D}_1 by perturbing D_1 . As discussed in Section 3.1.1, for each $X \in D_1 \cup D_0$, a membership score $d_{\tilde{D}_1}(X)$ is calculated. We then compute the AUC under the ROC curve of the membership score $d_{\tilde{D}_1}(X)$ in classifying $X \in D_1$ vs $X \in D_0$. AUC values near 0.5 indicate that synthetic data does not leak training samples and provides empirical support for privacy preservation. We select the largest value of the perturbation parameter $w \in (0, 1)$ such that the MIA AUC remains below 0.55. The selected perturbation size, \hat{w} , is different for each sub-study and reported in Table 5. This criterion balances the tradeoff between fidelity and privacy: as $w \rightarrow 1$, the synthetic output becomes more faithful to the original data (but may risk memorization of individual observations), whereas as $w \rightarrow 0$, the output resembles purely sampled noise from the latent prior, offering stronger privacy but potentially lower statistical utility. Figure 10 displays sub-study specific ROC curves for varying w value. The AUC values remain near 0.5 when w is small, indicating no detectable memorization. However, as w increases beyond a threshold (i.e., between 0.7 and 0.9), AUC values rise sharply to 1.0, which signals potential privacy leakage due to inadequate perturbation. This empirical trend is consistent across studies and reinforces the need to calibrate w based on an acceptable privacy-utility tradeoff.

To evaluate the privacy protection provided by selected \hat{w} , we additionally calculate the pairwise Euclidean Distances between real and synthetic samples and compare them with distances between two different real samples. If the distance between real and synthetic samples is very small, the risk of privacy leakage can be non-trivial as one may guess the real sample value from the released synthetic sample value. The empirical distributions of distances between real and synthetic samples and distances of two randomly selected real samples are plotted in Figure 11, suggesting pair-wise distances between real and perturbed samples are indeed small, but not universally smaller than those between two distinct real observations. We calculate the empirical probability of $\|X_j - X_i\|_2 < \|\tilde{X}_i - X_i\|_2$ for $i \neq j$ to quantify the relative closeness of original and synthetic samples, where X_i is a real observation in a given study, and \tilde{X}_i is its perturbed counterpart using \hat{w} in the generated synthetic dataset. The results are reported as **Probability** in Table 6 by sub-study. These probabilities range from 0.9% to 3.5%, also suggesting sufficient perturbation to alleviate the privacy concern. In Figure 11, we also plot the empirical distribution of distances between real and synthetic samples with $w = 0$, which provides 100% privacy protection. As expected, this distribution is almost the same as the distribution of distances between two randomly selected real samples. Coupled with the fact that the reported **Probability** corresponding to $w = 0$ is close to 50% in Table 6, this supports the selection of the latter as a reference distribution to evaluate the privacy protection from selected \hat{w} .

To further quantify the privacy protection with selected \hat{w} , for each real observation X_i in a study, we calculate the distance $\|X_i - \tilde{X}_i\|_2$ and the distances between X_i and other real observations:

$$D_i = \{\|X_i - X_j\|_2 \mid j = 1, \dots, i-1, i+1, \dots, n\}.$$

Then, we calculate the rank of $\|X_i - \tilde{X}_i\|_2$ among D_i , calculated as

$$r_i = \sum_{j \neq i} I(\|X_i - \tilde{X}_i\|_2 > \|X_i - X_j\|_2). \quad (26)$$

The medians of r_i for different w are summarized in Table 6. For instance, among male ARIC participants, it suggests that, on average, when $w = \hat{w} = 0.85$, the perturbation moves the original observation beyond its 16 nearest neighbors. In other words, the perturbation is likely sufficient, since there are many distinct real samples closer to X_i than its perturbed counterpart in the synthetic dataset. When $w = 0$, that is, when a perfect privacy protection is provided, the median rank is close to 50% of the sample size as expected. To visualize the effect of the proposed perturbation in synthetic data generation, Figure 12 shows trajectories for 3 randomly selected observations from the ARIC (Male) sub-study as they transition from $w = 0$ to $w = 1$.

Study	Size of Hidden Layer	Number of Hidden Layers	Number of Flows
ARIC (M)	128	1	5
ARIC (F)	64	1	4
CARDIA (M)	64	2	4
CARDIA (F)	128	1	4
CHS (M)	64	2	4
CHS (F)	64	1	5
MESA (M)	32	2	4
MESA (F)	32	2	5
Framingham (M)	64	1	5
Framingham (F)	64	1	4
Jackson Heart (M)	32	1	3
Jackson Heart (F)	32	2	3

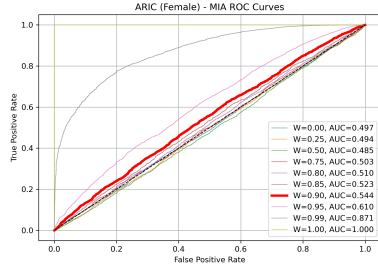
Table 4: The configurations of tuning parameters selected via cross validation for MAF training across 12 sub-studies.

Figures 13 and 14 further examine the fidelity of the synthetic data. Figure 13 compares real and synthetic joint distributions of SBP and survival time (time to CVD) in ARIC (Male) sub-study, where the synthetic data is generated using $w = 0$ and $w = 0.85$. Note that lines are drawn between the original and perturbed data points in each plot to highlight the effect of perturbation. These connecting lines reveal substantial movement for both $w = 0$ and $w = 0.85$, demonstrating that the synthetic data differ meaningfully from the original data on an individual level, which is crucial for ensuring privacy. At the same time, the overall joint distribution is well retained, indicating that the statistical utility is preserved.

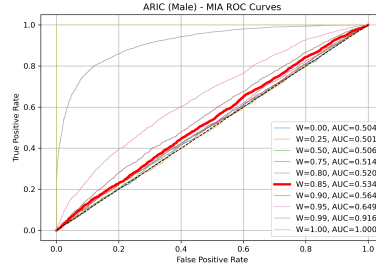
Figure 14 presents boxplots of the real versus synthetic distributions for key variables across all studies, using \hat{w} for each. These visual comparisons indicate that the synthetic data maintain close alignment with real data distributions, suggesting high quality of the trained MAF models.

4.4 Synthetic Data Analysis

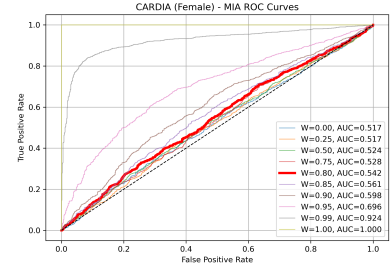
For generated synthetic data of each sub-study, we also fit two Cox Regression models and obtain relevant parameter estimates and their standard errors, which are then aggregated to generate a single estimator for the hazard ratio via the same meta analysis above. The results are reported in Figure 15. The results based on synthetic data are very consistent with those based on original data. For example, after adjusting for age, total cholesterol level, and HDL, the final estimated HR based on synthetic data generated using \hat{w} was 1.148 (95% CI: 1.111 to 1.185) for 10 mmHg difference in SBP, suggesting every 10 mmHg higher in baseline SBP is associated with a 14.8% increase in CVD hazard. This result is fairly close to that based on original data: HR of 1.171 (95% CI: 1.134 to 1.207). On the other hand, when $w = 0$, the HR estimate is further way from that based on original data. Specifically, the adjusted HR estimate is 1.121 (95% CI: 1.084 to 1.158). The results of unadjusted analysis follow a similar pattern. Overall, analyses results based on original data, synthetic data with $w = 0$, and synthetic data with $w = \hat{w}$ all suggest a statistically significant association between SBP level and CVD risk, with the results based on synthetic data generated with $w = \hat{w}$ better reproducing those based on original data. This trend is also observed for individual studies, especially studies with a large sample size.



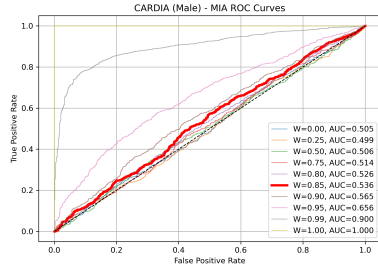
(a) ARIC (Female)



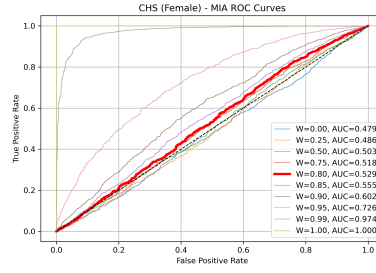
(b) ARIC (Male)



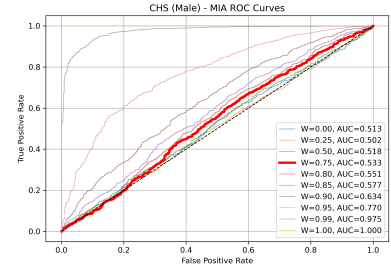
(c) CARDIA (Female)



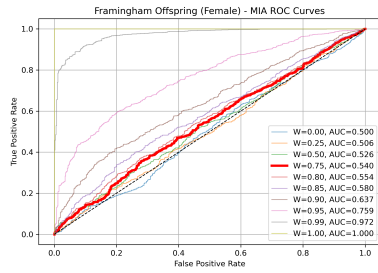
(d) CARDIA (Male)



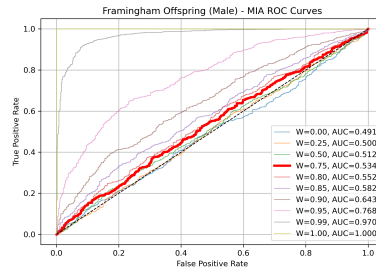
(e) CHS (Female)



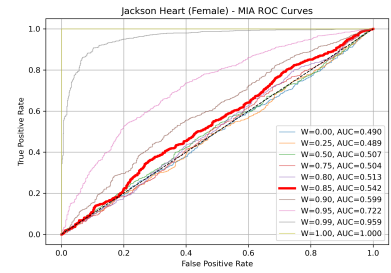
(f) CHS (Male)



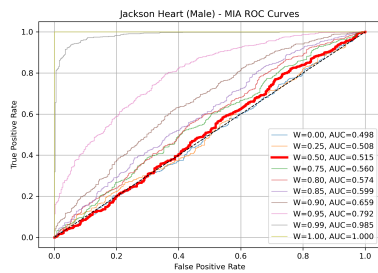
(g) Framingham (Female)



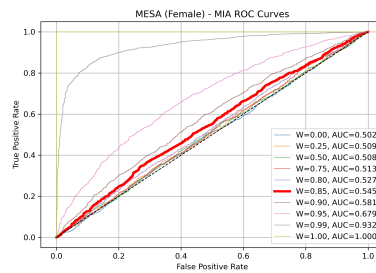
(h) Framingham (Male)



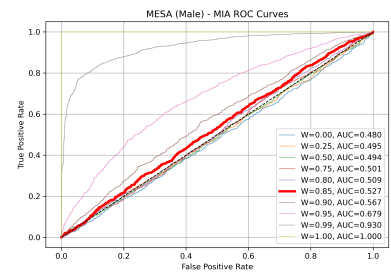
(i) Jackson Heart (Female)



(j) Jackson Heart (Male)



(k) MESA (Female)



(l) MESA (Male)

Figure 10: ROC curves of membership scores in MIA for different w in each sub-study. The red ROC curve corresponds to the selected perturbation size \hat{w} .

Table 5: Selected w for 12 sub-studies.

Study	Best $w = \hat{w}$
ARIC (M)	0.85
ARIC (F)	0.90
CARDIA (M)	0.85
CARDIA (F)	0.80
CHS (M)	0.75
CHS (F)	0.80
MESA (M)	0.85
MESA (F)	0.85
Framingham Off. (M)	0.75
Framingham Off. (F)	0.75
Jackson Heart (M)	0.50
Jackson Heart (F)	0.85

Table 6: The selected $w = \hat{w}$ across 12 sub-studies and privacy protection at $w = 0$. The median refers to the the median ranks (26), and the probability refers to the empirical probability (22). A higher median rank and empirical probability for a study indicates stronger privacy protection. n refers to the sample size of all 12 sub-studies.

Study	w	Median	Probability	n
ARIC (M)	0.00	3389	0.503	6762
	0.85	16	0.015	
ARIC (F)	0.00	4043	0.504	8101
	0.90	10	0.009	
CARDIA (M)	0.00	1156	0.513	2297
	0.85	9	0.027	
CARDIA (F)	0.00	1370	0.508	2743
	0.80	15	0.023	
CHS (M)	0.00	1184	0.479	2413
	0.75	18	0.029	
CHS (F)	0.00	1581	0.492	3254
	0.80	15	0.022	
MESA (M)	0.00	1539	0.506	3176
	0.85	7	0.014	
MESA (F)	0.00	1757	0.512	3552
	0.85	9	0.018	
Framingham (M)	0.00	745	0.489	1608
	0.75	11	0.034	
Framingham (F)	0.00	858	0.498	1766
	0.75	12	0.035	
Jackson Heart (M)	0.00	619	0.515	1196
	0.50	64	0.127	
Jackson Heart (F)	0.00	925	0.525	1913
	0.85	4	0.021	

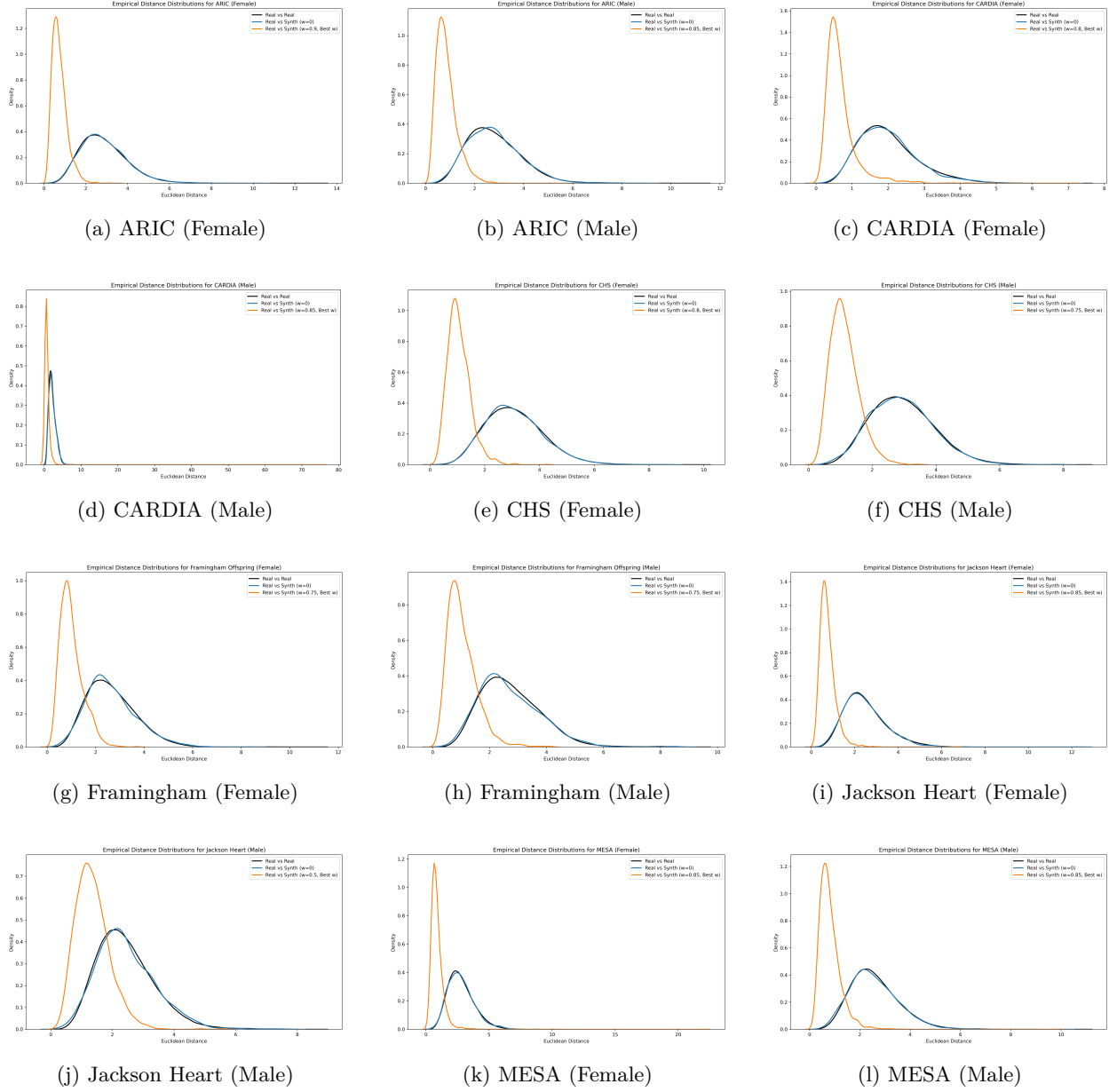


Figure 11: The empirical distribution of pairwise distances between two randomly selected real samples (black); the empirical distribution of pairwise distances between a real sample and its perturbed counterpart with $w = \hat{w}$ (orange); the empirical distribution of pairwise distances between a real sample and its perturbed counterpart with $w = 0$ (blue) for all 12 sub-studies.

Trajectory of Synthetic Data for ARIC (Male)
(3 Random Samples)

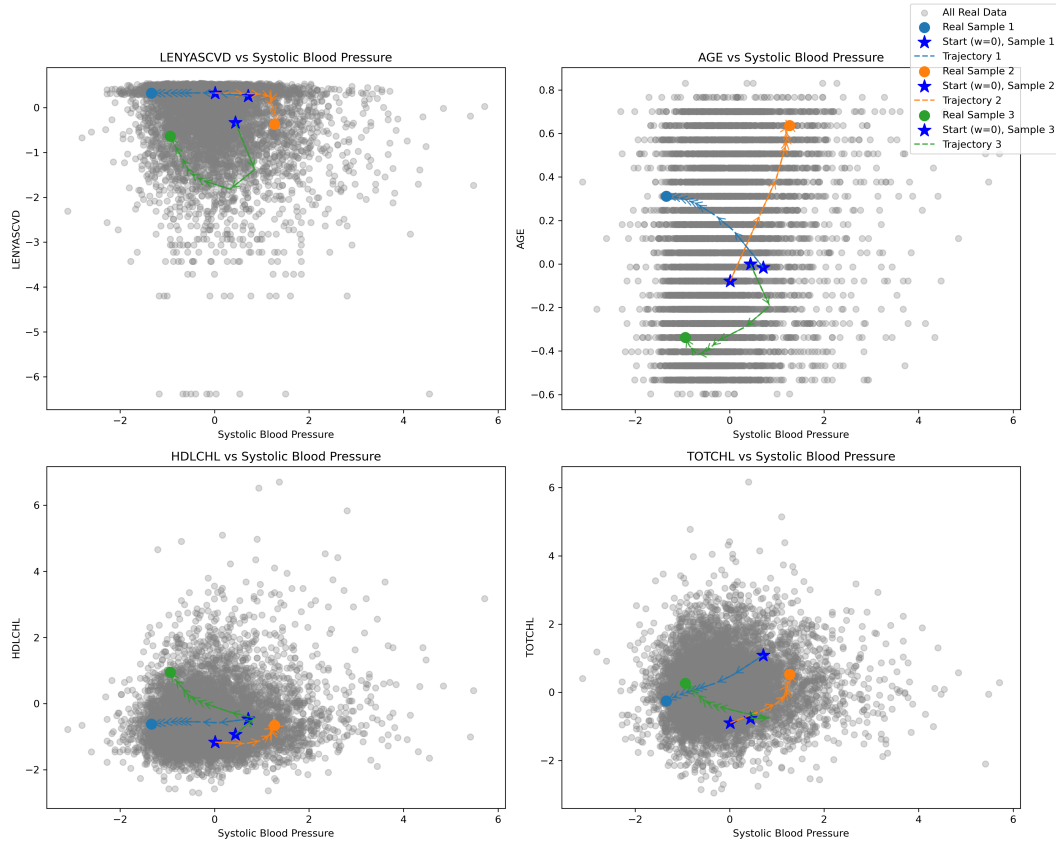
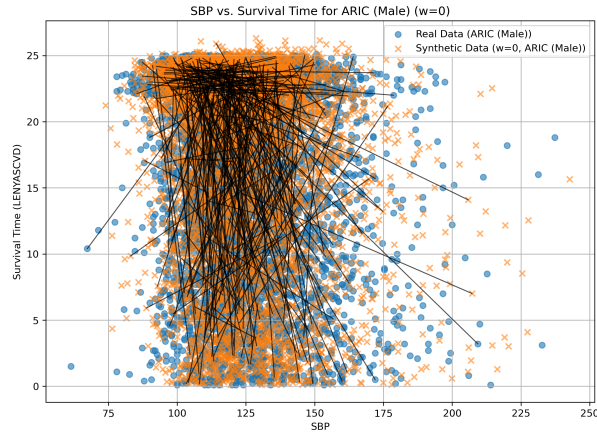
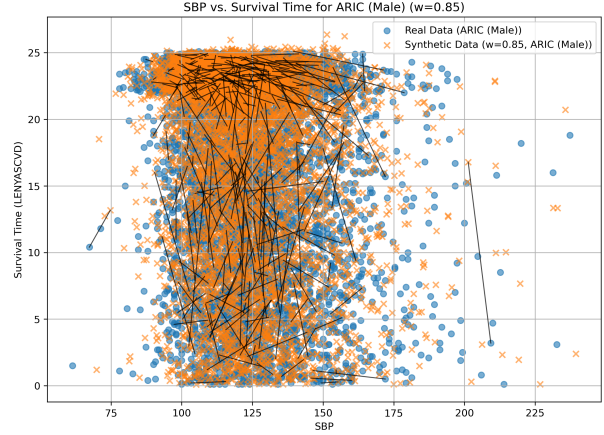


Figure 12: The evolution of 3 randomly selected records as the perturbation weight w increases from 0 to 1 in the ARIC–Male sub-study. All variables are standardized (a min-max logit transformation of years to CVD, and Z-score transformation of age, HDL, and total cholesterol). The scatter plots with SBP as the x-axis serve as a reference density to examine the effect of perturbation. For each of the three individuals, a colored curve starts from its fully perturbed draw at $w = 0$ (star) to its unperturbed value at $w = 1$ (solid circle).

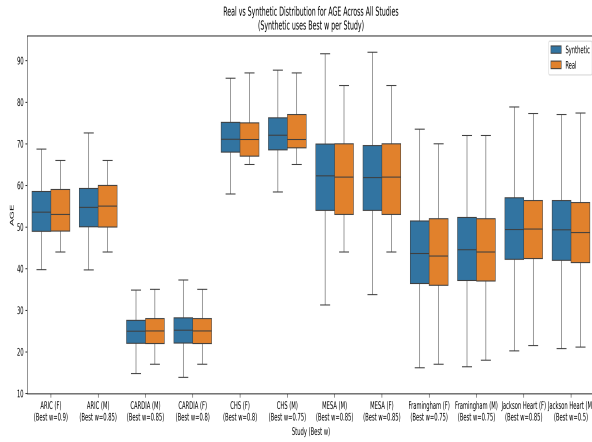


(a) SBP vs. Survival Time (ARIC (Male), $w = 0$), Randomly Sampled 300 Lines Connected

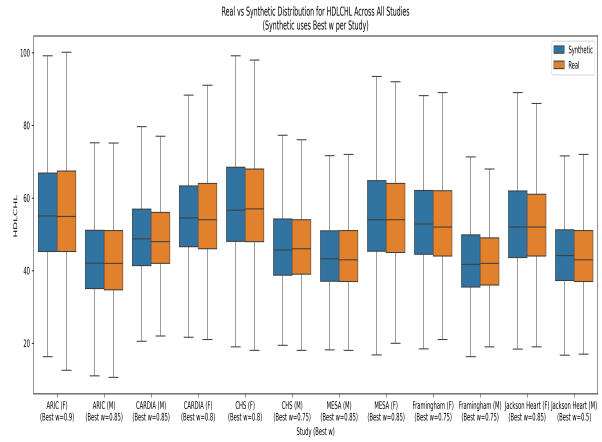


(b) SBP vs. Survival Time (Aric (Male), $w = 0.85$), Randomly Sampled 300 Lines Connected

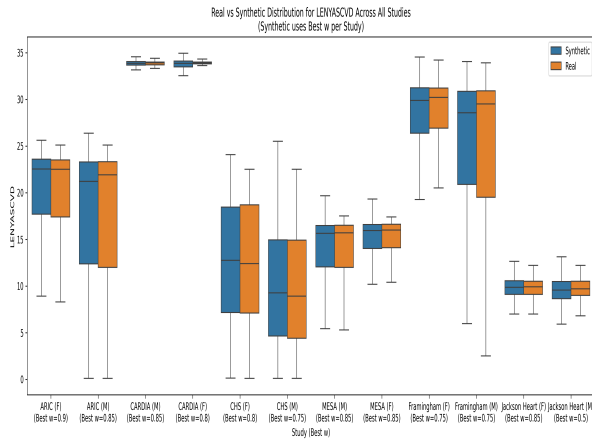
Figure 13: Relationship between SBP (mmHg) and time to CVD (year) in the ARIC–Male sub-study. The left panel shows the high-privacy protection setting with $w = 0$. The right panel shows the setting with selected $\hat{w} = 0.85$; blue circles are observed records and orange crosses are their perturbed counterparts. To visualize record-level perturbation, 300 randomly selected real–synthetic pairs are linked by black line segments.



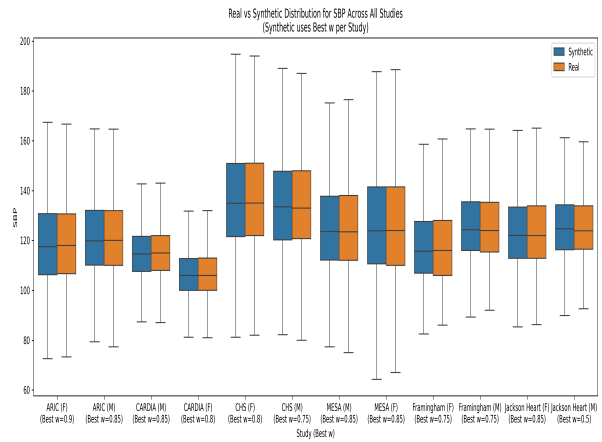
(a) Age (year)



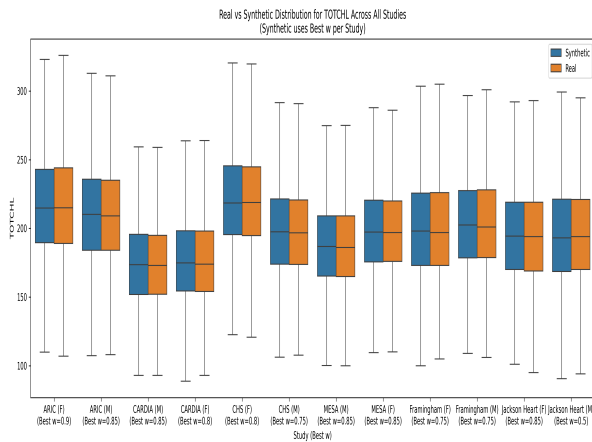
(b) HDL (mg/dL)



(c) Time to CVD Event subject to Right Censoring (year)

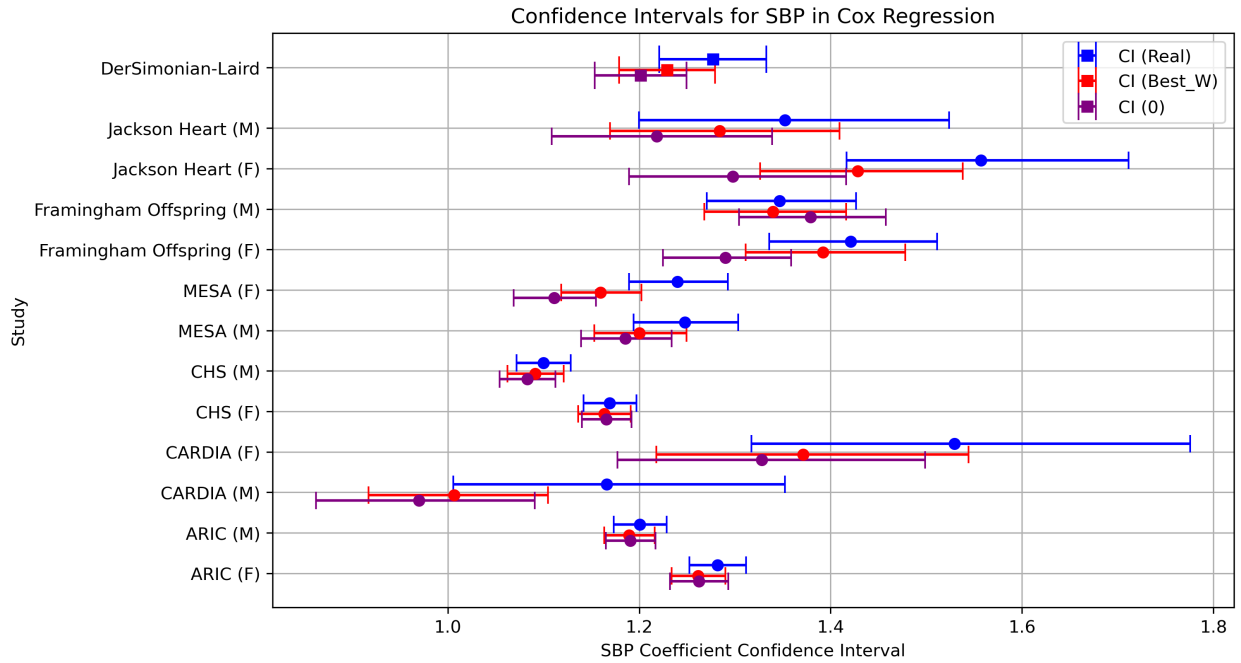


(d) SBP (mmHg)

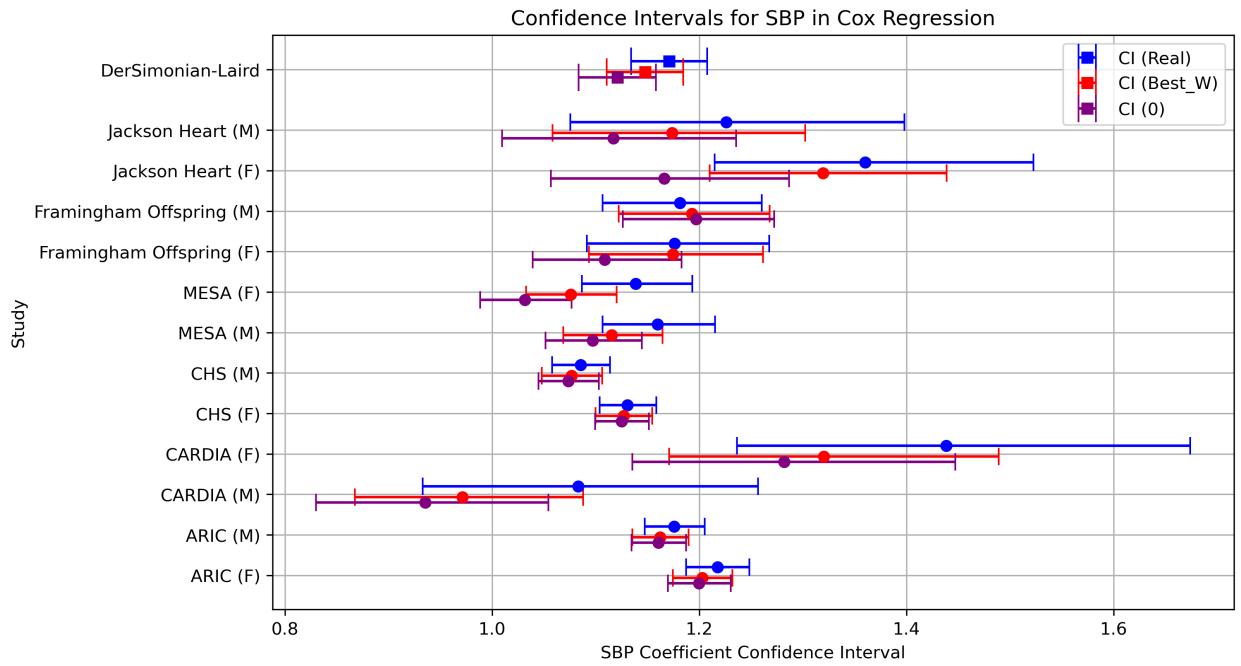


(e) Total Cholesterol Level (mg/dL)

Figure 14: The boxplot of the synthetic data generated with the selected \hat{w} (blue) against that of the real data (orange). A close alignment of medians and quartiles between the two distributions suggests that the synthetic generator preserves the marginal distribution of each variable across 12 sub-studies.



(a) Unadjusted Hazard Ratio Corresponding to 10 mmHg Difference in SBP



(b) Adjusted Hazard Ratio Corresponding to 10 mmHg Difference in SBP (adjusted for Age, Total Cholesterol Level and HDL)

Figure 15: The forest plots for estimated hazard ratio associated with an increase of 10 mmHg in SBP; point estimates and associated 95% CI from individual sub-studies and meta analysis are reported; estimates based on real data are colored blue; estimates based on synthetic data generated with $w = \hat{w}$ are colored red; and estimates based on synthetic data generated with $w = 0$ are colored purple.

By our Latent Noise Injection method and performing inference over K synthetically generated studies, we create a dual benefit: individual level privacy protection and valid statistical inference by retaining similar

statistical properties to support meta analytic conclusions.

4.5 Summary

Our empirical evaluation demonstrates that the MAF model effectively generates synthetic data that preserves the distribution of the original data, and the Latent Noise Injection method can provide reasonable privacy protection when the perturbation size is appropriately selected. With sufficient sample size, the synthetic data closely aligns with the real data and can reproduce results of statistical analysis, such as Cox regression analysis, based on real data reasonably well. When sample size is smaller, the difference in analysis results between synthetic and real data can be greater as expected. In general, the meta analysis results incorporating multiple studies with different sample sizes are even more reproducible with generated synthetic data.

5 Discussion

We proposed a novel method for synthetic data generation using MAF that achieves both high-fidelity replication of statistical properties and strong privacy protection. This is accomplished by coupling flexible generative modeling techniques from the machine learning literature with a simple noise injection mechanism in the latent space. By introducing appropriate perturbations while preserving a one to one mapping between real and synthetic samples, our approach enables accurate reproduction of downstream statistical inference results, including not only point estimates, but also standard errors, CIs, and p -values. Through simulation studies and real data applications, we demonstrated that the synthetic data preserves key associations between covariates and outcomes of interest and can replace the original data for many purposes. Moreover, our method supports valid meta analytic inference across multiple studies, an essential feature for distributed and collaborative research.

Despite these strengths, several limitations remain. First, while the method offers effective privacy protection for most individuals, it may be insufficient for “extreme” observations—those near the boundaries of the data support, where observations are relatively sparse. Intuitively, a larger perturbation is needed for those observations. It would be desirable to design perturbation mechanisms that adapt to individual observations while maintaining global fidelity. Second, although synthetic data is designed to approximate the original data, they remain inherently different due to injected noise and imperfections in the training of the Normalizing Flow. As a result, statistical analyses based on synthetic data always yield results that differ from those based on the original data. It is important to develop tools that allow users to quantify the potential discrepancy between analyses performed on synthetic versus real data using only the synthetic data itself. This is particularly relevant in light of our empirical findings that some parameter estimates can be highly sensitive to small perturbations in the observed data, highlighting the need for caution in finite-sample settings. Third, while MAF serves as a practical and interpretable generative model, more advanced approaches such as Diffusion Models have shown superior performance in high-dimensional settings. Exploring whether such models can replace MAF in our framework is an important direction for future research. Finally, training generative models like MAF typically requires large sample sizes. To address this, one could explore transfer learning approaches that leverage shared structure across datasets, thereby improving generative model training in meta analytic applications involving multiple studies.

References

- Ian Goodfellow, Jean Pouget-Abadie, Mehdi Mirza, Bing Xu, David Warde-Farley, Sherjil Ozair, Aaron Courville, and Yoshua Bengio. Generative Adversarial Networks. *Communications of the ACM*, 63(11): 139–144, 2020.
- Kingma, Diederik P and Welling, Max and Others. An Introduction to Variational Autoencoders. *Foundations and Trends® in Machine Learning*, 12(4):307–392, 2019.
- George Papamakarios, Theo Pavlakou, and Iain Murray. Masked Autoregressive Flow for Density Estimation. *Advances in Neural Information Processing Systems*, 30, 2017.

- Mathieu Germain, Karol Gregor, Iain Murray, and Hugo Larochelle. Made: Masked Autoencoder for Distribution Estimation. In *International Conference on Machine Learning*, pages 881–889. PMLR, 2015.
- George Papamakarios and Iain Murray. Fast ε -free Inference of Simulation Models with Bayesian Conditional Density Estimation. *Advances in Neural Information Processing Systems*, 29, 2016.
- Brooks Paige and Frank Wood. Inference Networks for Sequential Monte Carlo in Graphical Models. In *International Conference on Machine Learning*, pages 3040–3049. PMLR, 2016.
- David Greenberg, Marcel Nonnenmacher, and Jakob Macke. Automatic Posterior Transformation for Likelihood-free Inference. In *International Conference on Machine Learning*, pages 2404–2414. PMLR, 2019.
- Ricky TQ Chen, Yulia Rubanova, Jesse Bettencourt, and David K Duvenaud. Neural Ordinary Differential Equations. *Advances in Neural Information Processing Systems*, 31, 2018.
- Yuan Gao, Jian Huang, Yuling Jiao, and Shurong Zheng. Convergence of Continuous Normalizing Flows for Learning Probability Distributions. *arXiv preprint arXiv:2404.00551*, 2024.
- Shian Du, Yihong Luo, Wei Chen, Jian Xu, and Delu Zeng. To-flow: Efficient Continuous Normalizing Flows with Temporal Optimization Adjoint with Moving Speed. In *Proceedings of the IEEE/CVF Conference on Computer Vision and Pattern Recognition*, pages 12570–12580, 2022.
- Laurent Dinh, Jascha Sohl-Dickstein, and Samy Bengio. Density Estimation using Real Nvp. *arXiv preprint arXiv:1605.08803*, 2016.
- Durk P Kingma and Prafulla Dhariwal. Glow: Generative Flow with Invertible 1x1 Convolutions. *Advances in Neural Information Processing Systems*, 31, 2018.
- Laurent Dinh, David Krueger, and Yoshua Bengio. Nice: Non-linear Independent Components Estimation. *arXiv preprint arXiv:1410.8516*, 2014.
- Durk P Kingma, Tim Salimans, Rafal Jozefowicz, Xi Chen, Ilya Sutskever, and Max Welling. Improved Variational Inference with Inverse Autoregressive Flow. *Advances in Neural Information Processing Systems*, 29, 2016.
- Conor Durkan, Artur Bekasov, Iain Murray, and George Papamakarios. Neural Spline Flows. *Advances in Neural Information Processing Systems*, 32, 2019.
- Lynton Ardizzone, Carsten Lüth, Jakob Kruse, Carsten Rother, and Ullrich Köthe. Guided Image Generation with Conditional Invertible Neural Networks. *arXiv preprint arXiv:1907.02392*, 2019.
- Christina Winkler, Daniel Worrall, Emiel Hoogetboom, and Max Welling. Learning Likelihoods with Conditional Normalizing Flows. *arXiv preprint arXiv:1912.00042*, 2019.
- Brendan McMahan, Eider Moore, Daniel Ramage, Seth Hampson, and Blaise Aguera y Arcas. Communication-Efficient Learning of Deep Networks from Decentralized Data. In *Artificial Intelligence and Statistics*, pages 1273–1282. PMLR, 2017.
- Zhanglong Ji, Zachary C Lipton, and Charles Elkan. Differential Privacy and Machine Learning: a Survey and Review. *arXiv preprint arXiv:1412.7584*, 2014.
- Cynthia Dwork, Frank McSherry, Kobbi Nissim, and Adam Smith. Calibrating Noise to Sensitivity in Private Data Analysis. In *Theory of Cryptography: Third Theory of Cryptography Conference, TCC 2006, New York, NY, USA, March 4-7, 2006. Proceedings 3*, pages 265–284. Springer, 2006.
- Mengmeng Yang, Taolin Guo, Tianqing Zhu, Ivan Tjuawinata, Jun Zhao, and Kwok-Yan Lam. Local Differential Privacy and its Applications: A Comprehensive Survey. *Computer Standards & Interfaces*, 89:103827, 2024.

- Richard D Riley, Paul C Lambert, and Ghada Abo-Zaid. Meta-analysis of Individual Participant Data: Rationale, Conduct, and Reporting. *Bmj*, 340, 2010.
- Xiaotong Shen, Xuan Bi, and Rex Shen. Data Flush. *Harvard Data Science Review*, 4(2):10–1162, 2022.
- Will Grathwohl, Ricky TQ Chen, Jesse Bettencourt, Ilya Sutskever, and David Duvenaud. Ffjord: Free-form Continuous Dynamics for Scalable Reversible Generative Models. *arXiv preprint arXiv:1810.01367*, 2018.
- Yang Cao, Shengtai Li, and Linda Petzold. Adjoint Sensitivity Analysis for Differential-algebraic Equations: Algorithms and Software. *Journal of Computational and Applied Mathematics*, 149(1):171–191, 2002.
- Rebecca DerSimonian and Nan Laird. Meta-Analysis in Clinical Trials. *Controlled Clinical Trials*, 7(3):177–188, 1986.
- David A Harville. Maximum Likelihood Approaches to Variance Component Estimation and to Related Problems. *Journal of the American Statistical Association*, 72(358):320–338, 1977.
- Joanna IntHout, John PA Ioannidis, and George F Borm. The Hartung-Knapp-Sidik-Jonkman Method for Random Effects Meta-Analysis is Straightforward and Considerably Outperforms the Standard DerSimonian-Laird Method. *BMC Medical Research Methodology*, 14:1–12, 2014.
- John E Hunter. Methods of Meta-Analysis: Correcting Error and Bias in Research Findings. *Thousand Oaks, CA*, 2004.
- Haben Michael, Suzanne Thornton, Minge Xie, and Lu Tian. Exact inference on the random-effects model for meta-analyses with few studies. *Biometrics*, 75(2):485–493, 2019.
- Xinyu Tian and Xiaotong Shen. Enhancing Accuracy in Generative Models via Knowledge Transfer. *arXiv preprint arXiv:2405.16837*, 2024.
- Nicolas Fournier and Arnaud Guillin. On the Rate of Convergence in Wasserstein Distance of the Empirical Measure. *Probability Theory and Related Fields*, 162(3):707–738, 2015.
- Cynthia Dwork, Aaron Roth, et al. The Algorithmic Foundations of Differential Privacy. *Foundations and Trends® in Theoretical Computer Science*, 9(3–4):211–407, 2014.
- Ilya Mironov. Rényi Differential Privacy. In *2017 IEEE 30th Computer Security Foundations Symposium (CSF)*, pages 263–275. IEEE, 2017.
- Jamie Hayes, Luca Melis, George Danezis, and Emiliano De Cristofaro. Logan: Membership Inference Attacks against Generative Models. *arXiv preprint arXiv:1705.07663*, 2017.
- Dingfan Chen, Ning Yu, Yang Zhang, and Mario Fritz. Gan-leaks: A Taxonomy of Membership Inference Attacks against Generative Models. In *Proceedings of the 2020 ACM SIGSAC Conference on Computer and Communications Security*, pages 343–362, 2020.
- Takeru Miyato, Toshiki Kataoka, Masanori Koyama, and Yuichi Yoshida. Spectral Normalization for Generative Adversarial Networks. *arXiv preprint arXiv:1802.05957*, 2018.
- George C Casella. *Theory of Point Estimation*. Springer, 2001.
- Duanping Liao, Donna K Arnett, Herman A Tyroler, Ward A Riley, Lloyd E Chambless, Moyses Szklo, and Gerardo Heiss. Arterial Stiffness and the Development of Hypertension: the ARIC Study. *Hypertension*, 34(2):201–206, 1999.
- Maria Ines Schmidt, Bruce B Duncan, Heejung Bang, James S Pankow, Christie M Ballantyne, Sherita H Golden, Aaron R Folsom, Lloyd E Chambless, and Atherosclerosis Risk in Communities Investigators. Identifying Individuals at High Risk for Diabetes: The Atherosclerosis Risk in Communities Study. *Diabetes Care*, 28(8):2013–2018, 2005.

- Mercedes R Carnethon, Catherine M Loria, James O Hill, Stephen Sidney, Peter J Savage, and Kiang Liu. Risk Factors for the Metabolic Syndrome: the Coronary Artery Risk Development in Young Adults (CARDIA) Study, 1985–2001. *Diabetes Care*, 27(11):2707–2715, 2004.
- Gary D Friedman, Gary R Cutter, Richard P Donahue, Glenn H Hughes, Stephen B Hulley, David R Jacobs Jr, Kiang Liu, and Peter J Savage. CARDIA: Study Design, Recruitment, and Some Characteristics of the Examined Subjects. *Journal of Clinical Epidemiology*, 41(11):1105–1116, 1988.
- Linda P Fried, Nemat O Borhani, Paul Enright, Curt D Furberg, Julius M Gardin, Richard A Kronmal, Lewis H Kuller, Teri A Manolio, Maurice B Mittelmark, Anne Newman, et al. The Cardiovascular Health Study: Design and Rationale. *Annals of Epidemiology*, 1(3):263–276, 1991.
- Diane E Bild, David A Bluemke, Gregory L Burke, Robert Detrano, Ana V Diez Roux, Aaron R Folsom, Philip Greenland, David R Jacobs Jr, Richard Kronmal, Kiang Liu, et al. Multi-ethnic Study of Atherosclerosis: Objectives and Design. *American Journal of Epidemiology*, 156(9):871–881, 2002.
- Manning Feinleib, William B Kannel, Robert J Garrison, Patricia M McNamara, and William P Castelli. The Framingham Offspring Study. Design and Preliminary Data. *Preventive Medicine*, 4(4):518–525, 1975.
- Christopher T Sempos, Diane E Bild, and Teri A Manolio. Overview of the Jackson Heart Study: a Study of Cardiovascular Diseases in African American Men and Women. *The American Journal of the Medical Sciences*, 317(3):142–146, 1999.
- Jianfeng Lu, Zuowei Shen, Haizhao Yang, and Shijun Zhang. Deep Network Approximation for Smooth Functions. arXiv e-prints. *arXiv preprint arXiv:2001.03040*, 2020.
- Ernst Hairer, Syvert P. Nørsett, and Gerhard Wanner. *Solving Ordinary Differential Equations I: Nonstiff Problems*, volume 8 of *Springer Series in Computational Mathematics*. Springer, Berlin, Heidelberg, 2nd Revised ed. edition, 1993. ISBN 978-3-540-56670-0. doi: 10.1007/978-3-540-78862-1. URL <https://link.springer.com/book/10.1007/978-3-540-78862-1>.

6 Appendix

6.1 Assumptions and Basic Lemmas

Lemma 2. *Lipschitz Continuity via Spectral Normalization.* For a fixed j , let $f_j^{-1} = \phi^{(L)} \circ W^{(L)} \circ \dots \circ \phi^{(1)} \circ W^{(1)}$ be a neural network composed of linear layers $W^{(\ell)}$ and 1-Lipschitz Activation Functions $\phi^{(\ell)}$ with $f^{-1} = f_1^{-1} \circ \dots \circ f_k^{-1}$ and $l \in \{1, \dots, L\}$, where L is the total number of layers for transport map f_j . We assume the following:

- (a) For each $j \in \{1, \dots, k\}$ and for each layer $l \in \{1, \dots, L\}$, we apply spectral normalization to enforce Lipschitz Continuity:

$$W^{(l)} := \frac{W^{(l)}}{\sigma(W^{(l)})},$$

where $\sigma(W^{(l)})$ is the spectral norm (largest singular value) of $W^{(l)}$ for a layer l and transport map f_j . If spectral normalization is applied to each weight matrix,

$$\|W^{(\ell)}\|_2 = \sigma(W^{(\ell)}) \leq 1 \quad \text{for all } \ell \text{ and } j.$$

- (b) For each $j \in \{1, \dots, k\}$ and for each layer $l \in \{1, \dots, L\}$, $m \leq \sigma_{\min}(W^{(\ell)})$ for some fixed $m > 0$, where $\sigma_{\min}(W^{(\ell)})$ denotes the minimum singular value of $W^{(\ell)}$, and the inverse activations satisfy $\|(\phi^{(\ell)})^{-1}\|_{Lip} \leq 1$.

Then, f is bi-Lipschitz, with the network f^{-1} being 1-Lipschitz, i.e.,

$$\|f^{-1}\|_{\text{Lip}} \leq 1.$$

and f being m^{-kL} -Lipschitz. That is,

$$\|f\|_{\text{Lip}} \leq m^{-kL}.$$

Proof. In the case of a neural network f^{-1} composed of linear layers $W^{(\ell)}$ and 1-Lipschitz Activation Functions, spectral normalization ensures that:

$$\|f^{-1}\|_{\text{Lip}} \leq \prod_{\ell=1}^L \|W^{(\ell)}\| \cdot \|\phi^{(\ell)}\|_{\text{Lip}} \leq \prod_{\ell=1}^L \sigma(W^{(\ell)}),$$

where $\sigma(W^{(\ell)})$ is the spectral norm (largest singular value) of the weight matrix $W^{(\ell)}$. For a Normalizing Flow composed of k functions $f^{-1} = f_1^{-1} \circ \dots \circ f_k^{-1}$, each with L layers, we have:

$$\|f^{-1}\|_{\text{Lip}} \leq \prod_{j=1}^k \prod_{\ell=1}^L \sigma(W^{(\ell)}) \leq 1.$$

To obtain the bound for f , a similar argument shows that

$$\|f\|_{\text{Lip}} \leq \prod_{j=1}^k \frac{1}{m^L} = \frac{1}{m^{kL}}.$$

□

Lemma 3. *Bounded Latent Space.* Let f^{-1} be L -Lipschitz and $\mathcal{X} \subset \mathbb{R}^d$ be compact. Then, $f^{-1}(x)$ is bounded for any $x \in \mathcal{X}$.

Proof. For any $x \in \mathcal{X}$, we have by Triangle Inequality:

$$\|f^{-1}(x)\| \leq \|f^{-1}(x_0)\| + L \cdot \|x - x_0\|.$$

Taking the supremum over $x \in \mathcal{X}$, we obtain:

$$\sup_{x \in \mathcal{X}} \|f^{-1}(x)\| \leq \|f^{-1}(x_0)\| + L \cdot \text{diam}(\mathcal{X}),$$

where $\text{diam}(\mathcal{X}) := \sup_{x, x' \in \mathcal{X}} \|x - x'\|$. Note that it is sufficient to evaluate $f^{-1}(x)$ at a single point $x_0 \in \mathcal{X}$ to bound the inverse over the entire dataset. This relies on the Lipschitz Continuity of f^{-1} and the boundedness of \mathcal{X} . In practice, f^{-1} is implemented as a neural network with bounded weights and Lipschitz Activation Functions, and $\|f^{-1}(x_0)\|$ is finite for a real data point x_0 . Therefore, $f^{-1}(x)$ is bounded over \mathcal{X} . □

7 Proof of Theorem 1

Let $\hat{\theta} = \theta(\hat{P})$ be the estimator computed from the empirical distribution \hat{P} for a study, where \hat{P} is the probability measure induced by n i.i.d. observations in observed data $\mathbf{X} = \{X_1, \dots, X_n\}$. Similarly, $\tilde{\theta}_w = \theta(\hat{P}_w)$ is the estimator computed from the synthetic distribution \hat{P}_w generated by our mechanism with perturbation weight w . Here, $\theta(\cdot)$ is a functional with the first order expansion

$$\theta(\hat{P}) = \theta(\mathcal{P}) + \frac{1}{n} \sum_{i=1}^n l(\mathcal{X}_i) + o_p(n^{-1}),$$

where \hat{P} is the probability measure induced by the empirical distribution of n i.i.d. observations $\mathcal{X}_1, \dots, \mathcal{X}_n \sim \mathcal{P}$. We assume the following:

1. P_X has a continuously differentiable density function over a compact support on \mathbb{R}^d .

2. invertible transport map trained from the MAF, $\hat{f}(\cdot)$, converges to a deterministic invertible transport map $f(\cdot)$ in probability, where $Z = f^{-1}(X) \sim N(0, \mathbf{I}_d)$. Specifically, $\|\hat{f} - f\|_2 = O_p(\delta_{1n})$ for $\delta_{1n} = o(1)$.
3. $\hat{f}(\cdot)$ and $f(\cdot)$ are uniformly bi-Lipchitz Continuous on the support of X .
4. Both f and \hat{f} are members of a class of functions $\mathcal{F} = \{f_\theta\}$, and the class of functions

$$\mathcal{L} = \{l[\tilde{f}(\sqrt{w}\tilde{f}^{-1}(x) + \sqrt{1-w}z)] \mid w \in [0, 1], \|\tilde{f} - f\|_2 \leq \epsilon_n, \tilde{f}(\cdot) \in \mathcal{F} : \mathbb{R}^d \rightarrow \mathbb{R}^d\}$$

is a Donsker Class.

5. $l(\cdot)$ is continuously differentiable on \mathbb{R}^d .
6. $1 - w = o(\delta_{2n})$ for $\delta_{2n} = o(1)$.

Then, we have

$$\theta(\hat{P}_w) - \theta(\hat{P}) = O_p\left(\delta_{1n}^2 + \delta_{1n}\sqrt{\delta_{2n}}\right) + o_p(n^{-1/2}).$$

Proof. First, we show the result under $\theta(P_X) = E(X)$, and $X \sim P_X$. In the case where $\theta(P_X) = E(X)$,

$$\begin{aligned}\sqrt{n}\{\theta(\hat{P}) - \theta(P_X)\} &= \frac{1}{\sqrt{n}} \sum_{i=1}^n X_i, \\ \sqrt{n}\{\theta(\hat{P}_w) - \theta(P_w)\} &= \frac{1}{\sqrt{n}} \sum_{i=1}^n \hat{f}(\sqrt{w}\hat{f}^{-1}(X_i) + \sqrt{1-w}Z_i),\end{aligned}$$

where $X_1, \dots, X_n \sim P_X$ and $Z_1, \dots, Z_n \sim N(0, \mathbf{I}_d)$. Specifically, it follows from the stochastic equi-continuity guaranteed by the Donsker Class that

$$\sqrt{n}\{\theta(\hat{P}) - \theta(\hat{P}_w)\} = \sqrt{n}\{\theta(P_X) - \theta(P_w)\} + o_p(1),$$

where $1 - w = o(1)$. We may bound the difference

$$\begin{aligned}&\theta(P_w) - \theta(P_X) \\ &= E\{\hat{f}(\sqrt{w}\hat{f}^{-1}(X) + \sqrt{1-w}Z)\} - E(X) \\ &= E\{\hat{f}(\sqrt{w}\hat{f}^{-1}(X) + \sqrt{1-w}Z)\} - E\{\hat{f}(\sqrt{w}f^{-1}(X) + \sqrt{1-w}Z)\} + E\{\hat{f}(\sqrt{w}f^{-1}(X) + \sqrt{1-w}Z)\} - E(X) \\ &= E[\nabla\hat{f}\{\sqrt{w}f^{-1}(X) + \sqrt{1-w}Z\}\sqrt{w}\{\hat{f}^{-1}(X) - f^{-1}(X)\}] + E[\hat{f}\{f^{-1}(X)\} - \hat{f}\{\hat{f}^{-1}(X)\}] + O(\|\hat{f}^{-1} - f^{-1}\|_2^2).\end{aligned}$$

Note, to rigorously justify the last equality, we apply a first-order Taylor Expansion of the map \hat{f} at the point

$$u := \sqrt{w}f^{-1}(X) + \sqrt{1-w}Z$$

with perturbation

$$\delta := \sqrt{w}\{\hat{f}^{-1}(X) - f^{-1}(X)\},$$

so that

$$\sqrt{w}\hat{f}^{-1}(X) + \sqrt{1-w}Z = u + \delta.$$

Since \hat{f} from MAF is differentiable with Lipschitz Continuous Jacobian, we expand

$$\hat{f}(u + \delta) = \hat{f}(u) + \nabla\hat{f}(u) \cdot \delta + R,$$

where the remainder term satisfies $\|R\| = O(\|\delta\|^2) = O(\|\hat{f}^{-1}(X) - f^{-1}(X)\|^2)$. Then, from taking expectations on both sides, we obtain

$$\begin{aligned}&E[\hat{f}(\sqrt{w}\hat{f}^{-1}(X) + \sqrt{1-w}Z)] \\ &= E[\hat{f}(u)] + E[\nabla\hat{f}(u) \cdot \delta] + E[R],\end{aligned}$$

which yields

$$\begin{aligned} & E[\hat{f}(\sqrt{w}\hat{f}^{-1}(X) + \sqrt{1-w}Z)] - E[\hat{f}(\sqrt{w}f^{-1}(X) + \sqrt{1-w}Z)] \\ &= E[\nabla\hat{f}\{\sqrt{w}f^{-1}(X) + \sqrt{1-w}Z\} \cdot \sqrt{w}\{\hat{f}^{-1}(X) - f^{-1}(X)\}] + E\{O(\|\hat{f}^{-1}(X) - f^{-1}(X)\|_2^2)\}, \end{aligned}$$

where

$$E\{O(\|\hat{f}^{-1}(X) - f^{-1}(X)\|_2^2)\} = O\{E(\|\hat{f}^{-1}(X) - f^{-1}(X)\|_2^2)\} = O\{E(\|\hat{f}(Z) - f(Z)\|_2^2)\} = O(\|\hat{f} - f\|_2^2)$$

since $\hat{f}(\cdot)$ and $f(\cdot)$ are uniformly bi-Lipschitz Continuous by assumption. Finally, notice that $E[X] = E[\hat{f}\{\hat{f}^{-1}(X)\}]$ and $\sqrt{w}f^{-1}(X) + \sqrt{1-w}Z \sim N(0, \mathbf{I}_d)$. This justifies the third equality in the original derivation. Now, we note that

$$\begin{aligned} & \underbrace{E[\nabla\hat{f}\{\sqrt{w}f^{-1}(X) + \sqrt{1-w}Z\} \sqrt{w}\{\hat{f}^{-1}(X) - f^{-1}(X)\}]}_{(1)} \\ & \quad + \underbrace{E[\hat{f}\{f^{-1}(X)\} - \hat{f}\{\hat{f}^{-1}(X)\}]}_{(2)} + O(\|\hat{f} - f\|_2^2) \\ &= O(\|\hat{f} - f\|_2^2 + \sqrt{1-w}\|\hat{f}^{-1} - f^{-1}\|_2 + (1-w)\|\hat{f}^{-1} - f^{-1}\|_2) \\ &= O(\|\hat{f} - f\|_2^2 + \sqrt{1-w}\|\hat{f} - f\|_2). \end{aligned}$$

To bound (2), we have that

$$\begin{aligned} & E[\hat{f}(f^{-1}(X)) - \hat{f}(\hat{f}^{-1}(X))] \\ &= -E[\nabla\hat{f}(f^{-1}(X)) \cdot (\hat{f}^{-1}(X) - f^{-1}(X))] + E[O(\|\hat{f} - f\|_2^2)], \end{aligned}$$

where we used the bi-Lipschitz Continuous property of \hat{f} and f . To bound (1), we have that

$$E[\{\hat{f}^{-1}(X) - f^{-1}(X)\} m(w)] = E[\{\hat{f}^{-1}(X) - f^{-1}(X)\} [m(1) - \nabla m(1)(1-w) + o(|w-1|)]] \quad (27)$$

where $m(w) = \sqrt{w}\nabla\hat{f}\{\sqrt{w}f^{-1}(X) + \sqrt{1-w}Z\}$. Note that $E[\{\hat{f}^{-1}(X) - f^{-1}(X)\} m(1)]$ cancels with

$$-E[\nabla\hat{f}(f^{-1}(X)) \cdot (\hat{f}^{-1}(X) - f^{-1}(X))]$$

after taking expectation in (2). Moreover,

$$\begin{aligned} \nabla m(w) &= \frac{1}{2\sqrt{w}}\nabla\hat{f}\{\sqrt{w}f^{-1}(X) + \sqrt{1-w}Z\} \\ & \quad + \sqrt{w}\nabla^2\hat{f}\{\sqrt{w}f^{-1}(X) + \sqrt{1-w}Z\} \left(\frac{f^{-1}(X)}{2\sqrt{w}} - \frac{Z}{2\sqrt{1-w}} \right). \end{aligned} \quad (28)$$

Note that

$$\frac{1}{2\sqrt{w}}\nabla\hat{f}\{\sqrt{w}f^{-1}(X) + \sqrt{1-w}Z\} \rightarrow \frac{1}{2}\nabla\hat{f}\{f^{-1}(X)\}$$

and that

$$\frac{f^{-1}(X)}{2\sqrt{w}} - \frac{Z}{2\sqrt{1-w}} \sim -\frac{Z}{2\sqrt{1-w}},$$

so for the second term in (28),

$$\sqrt{w}\nabla^2\hat{f}\{\sqrt{w}f^{-1}(X) + \sqrt{1-w}Z\} \left(\frac{f^{-1}(X)}{2\sqrt{w}} - \frac{Z}{2\sqrt{1-w}} \right) \sim \frac{-\sqrt{w}Z\nabla^2\hat{f}\{\sqrt{w}f^{-1}(X) + \sqrt{1-w}Z\}}{2\sqrt{1-w}}.$$

Notice that we have an extra $(1-w)$ in front of $\nabla m(1)$ in (27), which cancels the denominator and so we have an extra $\sqrt{1-w}$ in the numerator which approaches 0 as $w \rightarrow 1$. In total,

$$\begin{aligned} E[\{\hat{f}^{-1}(X) - f^{-1}(X)\} m(w)] &= E[\{\hat{f}^{-1}(X) - f^{-1}(X)\} [-\nabla m(1)(1-w) + O((w-1)^2)]] \\ &= E[\{\hat{f}^{-1}(X) - f^{-1}(X)\} \left[-\frac{1}{2} \nabla \hat{f} \{f^{-1}(X)\} (1-w) + O((1-w)^2)\right]]. \end{aligned}$$

With regard to expectation and applying Cauchy Schwartz, we have

$$\begin{aligned} &E\left[\{\hat{f}^{-1}(X) - f^{-1}(X)\} \left[-\frac{1}{2} \nabla \hat{f} \{f^{-1}(X)\} (1-w) + O((1-w)^2)\right]\right] \\ &= O(\|\hat{f}^{-1} - f^{-1}\|_2 \sqrt{1-w}) + O((1-w) \|\hat{f}^{-1} - f^{-1}\|_2). \end{aligned}$$

The result follows from applying the bi-Lipschitz property of f . Thus,

$$\theta(\hat{P}) - \theta(\hat{P}_w) = O_p(\delta_{1n}^2 + \delta_{1n} \sqrt{\delta_{2n}}) + o_p(n^{-1/2})$$

follows. For the general case,

$$\begin{aligned} \sqrt{n}(\theta(\hat{P}) - \theta(P)) &= \frac{1}{\sqrt{n}} \sum_{i=1}^n l(X_i) + o_p(1), \\ \sqrt{n}(\theta(\hat{P}_w) - \theta(P_w)) &= \frac{1}{\sqrt{n}} \sum_{i=1}^n l\{\hat{f}(\sqrt{w} \hat{f}^{-1}(X_i)) + \sqrt{1-w} Z_i\} + o_p(1). \end{aligned}$$

It follows from the stochastic equi-continuity guaranteed by the Donsker Class that

$$\sqrt{n}\{\theta(\hat{P}) - \theta(\hat{P}_w)\} = \sqrt{n}\{\theta(P_X) - \theta(P_w)\} + o_p(1).$$

Since $l(\cdot)$ is continuous differentiable on a compact set, we may bound $\theta(P_X) - \theta(P_w)$ by $O_p(\delta_{1n}^2 + \delta_{1n} \sqrt{\delta_{2n}})$ as before. Therefore,

$$\theta(\hat{P}) - \theta(\hat{P}_w) = O_p(\delta_{1n}^2 + \delta_{1n} \sqrt{\delta_{2n}}) + o_p(n^{-1/2}).$$

□

7.1 Proof Sketch of the Convergence Rate of the Transport Map

Lemma 4 (Excess Risk of Flow Matching for s -Smooth Densities). *Assume Assumptions 1–2 in Gao et al. (2024) hold. In particular,*

1. *A1: the target distribution ν of the data is absolutely continuous w.r.t. Lebesgue Measure on \mathbb{R} and has zero mean.*
2. *A2: We have at least one of the following for the target distribution: strongly log concave, bounded support, and/or gaussian mixture tails. These are special cases that capture common distributions in generative modeling. See Assumption 2 of Gao et al. (2024) for Detail.*

We will also assume the underlying density belongs to $C^s([0, 1]^d) \subseteq W^{s, \infty}([0, 1]^d)$ with an integer smoothness index $s \geq 1$. Then,¹ if

$$NL \asymp n^{d/(2d+4s+2)}, \quad A \asymp \sqrt{\log n},$$

where N is the network width, L its depth, and A the parameter-norm bound in the hypothesis class, the excess risk incurred by the flow-matching estimator satisfies

$$E_{\mathcal{D}_n} E_{(t, X_t)} \|v_{\hat{\theta}}(t, X_t) - v_{\theta}(t, X_t)\|_2^2 \lesssim (nt^2)^{-\frac{2s}{2s+d+1}} \log n$$

up to polylogarithmic factors, where D_n is over the dataset of sample size n and $v_{\hat{\theta}}(t, X_t)$ is the estimated velocity field, $v_{\theta}(t, X_t)$ is the true velocity field, which were defined in (6).

Hence, the rate can be made arbitrarily close to the parametric order $n^{-1} \log n$ as $s \rightarrow \infty$.

¹Note, the proportionality symbols hide at most polylogarithmic factors in n and $\log(1/t)$. Moreover, constants may additionally depend on $d, \kappa, \beta, \sigma, D$ and R .

Proof Sketch. We follow the strategy of Gao et al. (2024, Thm. 5.12), extending it from the First-Order Sobolev Class $W^{1,\infty}$ to $W^{s,\infty}$. Specifically, the proof can be completed in three steps.

- **Bound the Approximation Error:** For any $f \in C^s([0, 1]^d)$ the constructive result of Lu et al. (2020, Thm. 1.1) states that for any $N, L \in \mathbb{N}^+$, there exists a function ϕ implemented by a ReLU feed forward neural network (FNN) with width $C_1(N+2)\log_2(8N)$ and depth $C_2(L+2)\log_2(4L)+2d$ such that

$$\|\phi - f\|_{L^\infty([0,1]^d)} \leq C_3 \|f\|_{C^s([0,1]^d)} N^{-2s/d} L^{-2s/d},$$

² where $C_1 = 17s^{d+1}3^d$, $C_2 = 18s^2$, and $C_3 = 85(s+1)^d 8^s$. Specializing this bound to the target vector field v_θ and inserting it into the Sobolev-Type Stability Estimate of Flow Matching in Corollary 5.9 of Gao et al. (2024) gives

$$\mathcal{E}_{\text{appr}} \lesssim A^2 (NL)^{-4s/d} + A^2 \exp(-C_3 A^2 / C_{\text{LSI}}),$$

where $C_3 > 0$ and $C_{\text{LSI}} > 0$ are constants. The exponential ‘‘tail’’ term is sub-dominant for the choice $A \asymp \sqrt{\log n}$ adopted below.

- **Bound the Stochastic Error:** Corollary 5.11 and Appendix C.4 of Gao et al. (2024) bounds the stochastic error by

$$\mathcal{E}_{\text{stoc}} \lesssim \frac{1}{n} A^4 t^{-2} (NL)^{2+2/d}.$$

- **Balancing the Errors:** Then, ignoring logarithmic factors in A and t , we equate the leading terms

$$\frac{1}{n} (NL)^{2+2/d} = (NL)^{-4s/d} \Rightarrow (NL)^{2+\frac{2}{d}+\frac{4s}{d}} = n \Rightarrow NL \asymp n^{d/(2d+4s+2)},$$

we get

$$NL \asymp n^{d/(2d+4s+2)}.$$

Substituting this choice and $A \asymp \sqrt{\log n}$ back into the dominant component of $\mathcal{E}_{\text{appr}}$ yields

$$E_{\mathcal{D}_n} E_{(t, X_t)} \|v_{\hat{\theta}}(t, X_t) - v_\theta(t, X_t)\|_{L^2}^2 \lesssim (nt^2)^{-2s/(2s+d+1)} \log n,$$

as the additional factor $(t^2)^{-2s/(2s+d+1)}$ appears after rescaling time in the flow-matching loss (cf. Lemma 5.2 of Gao et al. (2024)).

□

Theorem 4 (Convergence Rate for MAF with Sobolev Smoothness s). *We let the true transport map $f = f_k \circ \dots \circ f_1 : \mathbb{R}^d \rightarrow \mathbb{R}^d$ belong to the Sobolev Space $W^{s,\infty}([0, 1]^d)$ for some integer $s \geq 1$. We assume the assumptions of Lemma 4 hold. We also assume $v_{\hat{\theta}}$ and v_θ are both L' -Lipschitz with a uniform bound M .*

Now, set $\hat{f} = \hat{f}_k \circ \dots \circ \hat{f}_1$ to be the output of a flow-matching estimator (e.g., trained via MAF) with network width N , depth L , and parameter norm bounded by $A \asymp \sqrt{\log n}$. Then, under these assumptions and up to polylogarithmic factors in n , there exists width, depth, and Euler Discretization step size δ_n choices:

$$NL \asymp n^{d/(2d+4s)}, \quad \delta_n^s \asymp O(n^{-s/(2s+d+1)} \log n)$$

such that the estimator \hat{f} satisfies the excess risk bound:

$$E_{\mathcal{D}_n} \|\hat{f} - f\|_{L^2}^2 \lesssim n^{-\frac{2s}{2s+d+1}} \log n,$$

where \mathcal{D}_n denotes a dataset of n i.i.d. samples. Moreover, as $s \rightarrow \infty$, the rate approaches the parametric rate $n^{-1} \log n$.

²The boundedness of $\|f\|_{C^s([0,1]^d)}$ follows by assumption.

Proof Sketch. Rather than the Continuous-Time CNF considered in Gao et al. (2024), tailoring to the MAF in our setting, the only substantive change in the analysis is that the auxiliary time variable $t \in [0, 1]$ is absent.

Lemma 4 shows that under regularity conditions for Continuous Normalizing Flows with time component $t \in [t_0, T] = [0, 1]$ as in (5), the estimated velocity field $v_{\hat{\theta}}(t, x)$ converges to the true velocity field $v_{\theta}(t, x) \in W^{s, \infty}$ appearing in (6), which satisfies

$$\|v_{\hat{\theta}}(t, x) - v_{\theta}(t, x)\|_2 = O(n^{-s/(2s+d+1)} \log n). \quad (29)$$

We investigate what this velocity function becomes in the MAF setting as an intuitive guide.

First, assume $v_{\theta}(t, x) \in W^{1, \infty}$. The estimated transport map constructed from $v_{\hat{\theta}}$ is defined by a discretized Euler scheme over J_n time steps, which depends on sample size n and can be approximated as:

$$\begin{aligned} \hat{f}(z) &= \hat{x}_{J_n-1} + \delta_n v_{\hat{\theta}}(t_{J_n-1}, \hat{x}_{J_n-1}) \\ \hat{x}_{J_n-1} &= \hat{x}_{J_n-2} + \delta_n v_{\hat{\theta}}(t_{J_n-2}, \hat{x}_{J_n-2}) \\ &\dots \\ \hat{x}_2 &= x_1 + \delta_n v_{\hat{\theta}}(t_1, \hat{x}_1) \\ \hat{x}_1 &= z + \delta_n v_{\hat{\theta}}(t_0, z) \\ \hat{x}_0 &= z, \end{aligned}$$

where $0 = t_0, t_1, \dots, t_{J_n-1}, t_{J_n} = 1$ are $J_n + 1$ equal-spaced points in the unit interval $[0, 1]$ and $\delta_n = J_n^{-1}$, such that $t_j = j\delta_n$. This iterative update scheme defines an explicit Euler method for numerically integrating the estimated velocity field. Similarly, for the true velocity field v_{θ} ,

$$\begin{aligned} \tilde{f}(z) &= \tilde{x}_{J_n-1} + \delta_n v_{\theta}(t_{J_n-1}, \tilde{x}_{J_n-1}) \\ \tilde{x}_{J_n-1} &= \tilde{x}_{J_n-2} + \delta_n v_{\theta}(t_{J_n-2}, \tilde{x}_{J_n-2}) \\ &\dots \\ \tilde{x}_2 &= \tilde{x}_1 + \delta_n v_{\theta}(t_1, \tilde{x}_1) \\ \tilde{x}_1 &= z + \delta_n v_{\theta}(t_0, z) \\ \tilde{x}_0 &= z. \end{aligned}$$

Define $f(z) = x(1)$ from the exact ODE

$$\frac{dx_t}{dt} = v_{\theta}(t, x_t), \quad x_0 = z, \quad t \in [0, 1]. \quad (30)$$

Then, by Triangle Inequality,

$$\|\hat{f} - f\|_2 \leq \underbrace{\|\hat{f} - \tilde{f}\|_2}_{\text{Field Mismatch Error}} + \underbrace{\|\tilde{f} - f\|_2}_{\text{Euler Discretization Error}}.$$

By assumption, since $v_{\hat{\theta}}(t, x)$ and $v_{\theta}(t, x)$ are both L' -Lipschitz with a uniform bound M , then, the global bound (i.e., (Hairer et al., 1993)) gives

$$\|\tilde{f} - f\| \leq C_1 \delta_n, \quad C_1 = C_1(L', M),$$

where C_1 is a constant depending on L' and M . Set $e_j := \tilde{x}_j - \hat{x}_j$ ($e_0 = 0$). Note,

$$e_{j+1} = e_j + \delta_n (v_{\hat{\theta}}(t_j, \tilde{x}_j) - v_{\theta}(t_j, \hat{x}_j)) = e_j + \delta_n (v_{\hat{\theta}}(t_j, \tilde{x}_j) - v_{\theta}(t_j, \tilde{x}_j) + v_{\theta}(t_j, \tilde{x}_j) - v_{\theta}(t_j, \hat{x}_j)).$$

After taking norms, using Triangle Inequality, and applying the Lipschitz Continuity of v_{θ} ,

$$\|e_{j+1}\| \leq (1 + L'\delta_n)\|e_j\| + \delta_n \|v_{\hat{\theta}} - v_{\theta}\|.$$

The Discrete Gronwall Inequality implies

$$\|\hat{f} - \tilde{f}\| = \|e_{J_n}\| \leq C_2 \delta_n \|v_{\hat{\theta}} - v_{\theta}\|,$$

for some constant C_2 depending on L' . Then,

$$\|\hat{f} - f\| \leq C(\delta_n \|v_{\hat{\theta}} - v_{\theta}\|_2 + \delta_n), \quad C = \max\{C_1, C_2\}.$$

Then, choosing $\delta_n \asymp n^{-s/(2s+d+1)} \log n$ (i.e. $J_n \asymp n^{s/(2s+d+1)}/\log n$) gives

$$\|\hat{f} - f\|_2 = O(n^{-s/(2s+d+1)} \log n).$$

Now, specifying v_{θ} to be smoother with smoothing parameter $s \geq 1$, a higher-order of order s is used with the discretization term being $O(\delta^s)$. Balancing K and δ^s as above matches the same desired result. Thus, by assuming more smoothness on v_{θ} , we can establish a new convergence rate

$$\|\hat{f} - f\|_2 = o(n^{-s/(2s+d+1)+\delta_0}),$$

for any $\delta_0 > 0$. □

7.2 Proof of Lemma 1 and Theorem 2 for (ϵ, δ) Local Differential Privacy

Lemma 1. Set $\mathcal{M}(\cdot)$ to be the perturbation generated by applying Gaussian noise

$$\mathcal{M}(g(x)) = g(x) + N(0, \sigma^2 \mathbf{I}_d), \quad (31)$$

where $g(x) \in \mathbb{R}^d$ is a function such that its sensitivity

$$\Delta_2(g) = \sup_{\|x-y\|_2 \leq 1} \|g(x) - g(y)\|_2 \quad (32)$$

is bounded, i.e., $\Delta_2(g) \leq B$, for a constant $B > 0$. Then, the mechanism $\mathcal{M}(\cdot)$ satisfies (α, ϵ_R) Local RDP of order α with

$$\epsilon_R = \frac{\alpha \times \Delta_2(g)^2}{2\sigma^2}.$$

Proof. Observe that

$$D_{\alpha}(P||Q) = \frac{1}{\alpha-1} \log E_{x \sim Q} \left[\left(\frac{p(x)}{q(x)} \right)^{\alpha} \right]$$

where $\alpha > 1$. Then, if $P \sim N(\mu_1, \sigma^2 \mathbf{I}_d)$ and $Q \sim N(\mu_2, \sigma^2 \mathbf{I}_d)$, we get that

$$\begin{aligned} \frac{p(x)}{q(x)} &= \exp\left(\frac{1}{2\sigma^2} [\|x - \mu_2\|_2^2 - \|x - \mu_1\|_2^2]\right) = \exp\left(\frac{1}{2\sigma^2} [\|x - \mu_2\|_2^2 - \|x - \mu_2 + \mu_2 - \mu_1\|_2^2]\right) \\ &= \exp\left(\frac{1}{\sigma^2} (x - \mu_2)^T (\mu_2 - \mu_1) - \frac{1}{2\sigma^2} \|\mu_2 - \mu_1\|_2^2\right). \end{aligned}$$

Raising this to α and simplifying, we get that

$$D_{\alpha}(P||Q) = \frac{1}{\alpha-1} \log \left(\exp\left(-\frac{\alpha}{2\sigma^2} \|\mu_2 - \mu_1\|_2^2\right) E\left[\exp\left(\frac{\alpha \|\mu_2 - \mu_1\|_2}{\sigma} Z\right)\right] \right),$$

where $Z \sim N(0, 1)$. By MGF of Z , this simplifies to

$$D_{\alpha}(P||Q) = \frac{(\alpha^2 - \alpha)(\|\mu_2 - \mu_1\|_2^2)}{2\sigma^2(1 - \alpha)} = \frac{\alpha \|\mu_2 - \mu_1\|_2^2}{2\sigma^2}.$$

Specializing for our problem, our mechanism $\mathcal{M}(\cdot) = g(x) + N(0, \sigma^2 \mathbf{I}_d)$ satisfies Local (α, ϵ_R) RDP privacy with

$$\frac{\alpha \|g(x) - g(y)\|_2^2}{2\sigma^2} \leq \frac{\alpha (\Delta_2(g))^2}{2\sigma^2} = \epsilon_R. \quad \square$$

Theorem 2. First, consider a trained MAF transport map, $\hat{f} = \hat{f}_k \circ \dots \circ \hat{f}_1$, where each $\hat{f}_j, j \in \{1, \dots, k\}$ has mapping defined in (3). We assume the following:

1. each function $\mu_i(\cdot)$ and $\sigma_i(\cdot)$ in (3) are trained neural networks whose layers are spectrally normalized with the same number of layers L for each $\hat{f}_j, j \in \{1, \dots, k\}$. That is, each weight matrix has spectral norm at most 1.
2. the data domain $\mathcal{X} \subset \mathbb{R}^d$ is compact.
3. \hat{f} converges to a deterministic transport map f uniformly in probability as the sample size increases and the sensitivity of f^{-1} is bounded, i.e., $\Delta_2(f^{-1}) < C$ for a constant C .

Now, let

$$\tilde{\mathcal{M}}(x) = \sqrt{w}\hat{f}^{-1}(x) + \sqrt{1-w}Z, \quad (33)$$

where $w \in (0, 1)$ is a parameter controlling the perturbation size and $Z \sim N(0, \mathbf{I}_d)$. Then, the mechanism $\hat{f}\{\tilde{\mathcal{M}}(\cdot)\}$ satisfies (ϵ^*, δ) -Local DP for any $0 < \delta < 1$ and a prescribed $\epsilon^* > 0$ and some constant $C' > 0$, with

$$\epsilon^* = \frac{wC'^2}{2(1-w)} + \frac{C'\sqrt{2w\log(1/\delta)}}{\sqrt{1-w}}$$

in probability, i.e.,

$$\mathbb{P}\left(\mathbb{P}[\hat{f}\{\tilde{\mathcal{M}}(x)\} = y] \leq e^{\epsilon^*} \mathbb{P}[\hat{f}\{\tilde{\mathcal{M}}(x')\} = y] + \delta\right) \rightarrow 1$$

as $n \rightarrow \infty$ for any x, x' and y .

Proof. Define $\eta_n = \sup_{x \in \mathcal{X}} \|\hat{f}^{-1}(x) - f^{-1}(x)\|_2 \xrightarrow{P} 0$. For any $x \neq x'$ in the compact domain,

$$\|\hat{f}^{-1}(x) - \hat{f}^{-1}(x')\|_2 \leq \|f^{-1}(x) - f^{-1}(x')\| + 2\eta_n \leq C' + 2\eta_n,$$

for some constant $C' > 0$, where the last inequality follows from Lemmas 2 and 3, as f^{-1} is Lipschitz Continuous and $f^{-1}(x)$ is bounded for all $x \in \mathcal{X}$. From Theorem 1, $g(x) + N(0, \sigma^2 \mathbf{I}_d)$ satisfies Local (α, ϵ_R) RDP privacy for any $0 < \delta < 1$ with $\epsilon_R = \frac{\alpha(\Delta_2(g))^2}{2\sigma^2}$ with sensitivity being bounded by assumption.

If a mechanism satisfies Local $(\alpha, \epsilon_R(\alpha))$ -RDP, then it also satisfies Local (ϵ, δ) -DP for any $\delta > 0$ (Mironov, 2017), where:

$$\epsilon = \epsilon_R(\alpha) + \frac{\log(1/\delta)}{\alpha - 1}. \quad (34)$$

To minimize ϵ , the optimal α is given by taking the derivative and setting to 0. With some algebra,

$$\alpha^* = 1 + \sqrt{\frac{2\sigma^2 \log(1/\delta)}{\Delta_2^2 g}}. \quad (35)$$

Note that $\alpha^* > 1$. Substituting α^* into the conversion formula gives:

$$\epsilon^* = \frac{\Delta_2^2(g)}{2\sigma^2} + \frac{\Delta_2(g)\sqrt{2\log(1/\delta)}}{\sigma}. \quad (36)$$

Now, replacing g with $\sqrt{w}\hat{f}^{-1}$ and $\sigma^2 = 1 - w$, we get $\tilde{\mathcal{M}}(x)$ satisfies Local (ϵ^*, δ) Differential Privacy for any $\delta \in (0, 1)$ with

$$\epsilon^* = \frac{w(C' + 2\eta_n)^2}{2(1-w)} + \frac{(C' + 2\eta_n)\sqrt{2w\log(1/\delta)}}{\sqrt{1-w}},$$

since

$$\frac{w\Delta_2^2(\hat{f}^{-1})}{2(1-w)} + \frac{\Delta_2(\hat{f}^{-1})\sqrt{2w\log(1/\delta)}}{\sqrt{1-w}} \leq \frac{w(C' + 2\eta_n)^2}{2(1-w)} + \frac{(C' + 2\eta_n)\sqrt{2w\log(1/\delta)}}{\sqrt{1-w}}.$$

As $n \rightarrow \infty$, $\tilde{\mathcal{M}}(x)$ satisfies Local (ϵ^*, δ) Local DP, replacing $C' + 2\eta_n$ with C' .

Under this condition, by the Post Processing Theorem, which states that if $\tilde{\mathcal{M}}(x)$ is Locally (ϵ^*, δ) -Differentially Private, any function applied to the output also preserves the same privacy guarantees (Dwork et al., 2014), we conclude that by applying the MAF back to the observed space, the mechanism $\hat{f}(\tilde{\mathcal{M}}(x))$ is also Locally (ϵ^*, δ) -Differentially Private with $\Delta_2(\hat{f}^{-1}) \leq C' + 2\eta_n$. Then, from Appendix 7.1, since \hat{f} converges to f in L_2 , it also converges in probability as $n \rightarrow \infty$. Then, from (33), sending $n \rightarrow \infty$ the mechanism $\hat{f}(\tilde{\mathcal{M}}(x))$ satisfies Local (ϵ^*, δ) DP for any $0 < \delta < 1$ with

$$\epsilon^* = \frac{wC'^2}{2(1-w)} + \frac{C'\sqrt{2w\log(1/\delta)}}{\sqrt{1-w}}.$$

This completes the proof. \square

Without using Local RDP, we may directly prove the following theorem on the Local DP of our proposed mechanism.

Theorem 5. *First, consider a trained MAF transport map, $\hat{f} = \hat{f}_k \circ \dots \circ \hat{f}_1$, where each $\hat{f}_j, j \in \{1, \dots, k\}$ has mapping defined in (3). We assume the following:*

1. *each function $\mu_i(\cdot)$ and $\sigma_i(\cdot)$ in (3) are trained neural networks whose layers are spectrally normalized with the same number of layers L for each $\hat{f}_j, j \in \{1, \dots, k\}$. That is, each weight matrix has spectral norm at most 1.*
2. *the data domain $\mathcal{X} \subset \mathbb{R}^d$ is compact.*
3. *\hat{f} converges to a deterministic transport map f uniformly in probability as the sample size increases and the sensitivity of f^{-1} is bounded, i.e., $\Delta_2(f^{-1}) \leq C$ for a constant C .*

Let

$$\hat{f}(\tilde{\mathcal{M}}(x)) = \hat{f}\{\sqrt{w}\hat{f}^{-1}(x) + \sqrt{1-w}Z\}, \quad Z \sim N(0, \mathbf{I}_d).$$

Then, with $\hat{\Delta} = \|\hat{f}^{-1}(x) - \hat{f}^{-1}(y)\|_2$ and $\Delta = \|f^{-1}(x) - f^{-1}(y)\|_2$, the mechanism $\hat{f}\{\tilde{\mathcal{M}}(\cdot)\}$ satisfies (ϵ, δ) -Local DP Privacy in probability for any $0 < \delta < \frac{1}{2}$ if for sufficiently small w

$$w < \frac{1}{1 + \frac{\Delta^2}{\epsilon^2} (\epsilon - 2\log(2\delta))}, \quad (37)$$

i.e.,

$$\mathbb{P}\left(\mathbb{P}[\hat{f}\{\tilde{\mathcal{M}}(x)\} = y] \leq e^{\epsilon^*} \mathbb{P}[\hat{f}\{\tilde{\mathcal{M}}(x')\} = y] + \delta\right) \rightarrow 1$$

as $n \rightarrow \infty$ for any x, x' and y under (37) with sufficiently small w .

Proof. First, suppose we are in \mathbb{R} . Now, consider the input space $\tilde{\mathcal{M}}(x): \sqrt{w}\hat{f}^{-1}(x) + \sqrt{1-w}Z$, where $Z \sim N(0, 1)$. Note that $\sqrt{w}\hat{f}^{-1}(x) + \sqrt{1-w}Z \sim N(\sqrt{w}\hat{f}^{-1}(x), 1-w)$ and $\hat{f}^{-1}(x) - \hat{f}^{-1}(x') = \hat{\Delta}$, where $x, x' \in \mathcal{X}$, and $\hat{\Delta} \leq C' + 2\eta_n$ similar to the setup for the proof of Theorem 2 with some constant $C' > 0$. We first need to show that

$$\mathbb{P}\left(\log \frac{\mathbb{P}[\tilde{\mathcal{M}}(x) = y]}{\mathbb{P}[\tilde{\mathcal{M}}(x') = y]} > \epsilon\right) \leq \delta$$

for any $0 < \epsilon, \delta < 1$. Note that

$$\begin{aligned} & \log \left(\frac{\mathbb{P}[\tilde{\mathcal{M}}(x) = y]}{\mathbb{P}[\tilde{\mathcal{M}}(x') = y]} \right) \\ &= \frac{-(y - \sqrt{w}\hat{f}^{-1}(x))^2 + (y - \sqrt{w}\hat{f}^{-1}(x'))^2}{2(1-w)} \\ &= \hat{\Delta} \frac{2\sqrt{w}(\sqrt{w}\hat{f}^{-1}(x) + \sqrt{1-w}Z) - w(\hat{f}^{-1}(x) + \hat{f}^{-1}(x'))}{2(1-w)} \\ &= \hat{\Delta} \frac{2\sqrt{w(1-w)}Z + w\hat{\Delta}}{2(1-w)}. \end{aligned}$$

Then, we would like the following:

$$\begin{aligned}
& \mathbb{P} \left(\hat{\Delta} \frac{2\sqrt{w(1-w)}Z + w\hat{\Delta}}{2(1-w)} > \epsilon \right) \\
&= \mathbb{P} \left(Z > \frac{\epsilon\sqrt{1-w}}{\sqrt{w}\hat{\Delta}} - \frac{\sqrt{w}\hat{\Delta}}{2\sqrt{1-w}} \right) \\
&\leq \frac{1}{2} \exp \left\{ -\frac{1}{2} \left[\frac{\epsilon\sqrt{1-w}}{\sqrt{w}\hat{\Delta}} - \frac{\sqrt{w}\hat{\Delta}}{2\sqrt{1-w}} \right]^2 \right\} < \delta,
\end{aligned}$$

if

$$w < \frac{1}{1 + \frac{\hat{\Delta}^2}{\epsilon^2} (\epsilon - 2 \log(2\delta))}$$

To see the sufficient condition, we are given the quantity:

$$E(w) = \frac{\epsilon^2(1-w)}{w\hat{\Delta}^2} - \epsilon + \frac{w\hat{\Delta}^2}{4(1-w)},$$

and we want to find conditions on w such that

$$\frac{1}{2} \exp \left\{ -\frac{1}{2} \left(\frac{\epsilon\sqrt{1-w}}{\sqrt{w}\hat{\Delta}} - \frac{\sqrt{w}\hat{\Delta}}{2\sqrt{1-w}} \right)^2 \right\} < \delta.$$

Multiplying both sides by 2 and taking the natural logarithm, we get:

$$\begin{aligned}
-\frac{1}{2}E(w) &< \log(2\delta), \\
E(w) &> -2\log(2\delta).
\end{aligned}$$

Substituting the expression for $E(w)$ yields:

$$\frac{\epsilon^2(1-w)}{w\hat{\Delta}^2} - \epsilon + \frac{w\hat{\Delta}^2}{4(1-w)} > -2\log(2\delta).$$

Thus,

$$\frac{\epsilon^2(1-w)}{w\hat{\Delta}^2} + \frac{w\hat{\Delta}^2}{4(1-w)} > \epsilon - 2\log(2\delta).$$

Note, the left-hand side consists of two positive terms. Thus, a sufficient condition is obtained by focusing on the dominant term $\frac{\epsilon^2(1-w)}{w\hat{\Delta}^2}$, and requiring:

$$\frac{\epsilon^2(1-w)}{w\hat{\Delta}^2} > \epsilon - 2\log(2\delta).$$

Dividing both sides by $\epsilon^2/\hat{\Delta}^2$ and rearranging gives:

$$\frac{1-w}{w} > \frac{\hat{\Delta}^2}{\epsilon^2} (\epsilon - 2\log(2\delta)).$$

Thus,

$$w < \frac{1}{1 + \frac{\hat{\Delta}^2}{\epsilon^2} (\epsilon - 2\log(2\delta))}.$$

³ Now, let us partition R as $R = R_1 \cup R_2$, where

$$R_1 = \left\{ Z \in R : \hat{\Delta} \frac{2\sqrt{w(1-w)}Z + w\hat{\Delta}}{2(1-w)} \leq \epsilon \right\}, \quad R_2 = \left\{ Z \in R : \hat{\Delta} \frac{2\sqrt{w(1-w)}Z + w\hat{\Delta}}{2(1-w)} > \epsilon \right\}.$$

Now, fix any subset $S \subseteq R$, and set

$$S_1 = \{y \in S : \mathcal{M}(x) = y, \xi \in R_1\}, \quad S_2 = \{y \in S : \mathcal{M}(x) = y, \xi \in R_2\},$$

where $\xi \sim N(0, 1)$ is a noise realization in the mechanism. We have

$$\begin{aligned} \mathbb{P}[\tilde{\mathcal{M}}(x) \in S] &= \mathbb{P}[\tilde{\mathcal{M}}(x) \in S_1] + \mathbb{P}[\tilde{\mathcal{M}}(x) \in S_2] \\ &\leq \mathbb{P}[\tilde{\mathcal{M}}(x) \in S_1] + \delta \\ &\leq e^\epsilon \mathbb{P}[\tilde{\mathcal{M}}(x') \in S_1] + \delta \\ &\leq e^\epsilon \mathbb{P}[\tilde{\mathcal{M}}(x') \in S] + \delta, \end{aligned}$$

where the second inequality follows because the probability mass over R_2 is at most δ , and the third inequality follows from bounding the privacy loss over R_1 by ϵ .

Extending this to the multivariate setting, suppose $\hat{f}^{-1}(x), \hat{f}^{-1}(x') \in \mathbb{R}^d$ are neighboring points. Define $\hat{\Delta}_{\text{Vec}} = \hat{f}^{-1}(x) - \hat{f}^{-1}(x')$ and $\hat{\Delta} = \|\hat{f}^{-1}(x) - \hat{f}^{-1}(x')\|$. $\tilde{\mathcal{M}}(x)$ is $\sqrt{w}\hat{f}^{-1}(x) + \sqrt{1-w}Z$, where $Z \sim N(0, \mathbf{I}_d)$. Thus,

$$\tilde{\mathcal{M}}(x) \sim N(\sqrt{w}\hat{f}^{-1}(x), (1-w)\mathbf{I}_d), \quad \tilde{\mathcal{M}}(x') \sim N(\sqrt{w}\hat{f}^{-1}(x'), (1-w)\mathbf{I}_d).$$

Note, the privacy loss at output y is:

$$L(y) = \log \left(\frac{p_{\tilde{\mathcal{M}}(x)}(y)}{p_{\tilde{\mathcal{M}}(x')}(y)} \right) = \frac{1}{2(1-w)} (\|y - \sqrt{w}\hat{f}^{-1}(x')\|^2 - \|y - \sqrt{w}\hat{f}^{-1}(x)\|^2).$$

Applying $\|a\|^2 - \|b\|^2 = (a-b)^\top(a+b)$,

$$\|y - \sqrt{w}\hat{f}^{-1}(x')\|^2 - \|y - \sqrt{w}\hat{f}^{-1}(x)\|^2 = (\sqrt{w}\hat{\Delta}_{\text{Vec}})^\top (2y - \sqrt{w}(\hat{f}^{-1}(x) + \hat{f}^{-1}(x'))).$$

Substituting $y = \sqrt{w}\hat{f}^{-1}(x) + \sqrt{1-w}Z$,

$$\begin{aligned} 2y - \sqrt{w}(\hat{f}^{-1}(x) + \hat{f}^{-1}(x')) &= 2(\sqrt{w}\hat{f}^{-1}(x) + \sqrt{1-w}Z) - \sqrt{w}(\hat{f}^{-1}(x) + \hat{f}^{-1}(x')) \\ &= \sqrt{w}(\hat{f}^{-1}(x) - \hat{f}^{-1}(x')) + 2\sqrt{1-w}Z \\ &= \sqrt{w}\hat{\Delta}_{\text{Vec}} + 2\sqrt{1-w}Z. \end{aligned}$$

Thus,

$$\sqrt{w}\hat{\Delta}_{\text{Vec}}^\top (2y - \sqrt{w}(\hat{f}^{-1}(x) + \hat{f}^{-1}(x'))) = w\|\hat{\Delta}_{\text{Vec}}\|^2 + 2\sqrt{w(1-w)}\hat{\Delta}_{\text{Vec}}^\top Z$$

with

$$L(y) = \frac{1}{2(1-w)} \left(w\|\hat{\Delta}_{\text{Vec}}\|^2 + 2\sqrt{w(1-w)}\hat{\Delta}_{\text{Vec}}^\top Z \right).$$

Now,

$$Z' = \frac{\hat{\Delta}_{\text{Vec}}^\top Z}{\|\hat{\Delta}_{\text{Vec}}\|}, \quad \text{thus } Z' \sim N(0, 1).$$

Hence,

$$\hat{\Delta}_{\text{Vec}}^\top Z = \hat{\Delta} Z'.$$

Substituting,

$$L(y) = \frac{w\hat{\Delta}^2}{2(1-w)} + \frac{2\sqrt{w(1-w)}\hat{\Delta}Z'}{2(1-w)}.$$

³Since $0 < \delta < 1/2$, $\log(2\delta) < 0$ and $-\log(2\delta) > 0$, making the right-hand side well-defined and positive. Similarly, we may also explicitly derive a solution isolating w by solving a quadratic formula without any assumptions of $w \rightarrow 0$, only that $w \in [0, 1]$.

Simplifying,

$$L(y) = \hat{\Delta} \times \frac{2\sqrt{w(1-w)}Z' + w\hat{\Delta}}{2(1-w)}.$$

Thus, the final privacy loss for this multivariate Gaussian Mechanism is

$$L(y) = \hat{\Delta} \times \frac{2\sqrt{w(1-w)}Z' + w\hat{\Delta}}{2(1-w)}, \quad Z' \sim N(0, 1).$$

So, the same proof goes through in the \mathbb{R}^d case with

$$w < \frac{1}{1 + \frac{\hat{\Delta}^2}{\epsilon^2} (\epsilon - 2 \log(2\delta))}$$

for sufficiently small w , but with $\hat{\Delta}$ in the Multivariate Setting being with respect to L_2 Norm. Repeating our argument above, by the Post Processing Theorem (Dwork et al., 2014), we conclude that by applying the MAF back to the observed space, the mechanism $\hat{f}(\tilde{\mathcal{M}}(X))$ is also Locally (ϵ^*, δ) -Differentially Private with high probability when replacing $\hat{\Delta}$ with Δ as $n \rightarrow \infty$.

Repeating our argument above again, from Appendix 7.1, since \hat{f} converges to f in L_2 , it also converges in probability as $n \rightarrow \infty$. Then, from (33), the mechanism $\hat{f}(\tilde{\mathcal{M}}(x))$ satisfies Local (ϵ^*, δ) DP with high probability as $n \rightarrow \infty$ if

$$w < \frac{1}{1 + \frac{\Delta^2}{\epsilon^2} (\epsilon - 2 \log(2\delta))}$$

with sufficiently small w for any $0 < \epsilon < 1$ and $0 < \delta < 1/2$.

□

Remark 4. In Theorems 2 and 5, the sensitivity $\Delta_2(f^{-1})$ is assumed to be bounded from above. This is a consequence of Lemma 2 and Lemma 3.